Cardiff University

School of Engineering

Ph.D. Thesis

entitled

Wave propagation in quasi-crystalline generated phononic structure

Presented by: Abdelbaset Farhat

Student ID:1876891

Supervisor: Dr. Lorenzo Morini

Co-supervisor: Dr. Hanxing Zhu

Cardiff 2023

Abstract

Wave propagation in a class of two-phase phononic structures in which cells are generated according to Fibonacci sequences is investigated. The Fibonacci sequence is a one-dimensional quasi-crystalline rule. I studied axial waves in quasi-periodic infinite rods and flexural waves in quasi-periodic infinite beams.

In the axial wave case, two-phase phononic rods whose elementary cells are designed adopt the quasi-crystalline silver mean Fibonacci substitution rule. The stop/pass-band spectra are studied with the aid of a trace-map formalism, which provides a geometrical interpretation of the recursive rule governing traces of the relevant transmission matrices: the traces of two consecutive elementary cells can be represented as a point on a surface defined by an invariant function of the circular frequency, and the recursivity implies the description of an orbit on a surface called Kohmoto's surface. I showed that, for a sub-class of silver mean-generated waveguides, the orbits predicted by the trace map at specific frequencies are periodic. The configurations for which this occurs, called canonical, are also associated with periodic stop/pass-band diagrams along the frequency domain. Several types of periodic orbits exist, and each corresponds to a self-similar portion of the dynamic spectra whose scaling law can be studied by linearizing the trace map in the neighborhood of the orbit. The obtained results provide both a new piece of theory to better understand the behavior of classical two-phase composite periodic waveguides and an important advancement towards the design and realization of phononic quasi-crystalline-based metamaterials.

For flexural waves of quasiperiodic infinite beams designed by adopting the quasi-crystalline golden mean Fibonacci substitution rule, I investigated the effect of the axial pre-stress on the dispersion diagrams. I also investigated the frequency shift of the stop/pass band positions. The results show that pre-stress has a clear influence on the width of the pass/stop band, increasing or decreasing depending on the type of pre-stress applied.

This thesis gives a deep understanding of how waves propagate in quasiperiodic structures, giving broader options for designers of acoustic devices like waveguides and acoustic filters.

Declaration

This work has not been submitted in substance for any other degree or award at this or any other university of learning. It is not being submitted concurrently in candidature for any degree or other awarded.

Signed (Abdelbaset Farhat)

Date 20/04/2023

Statement 1

This thesis is being submitted in partial fulfilment of the requirements for the degree of Ph.D.

Signed (Abdelbaset Farhat)

Date 20/04/2023

Statement 2

This thesis is the result of my own work, except where otherwise stated. Other sources are acknowledged by footnote giving explicit reference. A bibliography is appended.

Signed (Abdelbaset Farhat)

Date 20/04/2023

Statement 3

I hereby give consent for my thesis, if accepted, to be available for photocopying and for inter-library loan and for the title and summary to be made available to an outside organisation.

Signed (candidate)

Date

ACKNOWLEDGEMENTS

The research presented in this thesis has been carried out at the Cardiff School of Engineering, Cardiff University with financially supported by the Libyan Ministry of Education under the supervision of Dr. Lorenzo Morini. I wish to express my deepest gratitude to them for the guidance, encouragement, patience, and support they have given me in the past few years and for providing the financial support, opportunity, and resources required in my study and completing this project.

First and foremost, I thank **ALLAH** for helping me to complete this thesis.

I would like to thank my current supervisor Dr. Lorenzo Morini and my previous supervisor Massimiliano Gei for their supervision, help and continuous support. My thanks go to them for accepting me to be one of their students in the School of Engineering at Cardiff University.

Big thanks are due to many members of staff at Cardiff University for taking time out of their busy schedules to help and support my project during my study at Cardiff University.

My most fantastic thanks are reserved for my family. Especially my mother, for her Doa, and unconditional love, support, and encouragement throughout the whole of my life. I will never forget her heart-warming support to me in tracking my progress and encouraging me continuously to reach my goals.

I would like to thank my country, Libya for funding my study and giving me this opportunity.

List of abbreviations and nomenclatures

F-B	Floquet-Bloch theory
TMM	Transfer Matrix Method
FBZ	First Brillouin Zone
GM	Golden Mean
SM	Silver Mean
GMs	Golden Mean structures
SMs	Silver Mean structures
T_i	Transfer matrix
tr	Trace of the transfer matrix
ω	Circular frequency
F_i	Fibonacci sequence
n_i	Fibonacci numbers
σ_g	Golden ratio
σ_s	Silver ratio
σ_b	Bronze ratio
L_A	Length of element A
L_B	Length of element B
S_A	Cross-section area of element A
S_B	Cross-section area of element B
E_X	Young's modulus
φ_X	Mass density per unit of volume
I(ω)	Kohmoto's invariant
$\bar{\omega}$	Normalized circular frequency
ω_{c_n}	Canonical frequency
R_C	Reflection coefficient
S	Bending stiffness
N	pre-stress
r	Radius of gyration
$\bar{N}$	Dimensionless pre-stress
M_i	Receptances matrix
SB	Stop Band
$k_2^{\pm}$	Silver Mean scaling factor (family 1)
$k_4^{\pm}$	Silver Mean scaling factor (familyno. 2 and 3)
$k_g^{\pm}$	Golden Mean scaling factor

Publications

Journals

Farhat, A.K.M., Morini, L. and Gei, M., 2022. Silver-mean canonical quasicrystalline-generated phononic waveguides. Journal of Sound and Vibration, 523, p.116679.

Conferences

Farhat, A.K.M., Chen, Z., Morini, L. and Gei, M. (2021). On generalised canonical axial waveguides. EM4SS'21 - Engineering Materials for Sustainable Structures, held online, Modena, Italy, 26-28 April 2021.

Farhat, A.K.M., Chen, Z., Morini, L. and Gei, M. (2021). Frequency spectra and stop-band optimisation of generalised canonical quasicrystalline phononic waveguides. Euromech Colloquium 626 – Mechanics of High-Contrast Elastic Composites, held online, Keele, UK, 6-8 September 2021.

Farhat, A.K.M., Chen, Z., Morini, L. and Gei, M. (2021). Generalised canonical quasicrystalline phononic waveguides. Metamaterials2021, held online, London, UK, 6-9 December 2021.

Farhat, A.K.M., Morini, L. and Gei, M. (2022). Silver mean canonical quasicrystalline-generated phononic structures. ESMC2022- 11th European Solid Mechanics Conference, Galway, Ireland, 4-8 July 2022.

Chapter of a books

Chen, Z., Farhat, A.K.M. and Gei, M. (2023). Universal representation of dynamic frequency spectra for canonical generalised quasi-crystalline-generated waveguides. In Mechanics of High-Contrast Elastic Solids, Eds. H. Altenbach (Advanced Structured Materials, vol. 187). Springer Nature, Switzerland, pp. 65-74.

Table of Contents

List of Figures

List of Tables

Chapter 1: General introduction

1.1 Background and motivation

Wave propagation in periodic structures has grown to become of essential importance in condensed matter physics due to the role that atomic vibrations (and electronic structure) play in describing the properties of crystals.

In eighteenth century, Brillouin started to investigate the physical properties of periodic structures. He studied the dynamic properties of these structures to understand the nature of wave propagation. Band-gap (BG) phenomenon is one of the most important features wherein any periodic structure displays a certain range of frequencies in which wave cannot propagate resulting in filtering properties (Brillouin, 1953). It has to be noted that the phenomenon of band gap which are also called stop band or attenuation zone is due to the fact that periodic structures possess two or more different faces and band gaps associate with the contrast between physical and geometrical properties of the different faces. In addition, we can assume two different materials to obtain band gap in the related dispersion relation. This type of behaviour is common to all periodic structures including mechanical, optical, magnetic, electromagnetic etc. where all these structures are periodic composite structures that have band gap behaviour. Another interesting feature of the periodic structures is their simplified calculation ways where due to the periodicity, analysing one subsystem is sufficient to deduce and understand wave propagation in the entire structure.

A huge number of research and studies about the properties of one-dimensional periodic structures have been performed. The simplicity of the geometry and analysis of these type of structures as well as their ability of coupling between adjacent cells have attracted many researchers (Brillouin, 1953; Mead, 1996; Ruzzene and Baz, 2001; *Liuet al, 2020*). Ungar (1966) has derived an expression describing the vibration of steady state of an infinite beam with uniformly supported on impedances. This formula provided ways analysing of the structures with fluid loadings. Later, the scientist Gupta was able to present a new analysis for periodically-supported beams systems that presented the concepts of unit cell and its transfer matrix. In addition, Gupta introduced the parameters' plots of the propagation and attenuation that are considered the base for future work of one-dimensional periodic structures (Gupta, 1970).

A study on mono-coupled periodic systems has been conducted by Faulkner and Hong. This study used analytical and finite element methods analysing the free vibration of mass-spring systems (Faulkner and Hong, 1985). In contrast, Mead and Yaman (1991) in their study investigated the response of one-dimensional periodic structures under the periodic load. The effects of the elastic support characteristics on the pass/stop characteristics of the beam are presented in this study.

Growing attention has been given in recent years to the investigation of elastic wave propagation in the phononic materials. Elastic or acoustic waves cannot propagate inside band gaps (BGs) created by Phononic materials which are artificial materials made of two or more materials with varying mechanical properties. The diverse physical features of BGs and their potential use in the creation of acoustic devices like noise reduction, waveguides, and acoustic filters are what have attracted a great attention to them (Yuan et al, 2014).

Phononic materials distinguish themselves from among other classical materials and composites by its unique ability to control acoustic and elastic vibrational waves where this material shows band gabs frequency in certain frequency range (Hussein et al, 2014). The notion of a “phonon” has emerged in the context of vibrations in a crystal lattice. "Formally defined as a quantum of vibrational energy in an elastic medium — which may be interpreted as a discrete particle-like quantity of sound in a solid". The term of a phonon has also been connected with classical axial waves like vibrations and acoustics, mainly in the field of periodic media. It has become normally to indicate to the periodic material, as a “phononic material,” or a “phononic structure.” In this thesis, I will study the dynamical properties of the phononic structures for axial waves which also called phonon in the field of solids which providing a possibility of designing a spectrum and predicting stop/pass band pattern.

This can be accomplished by arranging the material phases or geometry to take advantage of essential wave-material interactions, including resonance and interference. Due to these interactions, a phononic material allows the vibrational waves to pass at certain frequency bands, and prevents some vibrational waves from passing called here band gaps where wave propagation is forbidden. The feature of band gap can be useful to design waveguides, acoustic filters, and acoustic devices such as noise reduction.

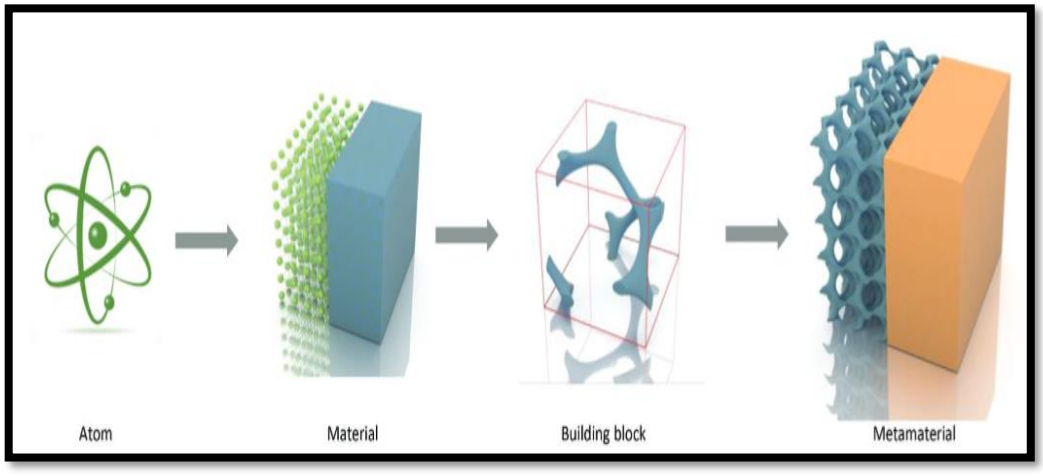

Figure 1: the transformation from conventional materials to phononic materials (metamaterials is an example) (Zheng et al, 2023).

According to (Frazier, 2015) resonance and interference are the two important mechanisms by which phononic materials exert control over vibrational wave propagation. These wave-material interactions can be exploited as a means in categorising phononic materials into two subsystems phononic crystals and metamaterials which can be created as illustrated in Figure 1.

Bragg scattering explains a process by which a light wave, upon passing via a crystal, is partially reflected at all planes of atom. Due to the spacing between planes, the reflected components may interfere with each other and the incident wave leads to prevent wave propagation through the crystal. Similarly, the artificial atoms of phononic crystals (i.e., the material/geometrical constituents) interact with vibrational waves.

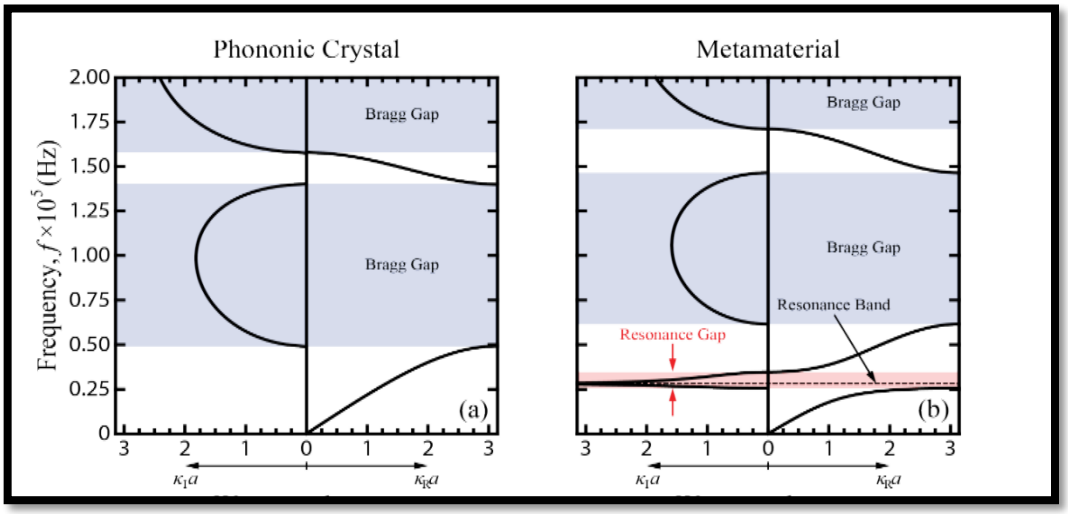

Figure 2:Dispersion band diagrams for a one-dimensional (a) phononic crystal with band gaps induced by Bragg scattering and (b) metamaterial featuring a resonance-induced gap before those of Bragg scattering (Liu et al, 2000).

In this context, the band gaps in the dispersion band diagram of phononic crystals are the result of the effect of Bragg scattering as illustrated in the Figure 2(a). Bragg scattering and interference have an influence within metamaterials, leading to band gaps in the dispersion band diagram. However, for metamaterials, the smallest gaps (sketched in red in figure 2(b)) are typically not the result of Bragg scattering, rather the result of a phenomenon of the local resonance (Liu et al, 2000). There are some potential applications of metamaterials include optical filters, smart solar power, and medical devices.

Over the past decades, the control of wave propagation in periodic structures has always been hotspot of the research. In this context, some typical examples of controlling wave propagation can be found such as supported beams, modulated rods, and plates (Liu et al, 2020).

starting in the early 1990s, the field of wave propagation in periodic structures has experienced a new rally with the introduction of phononic crystals (PnCs) which was a field of research of many researchers (Sigalas, 1992; Sigalas and Economou1993; Kushwahaet et al,1993;

Kushwahaet et al,1994; Vasseur et al,1994). Phononic Crystals (PnCs) are new synthetic periodic materials made up of at least two materials as illustrated in Figure 3 that can be used to regulate and manipulate the propagation of elastic (or acoustic) waves.

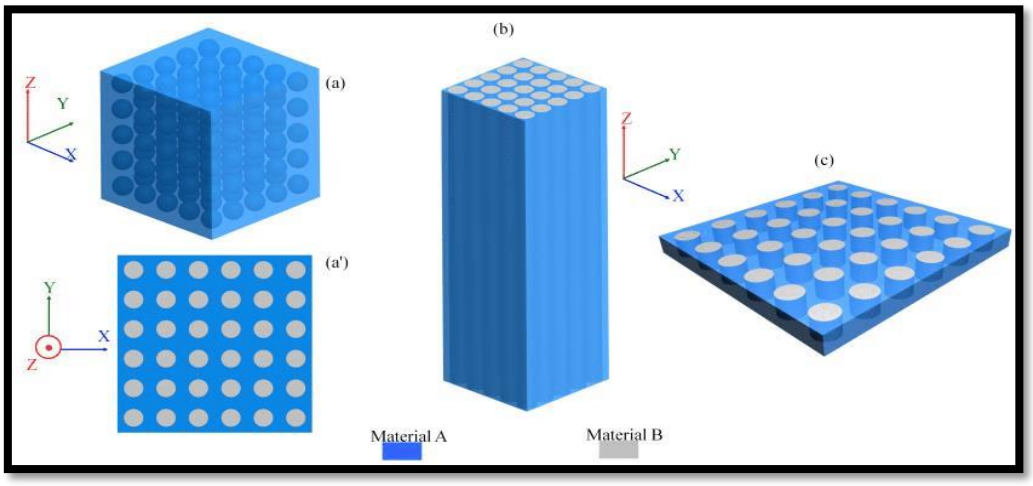

Figure 3: Schematic of periodic materials with different configurations. (a) 3D PC, (a') 2D PC for bulk waves, (b) 2D PC for surface waves, (c) PC for Lamb waves (2D) (Assouar et al, 2015).

The importance of the phononic crystals is the existing of band gabs (filtering property) in their structures (see Figure 4) which makes it possible to prevent the mechanical waves (i.e., acoustic and elastic waves) to propagate in a certain frequency range (Guillén-Gallegos et al,2019). The unique existing connection between both periodic materials and phonon physics has gained a substantial upgrade by introducing phononic crystals. An acoustic (or elastic) metamaterial, on the other hand, is also (usually) a periodic material with the added advantage of local resonance, or possibly other features, that can allow "unusual" dynamical behaviour, such as negative refraction or negative group velocity. In addition, metamaterials show an important foundation in electromagnetics, and the disciplines of acoustics and electrodynamics have been steering a parallel path in the improvement of this highly unique class of materials.

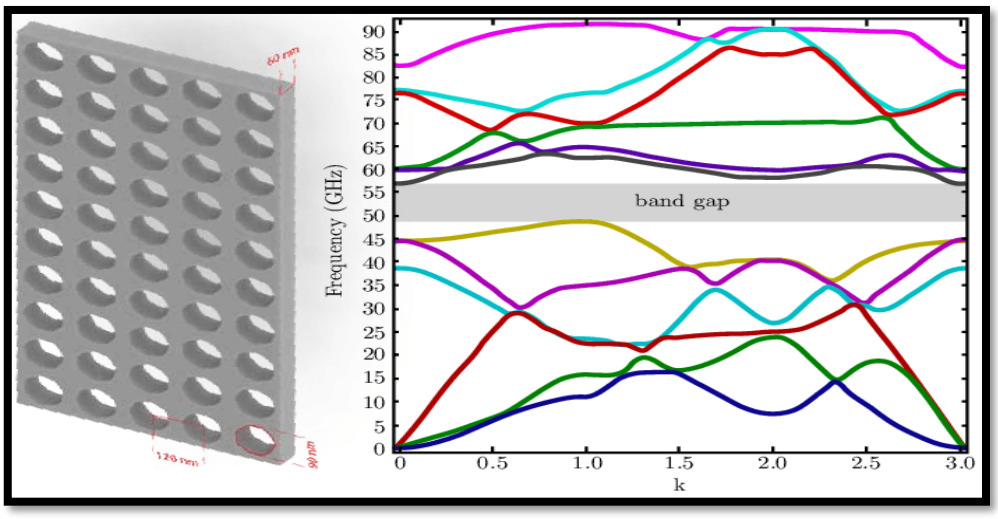

Figure 4: Simulated-phononic-band-structure-for-a-phononic-band-gap-material (Becker and Becher, 2017).

Phononic crystals and their optical counterpart, the so-called photonic crystals are now well-known for their ability to control, guide, and manipulate the propagation of acoustic and optical waves. These properties are fundamentally related to the existence of band gaps in their band structure which providing the possibility of localised modes and confined acoustic and optical waves (Penne and Djafari-Rouhani, 2019). As mentioned earlier, a remarkable feature of phononic materials research is the wide interest across disciplines. While research in composite materials and periodic structures has become the focus among civilians and mechanicals, the concept of artificial periodicity has also been especially attractive in the fields of electromagnetism and photonics (Elachi, 1976). The concept of photonic crystal was discovered by (Yablonovitch and John,1987) which quickly emerged for acoustic or elastic waves, which was subsequently called as a phononic crystal (Yablonovitch and John, 1987).

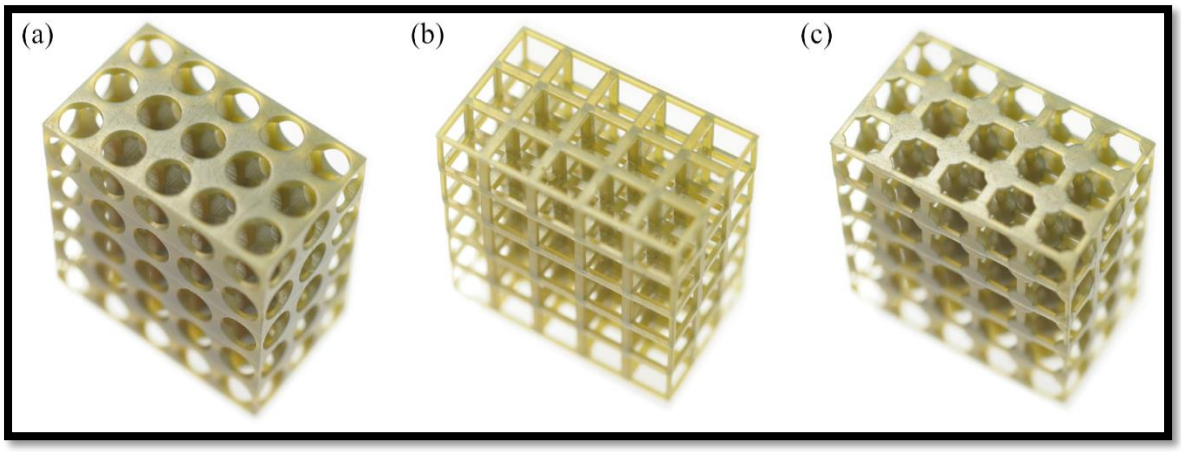

Figure 5: Fabrication of a simple cubic phononic crystals with 3mm lattice constant consisting of (a) three cylindrical holes; (b) rectangular scaffold; and (c) corner balls connected by cylindrical beams (Google image).

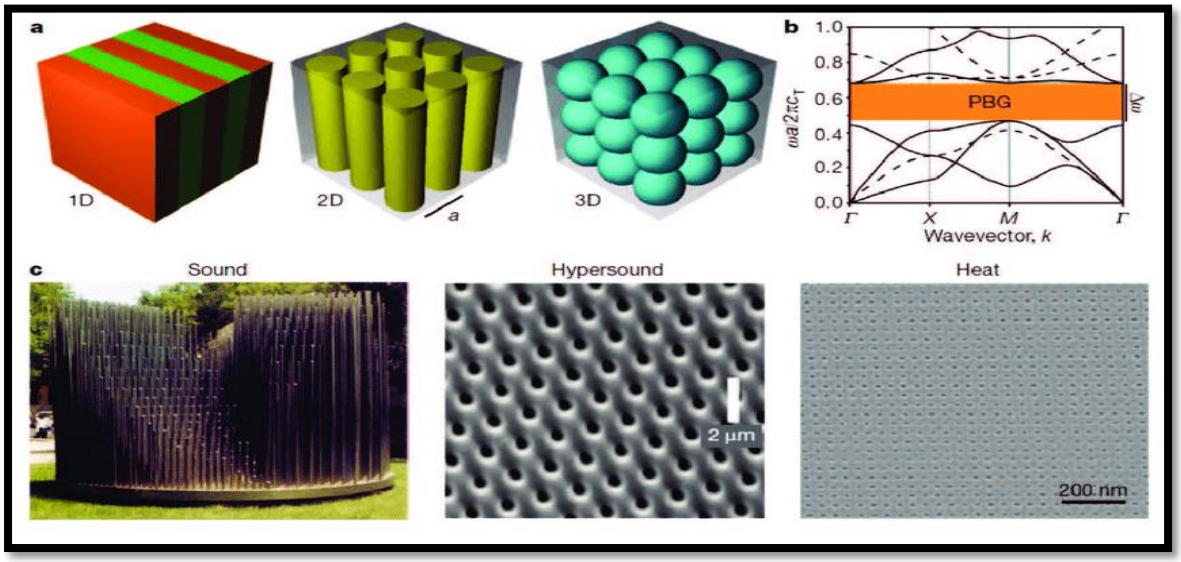

Figure 6: (a)Schematics of phononic crystal of different dimensionalities. (b) An example of phonon band structure. The orange area marks the forbidden band gap. (c) Examples of phononic crystals efficient at different wavelength scales (Zheng, 2017).

In the last twenty years, wave propagation in mechanical meta-materials and their applications in different areas of structural and mechanical engineering have gained an increasing interest. Many different phononic composites and structures have been designed and tested with the aim of achieving and controlling several innovative dynamical phenomena, such as frequency filtering, negative refraction, and non-reciprocal propagation.

Shmuel and Band (2016) showed that the frequency spectrum of two-component elastic laminates admits a universal structure, regardless of the particular physical attributes and periodic-cell shape. They also referred that we can rigorously derive the maximal width, the predicted width, and the density of the band-gaps ranges of frequencies at which waves cannot propagate thanks to the structure's compactness as illustrated in Figure 7(d). Specifically, they discover that these band-gaps' density is a characteristic shared by all laminate types. Following are guidelines for customizing laminates to meet required spectrum attributes. They demonstrated that different finitely deformed laminates have the same compact structure in their frequency spectrum as well.

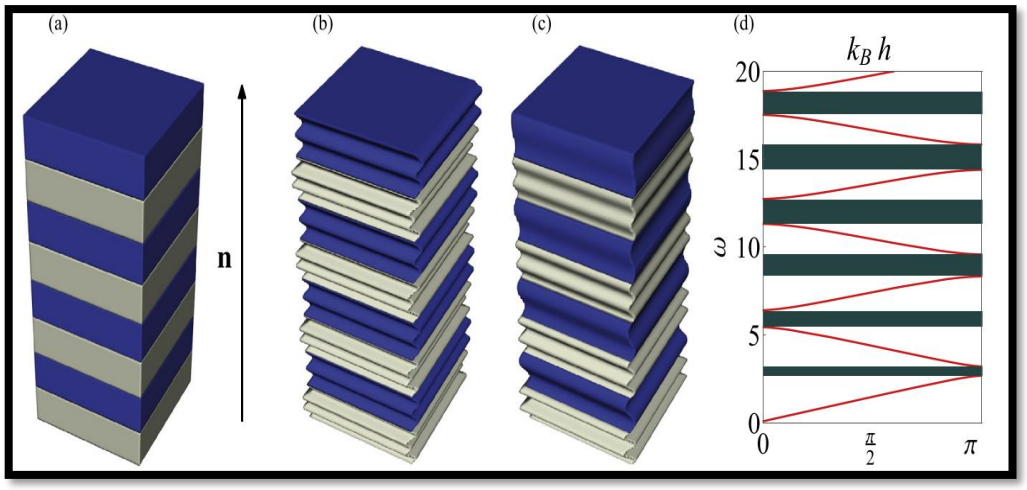

Figure 7: (a) A laminate comprising two alternating layers, repeated periodically in direction n. (b) Propagating waves.(c) Attenuating waves. (d) Representative band structure of exemplary laminate. Colored regions donate band-gabs (Shmuel and Band ,2016).

Another feature for wave propagation in mechanical meta-materials which is a negative refraction has been studied by (Srivastava, 2016). They have shown that it is possible to have a purely negatively refracted signal in the laminate that can be used to steer beams over large angles for small changes in the incident angles. Morini et al (2019a) also studied negative refraction in quasi-crystalline multi-layered metamaterials generated according to Fibonacci sequence. They have shown that with a trend that rises monotonically with increasing index, Fibonacci laminates can transmit negatively-refracted waves over a larger range of incidence angles; in certain circumstances, negative refraction is possible at any incidence angle.

Non-reciprocal wave propagation in discretely modulated spatiotemporal plates was studied by (Riva et al, 2020). They applied generalized Plane Wave Expansion Method (PWEM) to study a spatially discrete and temporally continuous elastic medium which embodies non-reciprocal capabilities. They computed group velocity plots and directivity, which are utilised to predict directional and non-reciprocal phenomena at specific frequencies. Theoretical solutions have been compared to numerical findings, proving that the generalized Plane Wave Expansion Method is suitable to describe wave propagation properties of discretely space-time modulated systems.

Recently, elastodynamics of composite beams following a quasi-periodic pattern have gained considerable attention (see e.g, Gei (2010); Sorokin (2019); Pal et al (2019); Xia et al (2020)). In particular, the non-standard dispersive properties of a class of two-phase periodic structured rods whose unit cells are generated according to the Fibonacci substitution rule based on the primary sequence commonly known as *golden mean* (GM) have been presented (Gei, 2010; Morini and Gei, 2018; Morini et al., 2019b). This class belongs to the subset of *quasi-crystalline* media (Poddubny and Ivchenko, 2010) and portions of Floquet-Bloch frequency spectra of its members display a self-similar pattern which scales according to factors linked to an invariant function, the so-called Kohmoto's invariant (Kohmoto and Oono, 1984).

All developments in past research in the field of wave propagation in quasi-periodic generated phononic structures, especially those related to the presence of frequency band gabs, have made it necessary to study the properties of wave propagation in these structures deeply. In this thesis, I will study the dynamical properties of another type of quasi-crystalline-generated waveguide, namely, that composed of elementary cells conceived by adopting a generalized Fibonacci substitution rule based on the binary sequence commonly known as silver mean (SM). Considering harmonic axial wave propagation, I will show that the corresponding Floquet-Bloch dynamic spectra can be fully determined by studying the behavior of the traces of the transfer matrices of three 'adjacent' elementary cells, which are related through recursive relationships. These connections allow us to apply the trace-map formalism (Kolar and Ali, 1989), which provides the geometrical representation of the traces as coordinates of points which describe orbits on a surface defined by the Kohmoto's invariant. Those orbits are studied in detail, to find that, for a sub-class of silver-mean (SM) waveguides, they are periodic at specific frequencies, called *canonical frequencies* in analogy to those determined for the standard Fibonacci sequence by Gei et al (2020). In particular, there exist three types of canonical frequencies and each of them can be associated with a well-defined configuration of the elementary cell called, likewise, *canonical configuration*.

Each of the three families of canonical configurations is characterized by self-similar properties of the layouts of stop and pass bands, a feature that can be linked to the periodic orbits on the invariant surface. By means of a linearization procedure of the trace map, we obtain analytical scaling factors governing the different self-similar ranges of the spectra for all three families of canonical rods. The scaling factors could be used to predict, design and optimize the unique filtering properties of a two-phase silver-mean generated structured rods.

This thesis also focuses on the effects of the axial pre-stress on the dispersion diagram of quasi-crystalline-generated waveguide whose elementary cells are built based on generalized Fibonacci substitution rule based on the primary sequence commonly known as *golden mean* (GM) by considering the propagation of a flexural wave in pre-stressed quasi-crystalline beam.

1.2 Aim and objectives

This project aims to investigate the dynamical properties of one-dimensional phononic quasi-crystalline structures whose elementary cell are generated according to Fibonacci substitution rule. The focus is on infinite two faces bar composed of the repetition of the elementary cells designed by adopting generalised Fibonacci substitution rules, some of which represent examples of one-dimensional quasi-crystals. Their dispersive features and stop/pass band spectra are computed and analysed by imposing Floquet–Bloch conditions and exploiting the invariance properties of the trace of the relevant transfer matrices.

I will demonstrate that an invariant function of the circular frequency, known as the Kohmoto's invariant, governs self-similarity (regular pattern of pass/stop band diagrams) and scaling of the stop/pass band layout within specified frequency ranges at increasing generation index for a family of generalized Fibonacci substitution rules, which correspond to the so-called precious means. The existence of specific frequencies, referred to as canonical frequencies, connected to closed orbits on the geometric three-dimensional representation of the invariant is also explained by the Kohmoto's invariant.

Morini and Gei studied the propagation of axial wave in one-dimensional bi-phase quasi-crystalline rods whose elementary cell produced according to Fibonacci Golden Mean (GM) sequence. The main focus of this study has been on the characteristics of the stop and pass band arrangements that are obtained in the same frequency range for various sequence indices.

Their research's primary finding illustrates how an invariant function of the circular frequency known as the Kohmoto's invariant contributes to the determination of those characteristics.

Despite a few attempts (Gei, 2010; Morini and Gei, 2018; Zhao et al, 2013) to investigate the dispersion properties of elastic Fibonacci generated waveguides, the understanding of these scaling phenomena for quasicrystalline and general quasiperiodic structures has not yet been

satisfactorily addressed in mechanics. Therefore, research is needed to identify the fundamental characteristics of dynamic spectra and offer the essential direction for their potential application in the creation of innovative architectural materials with readily controllable stop and pass band topology.

This thesis will focus primarily on the propagation of axial waves in Silver Mean (SM) structures. In addition, I will study the flexural waves in multi supported beam generated according to the generalised Fibonacci Golden Mean sequence.

Since this work is a continuation of what (Morini and Gei, 2018) have achieved for axial waves in Golden Mean rods and what (Gei, 2010) has done for flexural waves in multi supported beam, this work will follow the same pattern that Gei and Morini followed. Therefore, the objectives throughout this work are summarized in the following

• to follow Fibonacci sequences to create quasiperiodic quasi-crystalline structures.

• to provide a general framework to analyse axial wave propagation of quasi-crystalline generalized Fibonacci rods and also for flexural wave of multi supported quasi-crystalline beams.

• to highlight the role of trace mapping and that of an invariant function, the Kohmoto's invariant, in determining the properties of harmonic dynamics of such structures.

• to study the scaling properties of the dynamic spectra depending on the features of the Kohmoto's invariant.

• to investigate the occurrence of ultra wide stop bands occurring in the dynamic spectra whicg is can be useful in semiconductors.

• to introduce a special class of quasi-crystalline structures, named canonical structures, that display special conservation properties in the stop/pass band diagram.

• to introduce some properties at non canonical frequencies.

• to illustrate the role of the pre-stress on the dispersion diagram and Kohmoto's invariant for flexural waves.

The results obtained by this work give broader options for designers of acoustic devices like waveguides and acoustic filters.

1.3 Methodology

To achieve the above objectives, the following methodology was adopted

1. Reviewing previous work, with a particular focus on the findings of Gei (2010) and Gei and Morini (2018).
2. Follow Morini and Gei's approach in finding the dynamical properties of quasi-crystalline-generated structures as follows
    - Deriving all the equations of axial and flexural waves in one-dimensional quasi-crystalline rods and beams.
    - Analyse the properties of the trace of the transfer matrix (trT_i) associated with Fibonacci silver mean sequences.
    - Analyse the scaling and self-similarity of the stop/pass band layout for SM rods
    - studying the role of pre-stress in influencing the positions of pass and stop band in the dispersion diagram of GM pre-stressed beams
3. The results which are dispersion diagrams will be achieved using the MATLAB software by obtaining the trace of the transfer matrix.

1.4 Thesis structure

This thesis is organized as follows:

Chapter 2 introduces the concept of phononic periodic structure. The Floquet-Bloch theory will be presented in this chapter. At the end of this chapter, I will present some examples of applications of Floquet-Bloch theory.

Chapter 3 is about Quasi-crystalline-generated periodic structure. The chapter focuses on the Fibonacci sequences (Golden, Silver, and Bronze mean sequence: also called precious means) which are a typical examples of a one-dimensional quasi-crystalline pattern.

Chapter 4 analysis axial wave propagation in silver mean rods, in this chapter, the Floquet-Bloch theorem is applied to obtain the dispersion diagram for silver mean rod. I also studied the properties of trace of the related matrix ($tr\ T_i$) and how these features affect the frequency spectrum of silver mean rods. A nonlinear map determining the evolution of the auxiliary variable x_i for precious means structures and the so-called Kohmoto's surface for this map are found. The canonical structure which is a class of structure characterized by closed orbit is presented.

Chapter 5 gives a brief comparison of the behaviour of harmonic axial waves in Golden structures with their Silver counterpart.

Chapter 6 describes the effects of the axial pre-stress on dispersion diagrams for flexural vibration. The structure in this chapter is a quasiperiodic multi-supported pre-stressed beam generated according to the Fibonacci golden sequence.

Chapter 7 provides a summary of the entire thesis and gives some suggestions for future research.

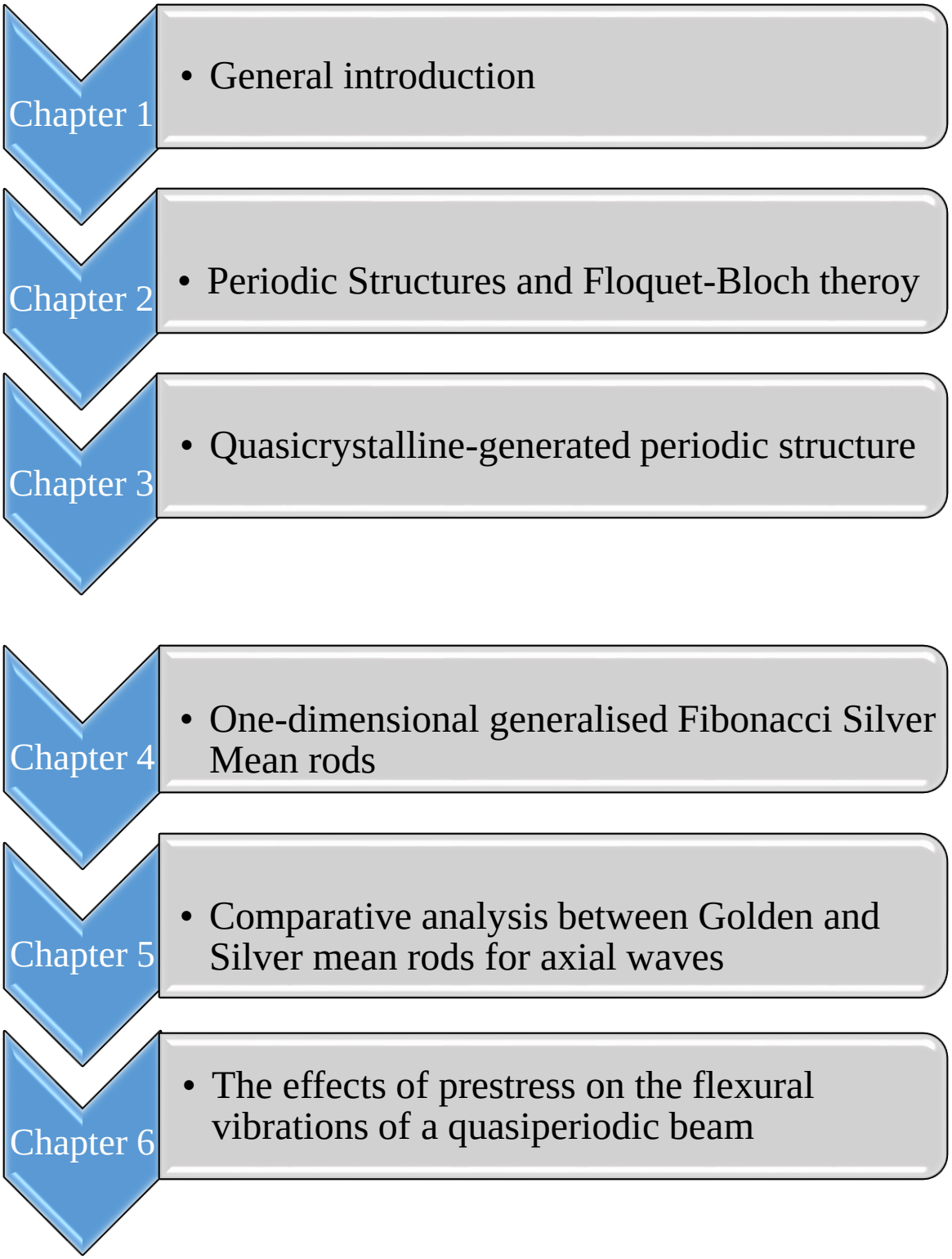

Figure 8: Thesis structure.

Chapter 2: Elastic Waves in Periodic Structures and Floquet-Bloch Theory

2.1 Overview

In this chapter, I will introduce the concept of periodic structures and how waves propagate in these structures which is very useful in many applications like filters and waveguides.

I will then introduce the Floquet-Bloch theory which is a mathematical theory that enables us to study elastic wave propagation in periodic structures and as examples of applications of Floquet-Bloch theory, we propose different 1-dimensional discrete systems. In details, this chapter will show how the periodic structure can be generated and find solution to waves propagation in periodic structures.

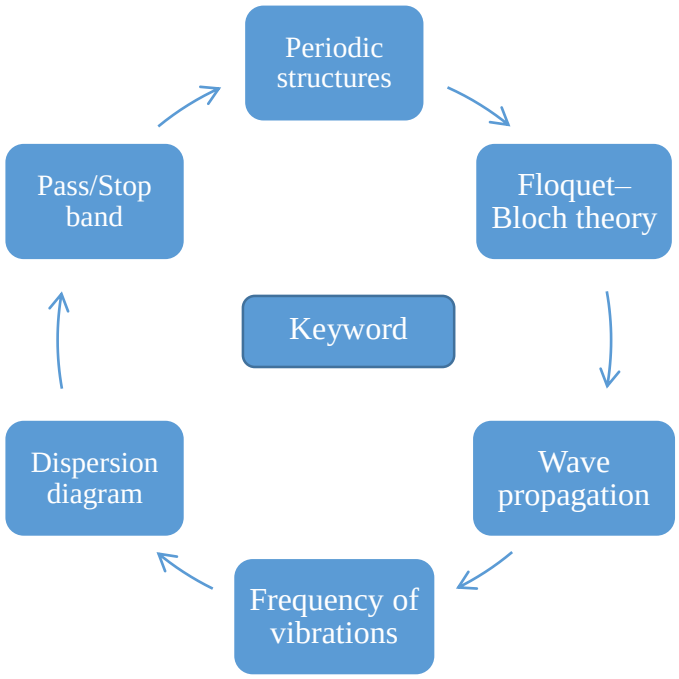

Figure 9: Chapter two key word.

2.1 Periodic structures

A periodic structure is a structure that is composed of the repetition of the periodic cell, as illustrated in Figure 10, where the periodic cell is sketched in red. The repetition of the periodic cell *N* times will lead to the creation of the entire structure. Reviewing the research carried out in the field of wave propagation in periodic structures, (Mead, 1996) defined a periodic structure as a structure formed mainly of two or more identical structural components connected together to compose a continuous structure. In a periodic structure, analyzing one subsystem (elementary cell or unit cell) is sufficient to deduce and understand wave propagation in the entire structure. This feature made the periodic structures easy to study their dynamical behaviour comparing with other non-periodic structures.

.

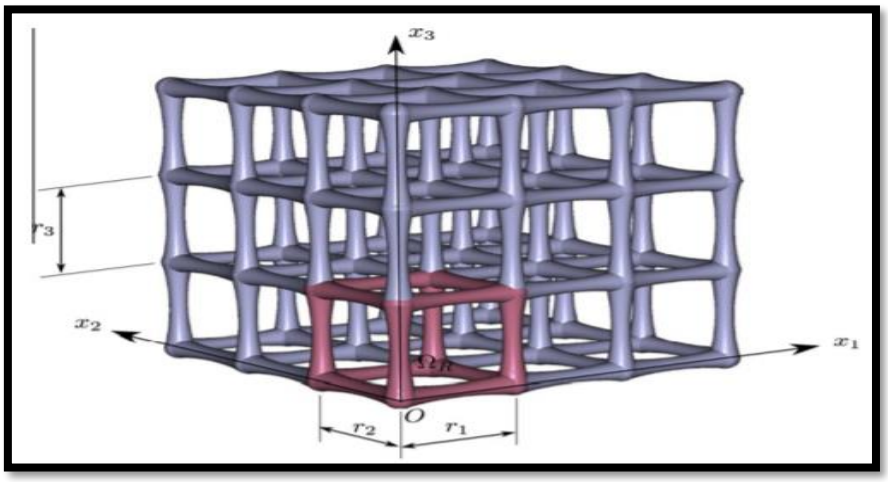

Figure 10: 3.D periodic structure, the red colour represents the elementary cell of the entire structure (Collet et al, 2011).

Periodic structures are found in many systems and materials. The regular arrangement of atoms, particles, or unit cells (periodic elements) which are connected together end-to-end or side-by-side in the system as illustrated in Figure 10 will produce a periodic system. The feature of controlling wave propagation in these systems has contributed to the growth of photonics and phononic fields. In addition, it is the periodic structure that allows interested scientists in photonics and semiconductors to take advantage of each other's preceding work.

All systems with periodic construction are widely spread in both nature and engineering systems around us such as multi-storey buildings, satellite solar panels and aircraft fuselage, etc. From the engineering point of view, the major point of these types of structures stems from the fact that it is easy to manufacture their structures, their ability to withstand high temperatures, high strength-to-weight ratios, and significant impact (Gibson and Ashby, 1999). In addition, structures with periodic features provide advantages in wave propagation characteristics which is very useful in filters and waveguides as illustrated in Figure 11. Given the vital role played by periodic structures, it is important to model and understand wave propagation phenomena in these structures (Ruzzene et al., 2003)

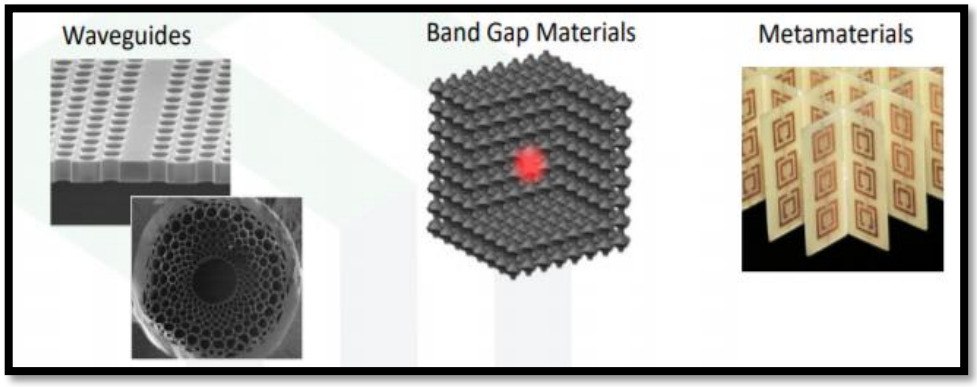

Figure: 11 Examples of the periodic structures.

In the field of periodic structures, we can have several directions of periodicity, we can have 1-D (periodic in one dimension such as rods and beams), 2-D (periodic in two dimensions such as flat and plates), or even 3-D (periodic in three dimensions such as curved shells) periodic structures (Mead, 1996) as illustrated in Figure 12. The structures generated according to Fibonacci sequence are one-dimensional structures. Therefore, this thesis will focus on mechanical wave propagation in one-dimensional structures which is periodic in one direction.

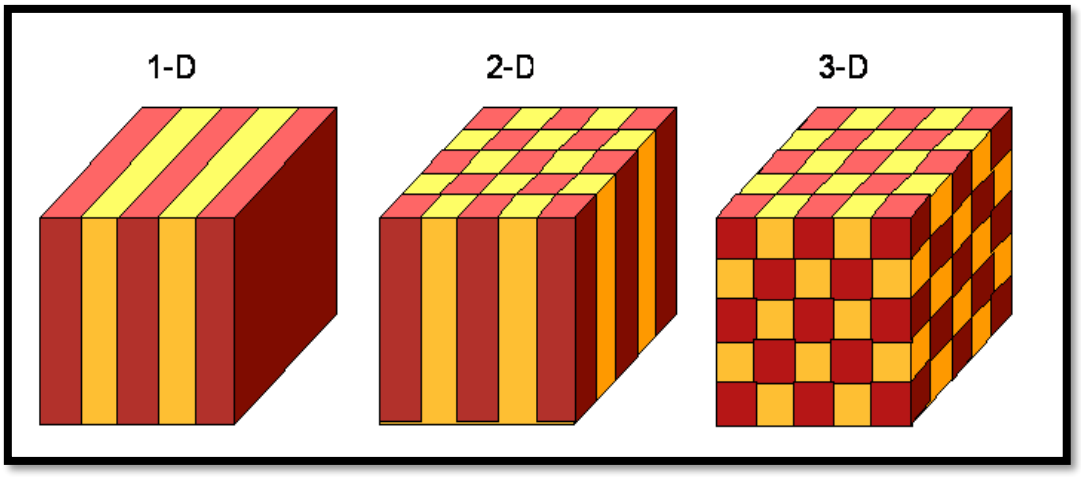

Figure 12: Periodic structures in several directions of periodicity.

Periodic materials modeling theories are not just restricted to the engineering area where physicists and the like were concerned with wave propagation behaviour in periodic materials. All these efforts help in understanding the properties of periodic material (Farzbod, 2010).

Engineers are primarily interested in the propagation of waves in periodic structures, such as sandwich beams and honeycomb panels for airplane fuselages, while physicists study the wave phenomena taking place in a microscopic periodic medium such as electron and phonon transport in crystals. These two approaches by engineers and physicists developed independently and in parallel until fairly recently, have both been referred to as the Bloch analysis (Farzbod, 2010). In the physical sciences, wavelike (hyperbolic) partial differential equations arise, which are parametrized by one or more periodic coefficients (Brillouin, 1946). Generally, these equations have often the form $\nabla^2\Psi(r) + \omega^2 F(r)\Psi(r) = 0$ in which $\Psi(r)$ is a field vector at position r and $F(r)$ is a periodic function. Floquet studied this equation when stated in one dimension and $F(r)$ is the cosine function. Bloch also solved a similar equation in quantum mechanics. In quantum mechanics, Bloch also solved an equation like this one. (Brillouin, 1946) solved the three-dimensional wave equation using the Bloch theorem. Since then, Bloch's approach has been applied to engineering problems as well as other physical sciences, such as acoustics and the study of sonic crystals (Miyashita, 2005).

The first work on a periodic one-dimensional lattice was a result of Newton's attempt to study and derive the formula for the velocity of sound in air. Since the differential equations at that time were not familiar, a natural approach would have consisted in discretising the continuous media supporting the propagation of sound into a chain of lumped masses that are connected by a lumped spring where $\rho, E,$ and A are the mass density, Young modulus, and cross-section area of the system respectively. This process, which is shown in Figure 13, leads to a periodic system, which is known to have a more complex wave behaviour than the original continuous system (Hussein et al., 2014).

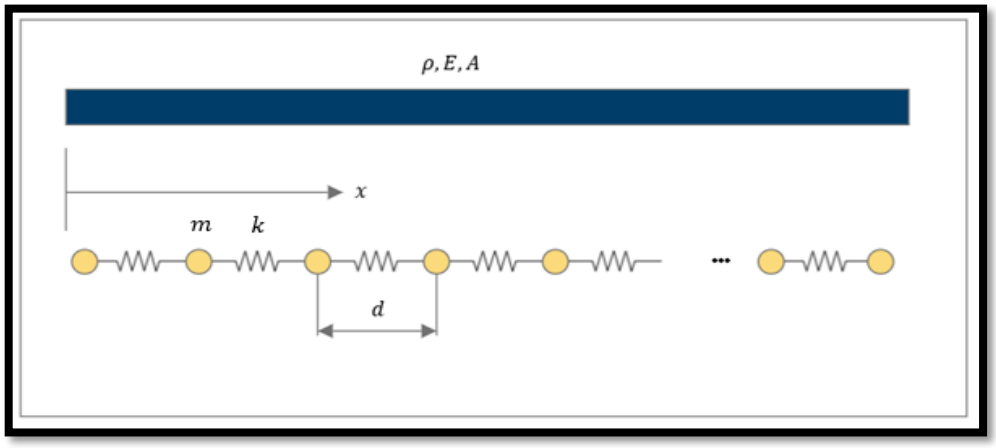

Figure 13: Discretization of a rod into a spring-mass system (Hussein et al, 2014).

The same system was later investigated by John Bernoulli and his son Daniel, who, in a series of studies starting in 1727, demonstrated that a system of *N* masses is characterized by *N* modes of vibration and associated frequencies, and essentially formulated the principle of superposition. Subsequent studies included the estimation of the velocity of wave propagation along one axis of a cubic lattice structure as a function of wavelength. Thanks to these efforts, wave dispersion has been seen for the first time from the estimation of the phase velocity's dependency on frequency.

In the field of the periodic structure, the equations of motion can be minimized to the lowest number of degrees of freedom utilizing the technique of Floquet–Bloch thus solving the wave equation on the boundaries of the unit cell.

Many scientists have used Floquet–Bloch theory which is a technique to solve wave equations and derive dispersion relations. In section 2.2 we will introduce the fundamental basics of Floquet–Bloch theory.

2.2 Floquet–Bloch theory

Floquet-Bloch's (F-B) theorem presents an effective and powerful strategy to analyse the behaviour of wave propagation in periodic systems. Floquet develop a theory for 1-D partial

differential equations with periodic coefficients obtained by Floquet (1883). Later Bloch generalised the results of Floquet to 3-D systems. This generalisation obtained a great description of the wave function associated with an electron moving through a periodic crystal lattice (Bloch, 1928).

F-B technique has become widely applied to compute the dispersion properties of periodic systems and predict their wave modes. Waves can propagate in any periodic systems (1-D, 2-D, 3-D, simple, complicated, etc.), but the equations related to waves propagation will be more complicated for 2-D and 3-D than 1-D periodic systems where we have to impose more than one directions. This thesis relies on Fibonacci sequences which are 1-D sequences in constructing the structures in which wave propagation is required to be studied.

Floquet–Bloch theory could deal with a representative cell describing the wave dispersion for the entire system. The F-B theory reduces the problem to calculations performed in the so-called unit cell, subject to certain specific boundary conditions derived from the F-B theory and elastodynamics (Collet et al, 2011). In this thesis will specify this theory to 1-D periodic systems.

Now I will introduce the basics of F-B theory and show how the concept of periodicity can be applied to introduce and derive a dispersion diagram.

Generally, Floquet-Bloch theory provides a strategy to obtain a set of solutions of a linear ordinary equations system of the form

$$F(x)= M(x)\, f\,(x) \qquad (1)$$

where f (x) is the solution vector, and M is the transfer matrix which give us the transmission of the state vector at the cell output as a function of state vector at the input of the cell.

Let us apply this concept to the analysis of axial wave propagation problems in infinite periodic material. To simplify the idea of this theorem, let us consider an infinite continuous rod consisting of equidistant atoms as illustrated in Figure 12 where each atom was represented by a round point having mass *m* while the spring constant *k* represents the wave vector.

F-B theorem provides an effective way to find a solution to the linear ordinary equations in the form

$$\varphi(x) = u_k(x)e^{ikx} \qquad (2)$$

Given the symmetricity of the atoms, at any distance $\varphi(x)$ will be written as follows.

$$\varphi(x + a) = u_k(x)e^{ikx}e^{ika}$$

Or

$$\varphi(x+a) = \varphi(x)e^{ika} \quad (3)$$

This equation gives the wave function $\varphi(x)$ at any distance where k is wave vector and $u_k(x)$ is a periodic part of wave function depends on wave vector (k) sometimes called Bloch wave. The results obtained are dispersion diagrams describing the propagation of the range of frequencies corresponding to waves along the structure (pass band). In parallel, these diagrams also clarify the width of the stop band called also band gap in which the range of frequencies associated with waves cannot propagate along the body (Gei, 2010).

In order to obtain Floquet–Bloch dispersion relation, we will use transfer matrix method.

2.3 Transfer Matrix Method

In this section we present and discuss a mathematical technique for the analysis of the wave propagation in one-dimensional structures. The method depends on the transfer matrix and is widely known as the transfer matrix method.

Generally, transfer matrix is a matrix providing us the output vector state as a function of input vector state. This matrix can be different according to system used. In other words, to derive the transfer matrix for periodic rods, displacement and axial force at the right-hand boundary of the elementary cell, respectively u_r and N_r, have to be identified in terms of those at the left-hand boundary, respectively u_l and N_l. For periodic beams, the transfer matrix depends on the rotation and its derivative at the boundaries of the cell. Transfer matrix contains all the properties that govern the waves propagation inside each phase of the system.

Transfer Matrix Method (TMM) is one of the most powerful methods of the contemporary theoretical physics. This method offers an accurate solution for the one-dimensional lattice (Myshlyavtsev, 2001).

The beginnings of using transfer matrix were in the early 1960s, as a result to joint effort between University of Southampton and Y. K. Lin's group at the University of Illinois.

Lin et al (1969) were pioneers in the field of the application of transfer matrices to the study of stiffened plate vibrations and periodic structures, emphasizing that the transfer matrix applies strictly to one-dimensional or quasi-one-dimensional systems.

In the University of Southampton, Mercer and Seavey (1967) confirmed that transfer matrices can be used to compute natural frequencies and modes of stiffened plates.

The Method is applied widely for the dynamic analysis of engineering structures analysis which is useful in the treatment of periodic structures. In general, the behaviour of the entire structure

can be described through the analysis of a single elementary cell, together with boundary conditions (Stephen, 2006).

The transfer matrix method was used to analysis the wave propagation of quantum particles, such as electrons (Kirkman and Pendry, 1984; Mello et al,1988; Ando,1989; Beenakker, 1997; Markos, 2006; others) and electromagnetic (Pendry and MacKinnon, 1992) acoustic (Morini and Gei, 218) and elastic waves. Once this technique is developed for one type of wave, it can easily be applied to any other wave problem.

2.3.1 Multiplication of Transfer Matrices

Consider a more complicated which is a unit cell of an infinite structure as illustrated in Figure 14 where Z donates the longitudinal axis. The general solution Ψ_z of the Schrödinger equation for the entire structure will be as follows

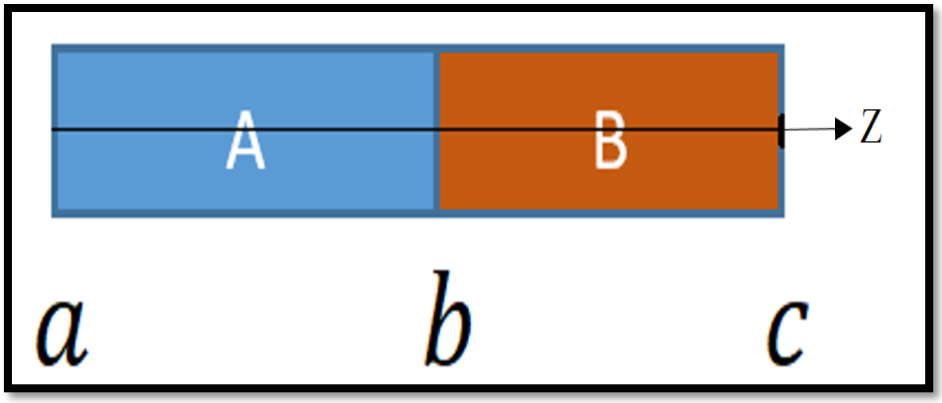

Figure 14: Representative of a unit cell of a periodic structure.

$$\begin{bmatrix}\Psi_b\,(+)\\ \Psi_b\,(-)\end{bmatrix} = \mathrm{M}_A \begin{bmatrix}\Psi_a\,(+)\\ \Psi_a\,(-)\end{bmatrix} \tag{4}$$

and

$$\begin{bmatrix}\Psi_c\,(+)\\ \Psi_c\,(-)\end{bmatrix} = \mathrm{M}_B \begin{bmatrix}\Psi_b\,(+)\\ \Psi_b\,(-)\end{bmatrix}. \tag{5}$$

By combining the Eq. (4) and (5), we will have

$$\begin{bmatrix}\Psi_c\,(+)\\ \Psi_c\,(-)\end{bmatrix} = \mathrm{M}_B\mathrm{M}_A \begin{bmatrix}\Psi_a\,(+)\\ \Psi_a\,(-)\end{bmatrix}. \tag{6}$$

As discussed above, we can express the entire system as represented by the transfer matrix

$$\mathrm{M}_{AB}=\mathrm{M}_B\mathrm{M}_A \tag{7}$$

Since the matrix M_{AB} is the transfer matrix of the entire system, its matrix elements determine the transmission and the reflection amplitudes for the entire system. This allows us to determine

the transmission and the reflection amplitudes of the whole system Figure 15 in terms of elements of the transfer matrices of the system's constituents.

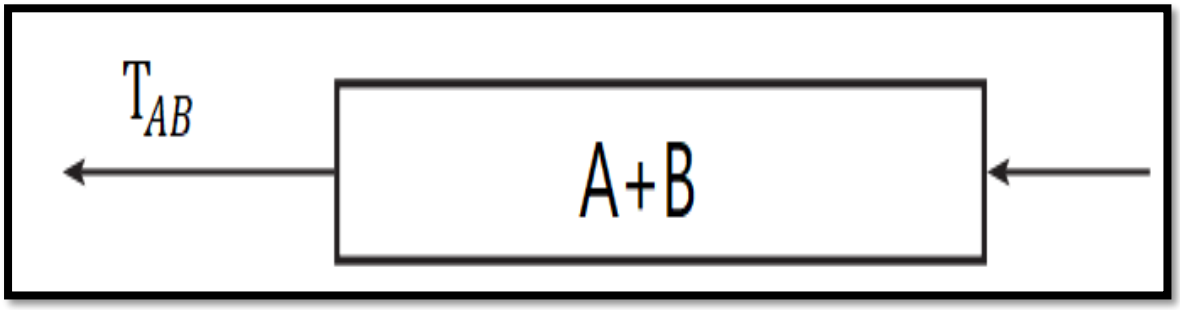

Figure 15: Transmission of electron through the entire system.

Based on above, the Eq. (6) can be written as follows

$$\begin{bmatrix}\Psi_c\,(+)\\ \Psi_c\,(-)\end{bmatrix} = \mathrm{M}_{BA}\begin{bmatrix}\Psi_0\,(+)\\ \Psi_0\,(-)\end{bmatrix} \tag{8}$$

where a=0

The superscripts + (–) indicate to the direction of propagation: + indicates that the electron moves from left to right in the positive direction and − means that the electron propagates from right to left as illustrated in Figure 16 Thus, $\Psi_L(\mathrm{z})$ is the wave function of the electron left of the sample, propagating to the right;

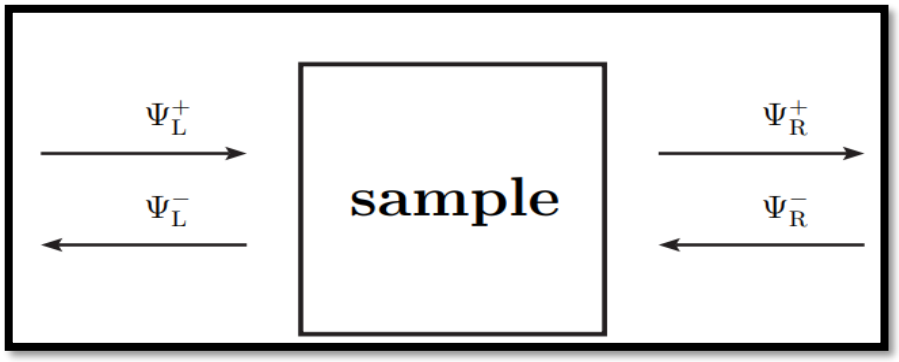

Figure 16: a typical scattering experiment. Incident waves $\Psi_L{}^+(z)$ and $\Psi_R{}^-(z)$ are scattered by the sample. Outgoing waves $\Psi_L{}^-(z)$ and $\Psi_R{}^+(z)$ consist of waves transmitted through the sample as well as waves reflected from the sample.

2.3.2 Propagating States

Consider a system with time-reversal symmetry. Then $\det M = 1$ and $tr\ (M)$ is real.

The two eigenvalues λ_1 and λ_2 of the transfer matrix are related by

$$\lambda_2 = 1/\lambda_1 \tag{9}$$

We will distinguish two cases. In the first case $|\lambda_1|$=1. Then λ_1 can be written as

$$\lambda_1 = e^{iql} \tag{10}$$

Where q is the wave vector which can be being real. As $\lambda_2 = e^{-iql}$ which lead to $tr\,(M) = \lambda_1 + \frac{1}{\lambda_1} = 2\cos ql$

Note that $|tr\,(M)| \leq 2$ (11)

In the second case, we have $|\lambda_1| \neq 1$. Then we have $|tr\,(M)| = \left|\lambda_1 + {\lambda_1}^{-1}\right| = 2\cos ql > 2$. Thus, we derive that Eq. (11) represents a sufficient condition for the existence of the propagating solution. Condition (11) is very useful in the analysis of complicated long systems. Following the Eq. (7), we can calculate the transfer matrix as a product of transfer matrices of individual subsystems. Then, Eq. (11) allows us to determine unambiguously if a given solution is propagating or not. In this way, we can estimate the entire spectrum of propagating solutions of the system.

The general solution of the infinite system is connected to the Floquet–Bloch as follows

$$\det\,[M_i - e^{\,ik} I] = 0 \tag{12}$$

where i denotes the imaginary unit and I denotes the $n \times n$ identity matrix .

The dispersion relation (12) gives the solution of complete Floquet-Bloch spectrum, which allows to obtain the stop/pass band distribution of the periodic structure.

Dispersion diagrams evaluated through the F-B technique are crucial in providing pass/stopband diagrams and these are important properties used to control wave propagation in periodic structures. According to different 1-D systems, we have a different expression of the determinates of the Floquet–Bloch will present them in the following section. In the rest of the next section, we will give different one-dimensional discrete systems as examples of the application of the Floquet-Bloch theory.

2.4 One-dimensional discrete structure

In this section, we will show how we can solve the equation of motion for undamped one-dimensional discrete systems using the Floquet-Bloch theory.

2.4.1Undamped monoatomic one-dimensional lattice material

Let us consider the discretised elastic rod as illustrated in Figure 17 in the form of a non-dissipative chain of equidistant masses (here, masses represent lattice atoms) linked by linear elastic springs. The symbols of d and k_s represent the distance between the masses and spring constant respectively and m is the mass of the material.

By applying Newton's second law in the case of the absence of an external load to the motion of the $n\text{-}th$ mass, the dynamic behaviour of the resulting spring-mass chain can be expressed by the following equation of motion

$$m\ddot{u}_n + 2k_s u_n - k_s u_{n-1} - k_s u_{n+1} = 0 \quad (13)$$

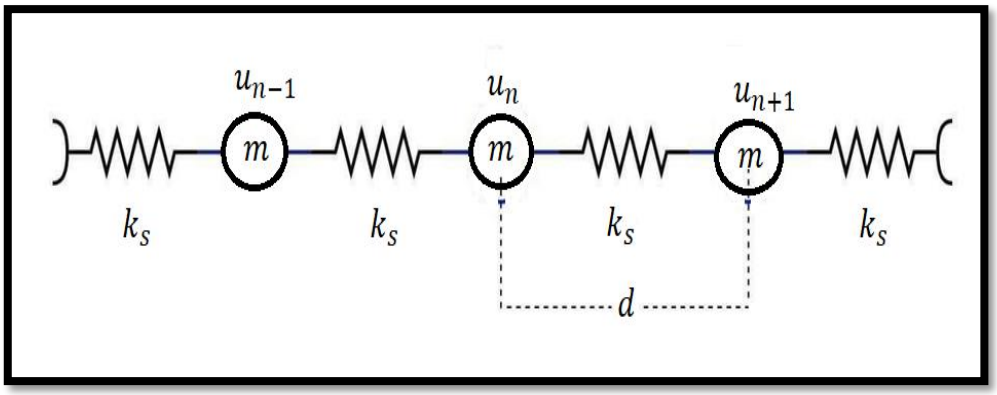

Figure 17: Undamped monoatomic lattice material.

Given the periodicity of the system, the displacement of any two neighbouring masses or cells can be described by Floquet-Bloch (F-B) theorem (Brillouin, 1953) in the following form

$$u_n = u_{n-1}\, e^{ikd} \text{ or } u_{n-1} = u_n\, e^{-ikd} \text{ and } u_{n+1} = u_n\, e^{ikd} \quad (14)$$

Let us find a solution of the form

$$u_n = \overline{u_n} e^{i\omega t} \quad (15)$$

This equation represents a traveling wave, in which all the masses vibrate with the same frequency ω at the same amplitude $\overline{u_n}$ and have wavenumber k.

Now substituting Eq. (14) and (15) into Eq. (13), we obtain

$$m^2 * \omega^2\, \overline{u_n} e^{i\omega t} = k_s \left(2\overline{u_n} e^{i\omega t} - \overline{u_n} e^{i\omega t} e^{-ikd} - \overline{u_n} e^{i\omega t}\, e^{ikd}\right). \quad (16)$$

Eq. (16) can be simplified and alternatively written in the form of

$$m * \omega^2 = k_s \left(2 - e^{-ikd} - e^{ikd}\right) = 2k_s(1 - cos\ k\ d)$$

Or

$$m * \omega^2 = 4k_s(sin^2 \tfrac{k\,d}{2}) \quad (17)$$

Leading to the final formula of the dispersion relation for the frequency which is as follows

$$\omega = \sqrt{\tfrac{4k_s}{m}} * \sin(\tfrac{k\,d}{2}). \quad (18)$$

Eq.(18) provides a relation between frequency of vibrations ω and wavenumber k, and therefore represents the dispersion relation the system illustrated in Figure 17. A non-dimensional form of the dispersion relation is introduced by defining the non-dimensional frequency. The dispersion diagram is a curve that represent the propagation of wave modes. The dispersion curve could be presented indifferent domain: frequency vs wave length; frequency vs wave number; group velocity vs frequency.

Let us introduce a non-dimensional frequency

$$\Omega = \frac{\omega}{\omega_0}, \text{ where } \omega_0 = \sqrt{\frac{k_s}{m}}$$

$$\Omega^2 = 2 * (1 - cos\ k\ d) \tag{19}$$

The dispersion relation expressed by Eq. (19) has several important properties as follows.

2.4.1.1 The symmetry of the dispersion relation

The dispersion diagram is symmetric about kd=0 and periodic with period of 2π. The behaviour of the relation is in the period of $kd \in (-\pi, +\pi)$.

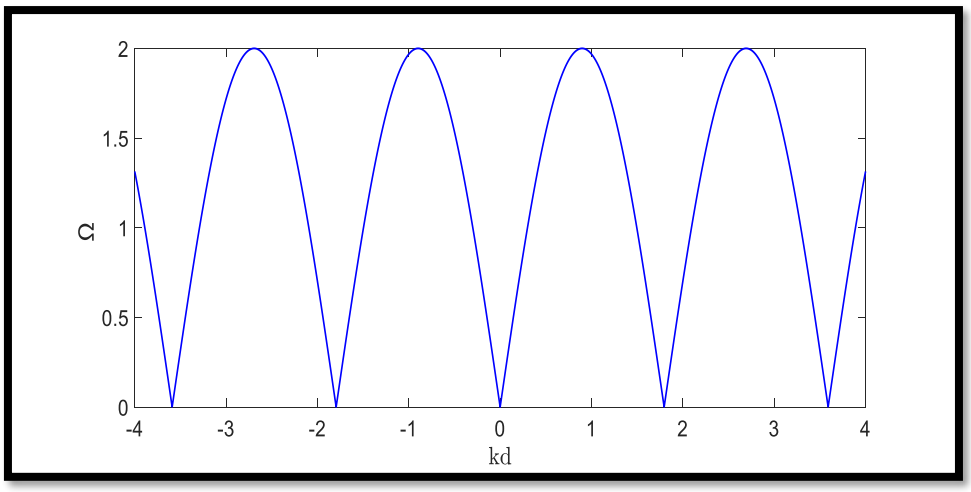

Figure 18: Dispersion relation for the 1D mass/spring system.

The range of wavenumbers determining the period of the dispersion relation, i.e., $kd \in [-\pi, +\pi]$, is known as "First Brillouin Zone" (FBZ), which is normally defined by the reciprocal lattice (Hussein et al, 2014). Given the symmetry of the dispersion relation, we can fully characterise the dispersion properties of the lattice by only studying half of the FBZ, i.e., $kd \in [0, +\pi]$, which defines the "Irreducible Brillouin Zone" (IBZ). More details can be found in (Hussein et al, 2014).

2.4.1.2 Propagation and attenuation bands (pass/stop band)

The dispersion relation solved by frequency against wavenumber provides a solution in a limited range, i.e., for $\Omega \in [0, 2]$. For $\Omega > 2$, there is no corresponding real-valued wavenumber (k), leading to stop propagating of harmonic waves. This means that the range of $\Omega > 2$ therefore belongs to stop band also known as the attenuation range. In contrast, when Ω located between 0 and 2, the wave will propagate without attenuation.

2.4.2 Undamped diatomic 1D-lattice material

Now we consider a discretised elastic rod as illustrated in Figure 19 which is one-dimensional lattice composed of two different masses m_1 and m_2 (here represent atoms) connected by linear elastic spring stiffness k_s in each unit cell with the distance between two adjacent masses d. It appears that the diatomic lattice possesses important features which is different from the monoatomic lattice.

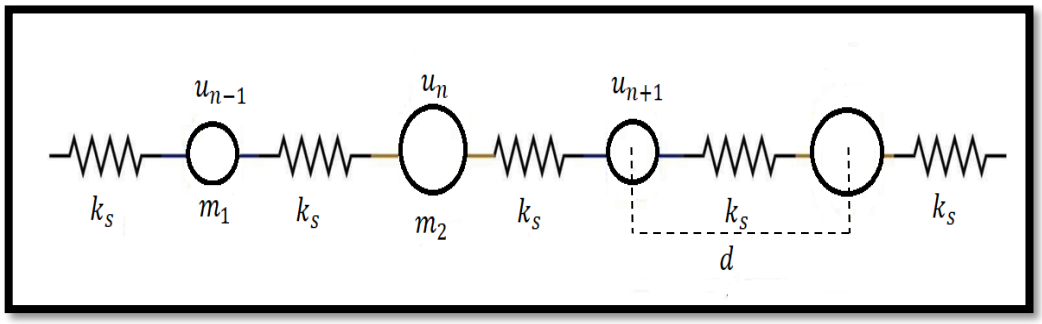

Figure 19: Undamped diatomic 1D lattice material.

Since we have two different masses in diatomic lattice, we have to derive two equations of motion using the similar way as for monoatomic lattice.

$$\begin{cases} m_1\ddot{u}_n + 2k_s u_n - k_s u_{n-1} - k_s u_{n+1} = 0 \\ m_2\ddot{u}_{n+1} + 2k_s u_{n+1} - k_s u_n - k_s u_{n+2} = 0 \end{cases} \tag{20}$$

Floquet-Bloch theorem in periodic system requires $u_{n+2} = u_n\, e^{i2kd}$ and $u_{n+1} = u_{n-1}\, e^{i2kd}$

Let us find solutions of the form

$$\begin{cases} u_n = \overline{u_1} e^{i\omega t} \\ u_{n+1} = \overline{u_2} e^{i\omega t} \end{cases}$$

Through a little algebra, the Eq. (20) can be also written in the matrix form as follows

$$\begin{bmatrix} m_1\omega^2 + 2k_s & -k_s(1 + e^{-i2kd}) \\ -k_s(1 + e^{i2kd}) & m_2\omega^2 + 2k_s \end{bmatrix} \begin{bmatrix} \overline{u_1} \\ \overline{u_2} \end{bmatrix} = \begin{bmatrix} 0 \\ 0 \end{bmatrix}. \tag{21}$$

We will have a nontrivial solution only if the determinant of the matrix is zero.

$$m_1 m_2 \omega^4 + 2k_s \omega^2 (m_1 + m_2) + 4k_s^2 - 2k_s^2 (1 + cos\ k\ 2d) = 0 \quad (22)$$

The relation between ω and k which is the dispersion relation of a diatomic one dimensional atomic is presented in Figure 20 using MATLAB where the gaps between the red line represent the domain where the range of frequency cannot propagate (band gaps)..

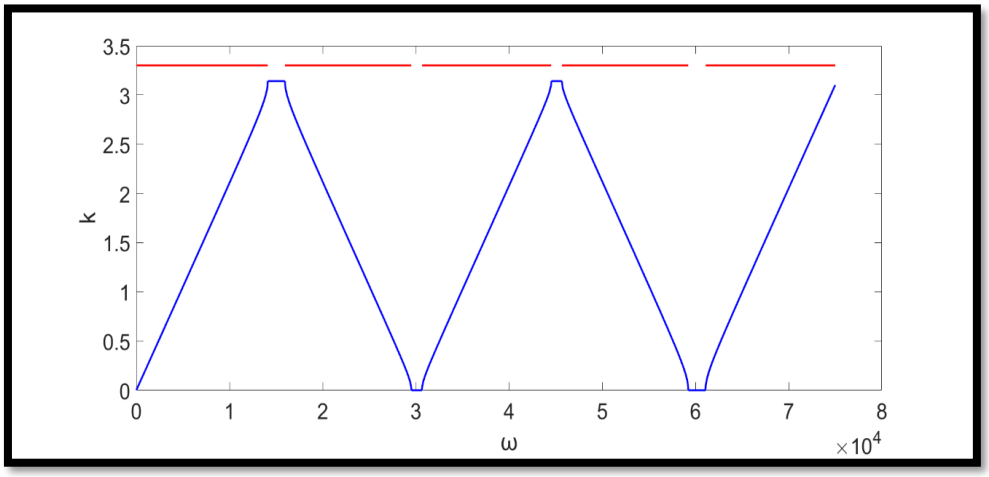

Figure 20: band gaps (cut-offs in the horizontal red line) in dispersion curve of 1D diatomic lattice assuming $m_2 = m_1 = 1, k_s = 1.$

Let us consider a solution depending on the wavevector in the form

$$\begin{cases} u_n = \overline{u_1} e^{iqnd} * e^{-i\omega t} \\ u_{n+1} = \overline{u_2} e^{iq(n+1)d} * e^{-i\omega t} \end{cases} \quad (23)$$

Where q is the wavevector and substituting this solution to Eq. (23), we will have this matrix

$$\begin{bmatrix} 2k_s - m_1\omega^2 & -2k_s \cos qd \\ -2k_s \cos qd & 2k_s - m_2\omega^2 \end{bmatrix} \begin{bmatrix} \overline{u_1} \\ \overline{u_2} \end{bmatrix} = \begin{bmatrix} 0 \\ 0 \end{bmatrix} \quad (24)$$

a nontrivial solution will be satisfied only if the determinant of the matrix is zero.

$$(2k_s - m_1\omega^2) * (2k_s - m_2\omega^2) - 4k_s^2\ cos^2\ qd = 0 \quad (25)$$

Solving this quadratic equation to ω^2, we will obtain

$$\omega^2 = k_s * (\frac{1}{m_1} + \frac{1}{m_2}) \pm 2k_s \sqrt{(\frac{1}{m_1} + \frac{1}{m_2})^2 - \frac{4 * k_s * cos^2\ (qd)}{m_1 * m_2}}. \quad (26)$$

This equation represents the dispersion relation of a diatomic one-dimensional atomic chain which has two different solutions corresponding to two different dispersion curves as shown in the Figure 21.

$$\omega_+^2 = k_s * \left(\frac{1}{m_1} + \frac{1}{m_2}\right) + k_s \sqrt{\left(\frac{1}{m_1} + \frac{1}{m_2}\right)^2 - \frac{4 * sin^2\ (qd)}{m_1 * m_2}}. \quad (27)$$

(Referring to optical branch) The boundaries of optical branch are as follows

When q= 0, $\omega = \sqrt{2k_s * \left(\frac{1}{m_1} + \frac{1}{m_2}\right)^2}$ and $q = \frac{\pi}{2d}$, $\omega = \sqrt{\frac{2k_s}{m_1}}$

$$\omega_{-}^{2} = k_s * \left(\frac{1}{m_1} + \frac{1}{m_2}\right) - k_s\sqrt{(\frac{1}{m_1} + \frac{1}{m_2})^2 - \frac{4 * sin^2(qd)}{m_1 * m_2}}. \quad (28)$$

(Referring to acoustic branch) The boundaries of acoustic branch are as follows

When $q = 0$, $\omega = 0$ and $q = \frac{\pi}{2d}$, $\omega = \sqrt{\frac{2k_s}{m_2}}$.

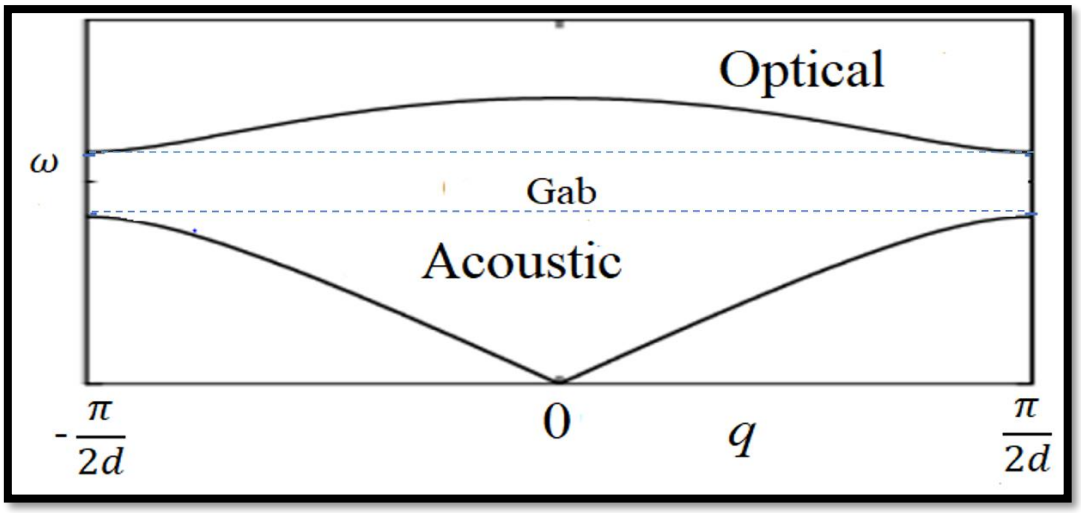

Figure 21: Dispesion curve of 1D diatomic lattice.

The upper curve is called the optical branch where the frequency directly proportional to the q in a linear relation starting from $q = 0$ up to $q = \frac{\pi}{2d}$. The lower curve represents the acoustic branch. The range of wavenumbers determining the period of the dispersion relation, i.e.

$$qd \in [-\frac{\pi}{2d}, +\frac{\pi}{2d}]$$

is known as "First Brillouin Zone" (FBZ). The difference between these two branches can be easily seen at $q = 0$.

For the acoustic branch ω = 0 and $\overline{u_1}$= $\overline{u_2}$. This means that the two atoms m_1 and m_2 in the elementary cell have the same amplitude and the phase dispersion is linear for small q. Therefore, the molecules vibrate as a rigid body. In contrast, the optical oscillation moves in such a way that the centre of mass of an atom remains fixed. The two atoms move in out of phase. The frequency of these vibrations occurs in infrared region which is the reason for calling this branch as optical. The area between the two dashed blue horizontal lines whose boundaries are $\omega = \pm\sqrt{\frac{2k_s}{m1}}$ and $\omega = \pm\sqrt{\frac{2k_s}{m2}}$ is the area where the frequency cannot propagate (band gap). A large energy separation between the acoustic and optical modes implies that the

ionic bonds between the atoms are very "rigid" and thus "hard" to vibrate leading to band gab between the two modes.

2.4.3 Undamped 1-D diatomic lattice with internal resonator

Let us consider a diatomic periodic cell in the form of mass-in-mass lattice as illustrated in the Figure 22. This lattice consists of two overlapping atoms, let us say primary atoms with translational mass m_1 represented as a stiff and rigid ring, and secondary atoms m_2 entered inside the primary atoms (rings) in an infinite chain. In addition, the unique degree of freedom of the primary atom can be described by displacement u of the configurational node 1 while displacement v is related to the internal inclusion (secondary atom). k_1 represents the elastic spring stiffness of the linear interaction between two adjacent cells whereas k_2 is elastic spring stiffness that linked the primary atom with secondary atom. This configuration will produce a bandgap along the frequency range.

The bandgaps we have studied for monatomic and standard diatomic lattices in the sections above depends on the size of the unit cell. In contrast to that, the internal resonance gaps are not related to wavelength, and therefore in principle can be observed at arbitrarily long wavelengths / low frequencies. This is the result of interference produced by the interaction of scattered and incident waves at the unit cell boundaries, which is the phenomenon often called as Bragg scattering. Due to the significant implications of internal resonance bandgaps' wavelength independence, numerous investigations have been conducted to put the theory into practice. (Liu et al, 2000) have created sonic crystals with spectral gaps that have a lattice constant two orders of magnitude less than the relevant wavelength, based on the concept of localized resonant structures which lead to applications in seismic wave reflection and ultrasonic. Local resonator-based sonic crystals produce significant attenuation bands at specific frequencies and perform far better than usual sonic crystals (based only on Bragg's scattering) (Hirsekorn et al, 2004).

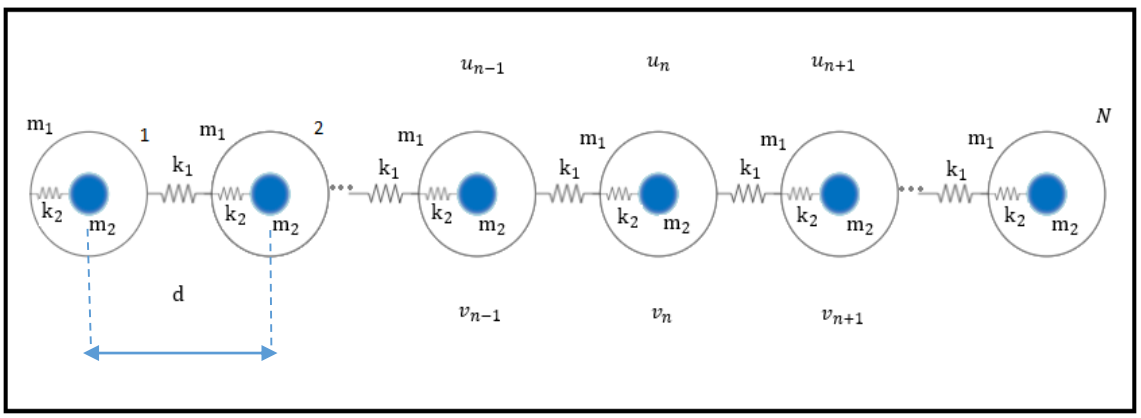

Figure 22: Undamped diatomic lattice metamaterial.

In the small-amplitude range of oscillations, the secondary atoms play the role of inertial resonators, if their linear frequencies are properly tuned with certain wave frequencies of the principal atom chain. The equations of motion of the elementary cell in the form of ordinary differential equations written as follows

$$\begin{cases} m_1\ddot{u}_n + 2k_1u_n - k_1u_{n-1} - k_1u_{n+1} + k_2(u_n - v_n) = 0 \\ m_2\ddot{v}_n + k_2(v_n - u_n) = 0 \end{cases} \quad (29)$$

The free propagation of elastic waves through the 1-D diatomic lattice with internal resonator can be described by means of the Floquet-Bloch theory as follows

$$u_n = u_{n-1}\, e^{ikd} \quad \text{and} \quad u_{n+1} = u_n\, e^{ikd} \quad (30)$$

Let us find a solution of the form

$$\begin{cases} u_n = \overline{u_1} e^{i\omega t} \\ v_n = \overline{u_2} e^{i\omega t} \end{cases} \quad (31)$$

Substituting Eq. (30) and (31) into Eq. (31), we will have

$$\begin{bmatrix} m_1\omega^2 + 2k_1(1 - \cos kd) + k_2 & -k_2 \\ -k_2 & m_2\omega^2 + k_2 \end{bmatrix} \begin{bmatrix} \overline{u_1} \\ \overline{u_2} \end{bmatrix} = \begin{bmatrix} 0 \\ 0 \end{bmatrix}. \quad (32)$$

In the case of $k_1 = k_2 = k_s$ (simple case), a nontrivial solution will be satisfied only if the determinant of the matrix is zero.

$$2{k_s}^2 - 2{k_s}^2 \cos(kd) + k_s m_1\omega^2 + 3k_s m_2\omega^2 + m_1 m_2\omega^4 - 2k_s m_2 = 0 \quad (33)$$

Solving this equation allow to obtain a nonlinear dispersion property for resonant lattices.

$$\omega_{1,2} = \pm \frac{\left(-k_s m_1 - k_s\left(k_s {m_1}^2 + 9k_s {m_2}^2 + 8m_1 m_2 - 2k_s m_1 m_2 + 8k_s m_1 m_2 \cos(kd)\right)^{0.5}\right.}{\sqrt{(2m_1 m_2)}} \quad (34)$$

$$\omega_{3,4} = \pm \frac{\left(-\left(\left(k_s\left(k_s {m_1}^2 + 9k_s {m_2}^2 + 8m_1 m_2 - 2k_s m_1 m_2 + 8k_s m_1 m_2 \cos(kd)\right)^{0.5}\right.\right.\right.}{\sqrt{(2m_1 m_2)}} \quad (35)$$

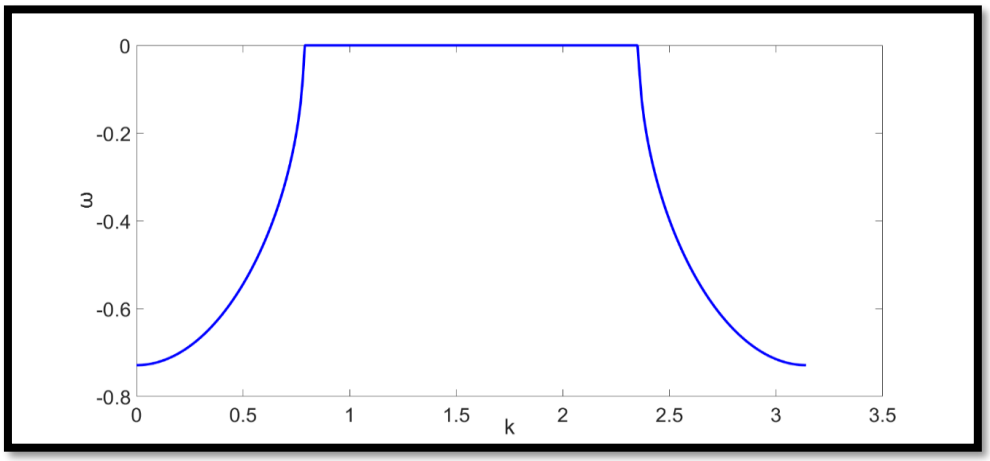

Figure 23: dispersion curve of 1D diatomic lattice with internal resonator.

The presence of the internal resonators in the unit cell will split the dispersion curve into two branches separated by observed bandgap (*the straight horizontal blue line in Figure 23*). This bandgap is centred at the tuning frequency Ω_R (frequency of resonance), over a range which is also characterised by the nonzero attenuation parameter (imaginary part of the propagation constant). The presence of dissipation in the system will impact the dispersion curve in such a way that the two branches to merge into only one curve.

The frequency of resonance Ω_R can be chosen to obtain attenuation over a certain band, without any constraint imposed by wavelength. Indeed, low frequency attenuation requires low stiffness and large value of mass, which make a challenge for the implementation of this concept.

2.5 Summary

This chapter is devoted to introducing periodic structures which can be built in several directions. The Floquet-Bloch's (F-B) theorem is presented which is an effective method to analyse the behaviour of wave propagation in periodic systems. The transfer matrix method and an example of how to derive it are also presented.

Two different reasons for having band gabs are presented in three examples of different one-dimensional discrete systems. The band gaps observed in monatomic and diatomic lattices are strictly constrained by the unit-cell dimensions. In contrast, 1-D lattice with internal resonator which is a lattice consists of two overlapping atoms which led to a configuration characterized by internal resonances centred at the resonant frequency of the oscillators. This produces a bandgap in the vicinity of frequency of the oscillators.

Chapter 3: Quasicrystalline-generated periodic structure

3.1 Overview

In this chapter I will introduce the term Quasi-crystalline and its presence in nature and other fields. Quasicrystals are expected to exhibit unusual properties. Both their elastic and electronic behaviour distinguish quasicrystals from other ordinary crystalline metals. Elastic response may be studied by measuring the speed of sound waves propagating through the metal. Quasicrystalline have many potential applications in several forms. Metallic quasicrystalline coatings can be applied by thermal spraying or magnetron sputtering. Quasicrystals can be used to develop heat insulation. Quasicrystalline structures can be useful to study the behaviour of waves propagation. Generalized Fibonacci sequence (golden ratio, silver ratio, and bronze ratio) which is a typical example of Quasi-periodic sequences is presented in detail. One of the ways quasicrystals can be created is through these ratios, which can be calculated using Fibonacci sequence.

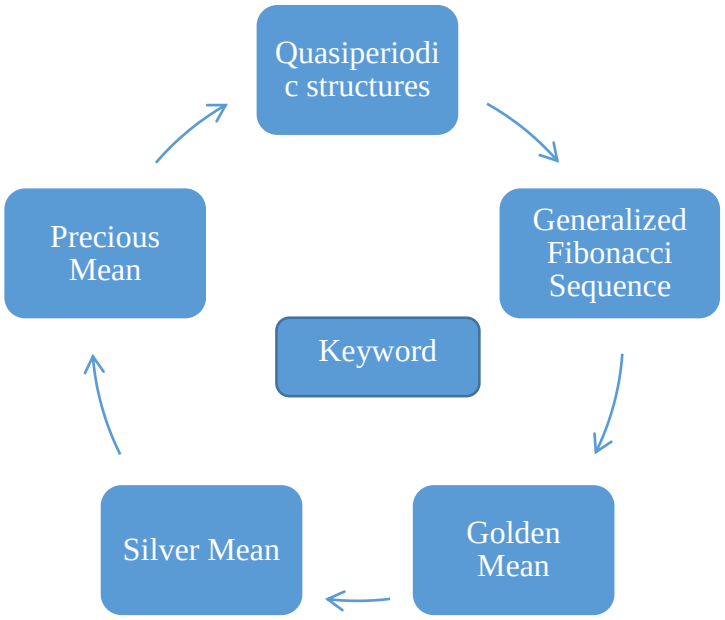

Figure 24: Chapter three key word.

3.2 Quasi-crystalline in nature

In nature, the spiral of Fibonacci can be used as a guide to place features in art and architecture, in order to give a pleasing visual effect where the number of spirals on pineapples, pinecones, and several flowers is always a Fibonacci number as illustrated in Figure 25. In biology the Fibonacci golden sequence is also seen in the inheritance tree of the human X chromosome, the population growth of rabbits as well as in the lineage of a male bee.

Figure 25: The golden spiral in nature.

In architecture, the golden mean shows an aesthetic glimpse on buildings, especially historical ones. Many people assume that the Parthenon in Athens is built using the golden ratio as illustrated in the left side of Figure 26. Boussora and Mazouz (2004) indicated the presence the golden mean in the design of the great mosque in the city of Kairouan in many parts such as the court, and the minaret, and dimensioning of the prayer space. The Great Pyramid of Egypt, its base, height, and hypotenuse appear to be built on the base of the golden mean but missing the absence of the mention of golden mean in ancient Egyptian history has made it difficult to prove using this ratio. In Japan, the application of the golden mean in design is almost non-existent. According to them, the silver mean creates a more beautiful and calm design than the Divine proportion. Because the silver mean yields a smaller proportion, the buildings created using it are squarer than those created using the Western proportion. Horyu-ji Temple in Ikagura is a well-known example of the utilisation of the silver mean.

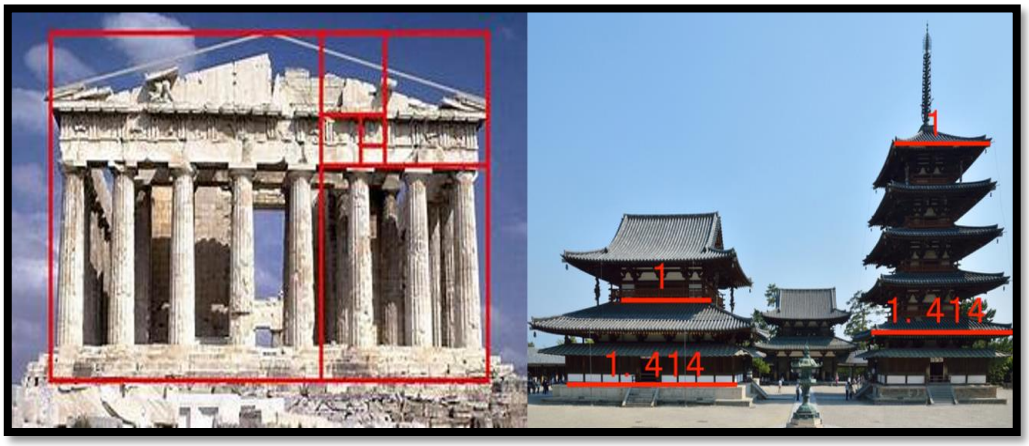

Figure 26: Applications of golden and silver ratios in architectures, Parthenon in Athens (golden ratio) Horyu-ji Temple in Japan (silver ratio) (Google image).

In design, according to some sources, the golden ratio is widely employed in everyday design, such as postcards, playing cards, posters, wide-screen televisions, pictures, light switch plates, and automobiles (Jones, 1971; Tschichold, 1991). Some members of the metallic means like golden mean and silver mean appeared already in many ancient civilizations of Turkey, India, Egypt and China (Hretcanu and Crasmareanu, 2013).

In the field of music, the golden mean was used by French composer Erik Satie in several of his works. The golden mean can also be seen in Debussy's Reflets dans l'eau (Reflections in Water), from Images (1st series, 1905), where "the succession of keys is marked out by the intervals 34, 21, 13 and 8, and the primary climax lies at the golden ratio position (Jones, 1971).

3.2 Quasi-periodic sequences

By 2003 more than 22 million different chemical substances were discovered. The crystal structure of more than 400,000 substances became available. Although the existence of hundreds incommensurately modulated structures and composite structures, there was no reason to doubt that he ground state (i.e. the thermodynamic equilibrium state at 0 K) of all these compounds and of condensed matter in general is represented by a periodic crystal structure (Steurer, 2004). On April, 1982, D. Shechtman discovered a novel phase with icosahedral diffraction symmetry in rapidly solidified Al86Mn14 alloy. This was the first discovery of quasicrystals, which mainly changed our concept of structural order on atomic scale.

In periodic systems, the impedance mismatch caused by periodic discontinuities in the geometry, which acts as a waveguide, and/or in the material, can create destructive wave interference phenomena over specified frequency range known as "stop bands" or "band gaps" (BG) (Spadoni et al, 2007). However, imperfections (i.e. defects or irregularities) in the structure, such as those caused by the manufacturing process or inaccurate reconstructions of the boundary conditions, cause the structure to lose its periodicity, which can have a significant influence on the vibrational behaviour of elastic structures. This scenario leads to refer to quasi-periodicity, which is a feature of a structure with irregular periodicity. Repeated substructures with asymmetric translations in each direction in Euclidian space can be idealized as a quasi-periodic structure. It can be thought of as a cross between a periodic and a random elastic medium (Velasco and Zarate, 2001). "Quasi-periodic behaviour is thus a pattern of recurrence with a component of unpredictability that does not lend itself to a precise measurement".

A *quasicrystal is an example of a natural quasi-periodic structure*. Levine and Steinhardt (1984) were the first to introduce the term quasicrystal as a non-periodic structure with perfect long-ranged order into solid-state physics. At present, it has become clear that, in addition to the state of crystalline and random materials, there exists a third state of solids which may help

in filling the gap between the two well-defined condensed-matter states. Figure 27 gives an idea of the difference between periodic and quasi-periodic structures.

Moreover, this intermediate category of materials called aperiodic deterministic structures includes in addition to Fibonacci sequences, other quasicrystals which can be described by a projection onto the m-dimensional space (m=1,2,3). Good examples of such aperiodic structures which differ from quasicrystals are Thue–Morse and period-doubling sequences (Morini and Gei, 2018; Tamura and Nori, 1989).

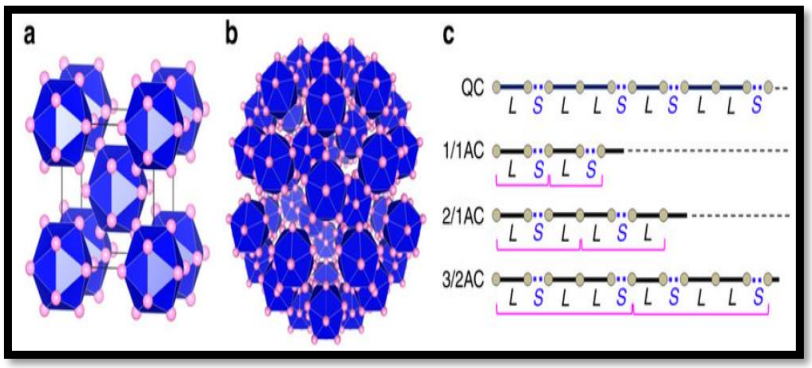

Figure 27: Periodic and quasiperiodic arrangement of atoms. a: An example of cubic unit cell in which the icosahedron occupies the corner and body-centered positions. Pink balls indicate atoms. b: An example of the quasicrystal. c: Fibonacci sequence.

One-dimensional quasiperiodic systems have been studied experimentally more frequently since their manufacturing is easier than that of two and three-dimensional systems. On the other hand, they still discover the key fundamental features of light propagation in aperiodic media. The simplest realization of one-dimensional quasiperiodic systems is a binary aperiodic chain, which is a repetition of the layers made of two phases *A* and *B*. The arrangement of layers is determined by the rule specifying the particular structure.

There are three definitions of the quasi-crystalline systems: (a) the incommensurate chains, (b) the substitution rules, and (c) the cut-and-project method which is a mean generating quasicrystal starting from a higher dimensional lattice (McColm, 2021). The incommensurate chains and related structures have been studied since the 1960s, even before the concept of quasicrystal was introduced (Azbel, 1964). In the one-dimensional setting, an accurate method of classification for the different quasiperiodic patterns was proposed by Kolar (1993). By following his criterion, we define a different one-dimensional quasiperiodic chain composed of two distinct segments, say *A* and *B*, generated according to the generic substitution rule

$$\mathrm{A} \rightarrow \varsigma\,(\mathrm{A}) = M_{\alpha\beta}\,(\mathrm{A}, \mathrm{B}), \quad \mathrm{B} \rightarrow \varsigma\,(\mathrm{B}) = N_{\gamma\delta}\,(\mathrm{A}, \mathrm{B}). \tag{36}$$

where the quantity of $M_{\alpha\beta}$ and the quantity of $N_{\gamma\delta}$ are two building blocks containing of a certain permutation of $\alpha + \beta$ and $\gamma + \delta$, α and β indicate to the number of elements A and B

in ς (A), respectively, whereas both parameters γ and δ indicate to the number of elements A and B in ς (B). The correspondence between the two definitions is established by the relation $t = (1 + \lambda_1 - \alpha)/\gamma$ between a value of t and indices α , β , γ , δ ,where $\lambda_1 = (v\sqrt{v^2 + 4w})/2$, $v = \alpha + \delta$ and $w = \beta\gamma - \alpha\delta$. It is worth to point out that $w = \pm 1$ *is the condition for having a quasi-crystalline system.*

A typical but not the only example of one-dimensional quasi-crystalline pattern is represented by the generalized Fibonacci sequences for which

$\alpha = \beta = \gamma = 1$ and $\delta = 0$.

3.3 Generalized Fibonacci sequence

Various studies on multi-component systems generated according to the Fibonacci sequences for different aims began in the eighties of the last century. Fibonacci sequence is neither periodic nor random, but has been described as an intermediate between them (Morini and Gei, 2018).

Kolar and Ali (1989b) indicated that the attractors connected to certain volume-non-preserving generalized Fibonacci trace maps are the subject of this research. It is demonstrated that several pseudo-invariants play a key role in their behaviour. They demonstrate the coexistence of regular and Cantor-like excitation spectra based on the existence of these attractors.

Maciá (1998) investigated light's resonant transmission over multilayers of Fibonacci dielectric dielectrics. renormalization via transfer matrix method application. For any given incidence angle, we provide closed analytical equations for the transmission coefficient. They examine the connection between the quasiperiodic structure of the substrate and the resonant wavelengths, indicating that arrays with varying widths of Fibonacci dielectric multilayers could be used to create optical microcavities.

(Gei, 2010; Morini and Gei, 2018; Morini et al, 2019b) studied the propagation of waves in systems generated according to Fibonacci sequences. The stop/pass-band spectra are studied with the aid of the trace-map formalism. These studies shown that the spectrum of this class of structures is characterised by specific self-similar properties, different from those pertaining to other quasi-crystalline-generated waveguides. They also indicated that some factors affect the propagation of waves, such as pre-stress and the geometry of the structures.

Very recently, there is a major interest in modern engineering and material science in the application of Fibonacci numbers (Falcón and Plaza, 2007). The general Fibonacci elementary cell here is denoted by F_i whereas the general Fibonacci numbers here is denoted by n_i which are the terms of the sequence in which each number is the sum of the two preceding numbers,

beginning with the values n_0= 1, and n_1= 1. On the other hand, the ratio of two consecutive Fibonacci numbers is very close to the precious means or precious ratios (Golden, Silver and Bronze), which can be seen in modern research in many fields from nature (human body), art and architecture (pentagon) (Spinadel, 1999; Bolat and Köse, 2010).

The generalised Fibonacci sequence F_i is a class of quasi-periodic lattices produced by the general substitution rule where two distinct phases, say *A* and *B* are arranged in a chain according to the generalised Fibonacci sequence (Trabelsi et al., 2009)

$F_i = F^m{}_{i-1}F^z_{i-2}$, with m and $z \geq 1$ (37)

where the parameters m and z denote the frequency of the previous sequences in following sequence, i.e., $A^3 = AAA$ (m times).

with initial conditions F_0 =B and F_1=A

The structures (supported beams, rods, plates, and 3-D structures) based on generalised Fibonacci sequence are quasi-periodic structures. According to the general criterion for the classification of the one-dimensional quasiperiodic patterns proposed by Kolar (1993), the precious mean arrangement is quasi-crystalline. Quasi-crystalline systems possess unique properties that make them an intermediate class between periodic and disordered systems (Steurer, 2004; Steurer and Deloudi, 2008). Previous studies have shown that although quasi-crystalline systems are not totally periodic, their features can be described theoretically using quasiperiodic approximants (Kohmoto et al, 1983; 1987; Kolar and Ali, 1989b). The replication of the elementary cell built based on the ***precious means*** leads to a global periodicity along the axis and then the possibility of applying Floquet-Bloch technique to investigate wave propagation in these systems

3.3.1 Fibonacci Golden Mean Sequence

By setting the exponent $m = 1$, z=1 we will have a class of quasi-periodic structure referred here as Golden Mean structures (GMs) where its elementary cell obey to the general substitution rule illustrated in Eq. (38) as follows

F_2=AB, F_3=ABA F_4=ABAAB as shown in Figure 28.

We can also express F_4=(ABA)(AB) where the brackets separate the sequences F_3 and F_2.

The exponents m and z denote the frequency of the element in the chain i.e., A^m = AAA (m =3 times).

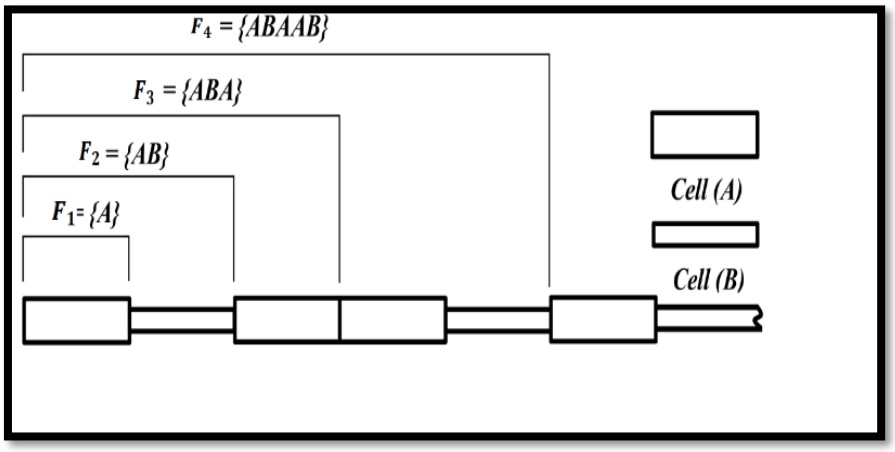

Figure 28: Configurations of quasi-periodic structure following a Fibonacci golden sequence.

The total number of elements n_i in each sequence F_i is given by the recurrence relation

$$n_i = mn_{i-1} + zn_{i-2}. \quad (38)$$

$n_i = n_{i-1} + n_{i-2}$, with initial conditions as mentioned above n_0= 1, and $n_1 = 1$

An example of this relation is n_2= 1+1=2 and n_3 = 2+1=3 n_4=3+2=5

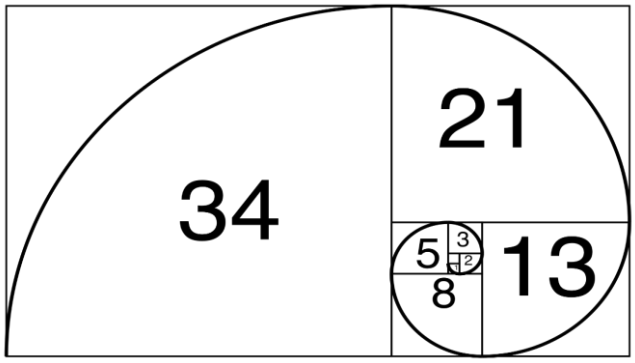

Figure 29: Fibonacci golden spiral.

From the above, the Fibonacci numbers based on Golden Mean (GM) are (1,1,2,3,5,8,13…). These numbers can be seen in Fibonacci spiral also called as golden spiral illustrated in the Figure 29.

The limit σ of the ratio for $i \to \infty$ will be as follows

$$\sigma = lim_{i\to\infty} \frac{n_{i+1}}{n_i} = \frac{m+\sqrt{m^2+4z}}{2} \quad (39)$$

where in the golden mean case we have $m = 1$, z=1.

As a result, $\sigma_g = \frac{1+\sqrt{5}}{2}$ which is corresponding to the Golden ratio 1. 618.

This means that any number in the Fibonacci sequence divided by the previous has a quotient of approximately 1.618. For the first few numbers, this is not the exact approximation, but as the number (n) increases, the quotient coincides more exactly with this value.

3.3.2 Fibonacci Silver Mean Sequence

Let us assume a different value of the exponents in which $m = 2, z$=1. Now we have a different class of quasi-periodic structure referred here as Silver Mean structures (SMs) where its elementary cells obey to the same general substitution rule as follows

F_2=(AAB), F_3=(AABAABA), and F_4= (AABAABAAABAABAAAB) as shown in Figure 30.

We can also express F_4= (AABAABA)(AABAABA)(AAB) where the brackets separate the sequences F_3 (two times) and F_2. The total numbers of elements in each sequence F_i will be as follows

$$n_i = 2n_{i-1} + n_{i-2} \tag{40}$$

with initial conditions n_0= 1, and $n_1 = 1$, this means that n_2= 2+1=3 and n_3=2*3+1=7.

The Fibonacci numbers based on Silver Mean (SM) are (1,1,3,7,17,41, 99…...).

In the silver mean case, we impose ($m = 1, z$=2) leads to $\sigma_s = (1 + \sqrt{2})$ which is corresponding to the silver ratio 2.414.

This means that any number in the Fibonacci sequence divided by the previous has a quotient of approximately 2.414. For the first few numbers, this is not the exact approximation, but as the number (n) increases, the quotient coincides more exactly with this value.

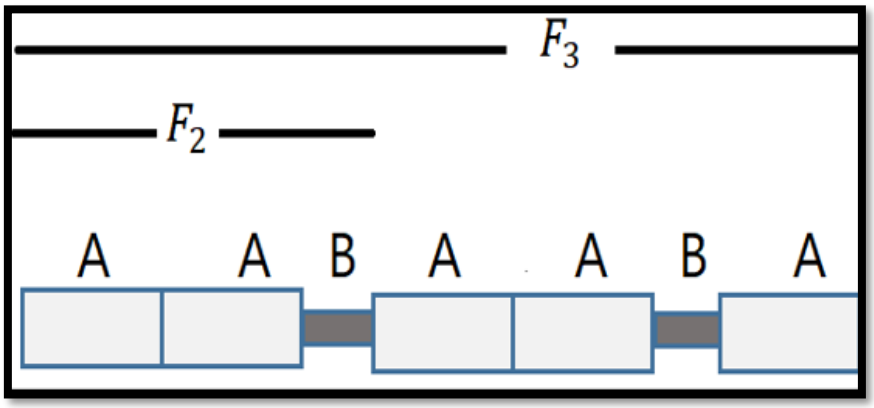

Figure 30: Configurations of quasi-periodic structure following a Fibonacci silver sequence.

3.3.3 Fibonacci Bronze Mean Sequence

Assuming an alternative value for the exponents in which $m = 3$, z=1 we will have a third class of quasi-periodic structure referred here as Bronze Mean structures (BMs) whose elementary cells follow the same general substitution rule 1. As follows

F_2=AAAB, F_3= AAABAAABAAABA.

In the bronze mean case, we impose ($m = 1, z$=3) leads to $\sigma_b = \frac{3+\sqrt{13}}{2}$ which is corresponding to the bronze ratio 3.303.

This class of quasiperiodic structure called bronze mean structures and the number of elements in each sequence can be calculated using the following rule

$$n_i = 3n_{i-1} + n_{i-2} \quad (41)$$

n_2= 3+1=4 n_3=3*4+1=13.

To this end, The Fibonacci numbers based on Bronze Mean (BM) are (1,1,4,13,43,142,469, 1549…...).

From the above, all structures built according to the general metallic ratio $\sigma = \frac{m+\sqrt{m^2+4z}}{2}$ of orders m (1, 2, and 3) and z=1 s precisely the Golden ratio, the Silver ratio, and the Bronze ratio respectively are quasicrystalline (Sivaraman, 2020). In this thesis, we will refer to these metallic ratios ($\sigma_g, \sigma_s,$ and σ_b) as *precious means* and their structures as precious means structures.

The copper ratio ($\sigma_g = 2$) and the nickel ratio ($\sigma_n = 2.302$) (metallic means as they are referred to here) are obtained by setting $w = z = 2$ for copper and $w = z = 3$ for nickel in the relation (36) are non-quasicrystalline, quasiperiodic systems (Morini and Gei, 2018).

Fibonacci sequences F_i	Golden Mean	Silver Mean	Bronze Mean
F_0	B	B	B
F_1	A	A	A
F_2	AB	AAB	AAAB
F_3	ABA	AABAABA	AAABAAABAAABA
F_4	ABAAB	AABAABAAABAABA AAB	AAABAAABAAABAAAABAAABAAABAAAABAAABAAABA AAAB
F_5	ABAABABA	AABAABAAABAABAAABAABAABAAABAABAAAB	AAABAAABAAABAAAABAAABAAABAAAABAAABAAABA AAABAAABAAABAAABAAAABAAABAAABAAAABAAABAAA BAAAABAAABAAABAAABAAAABAAABAAABAAAABAAA BAAABAAAABAAABAAABAAABA

Table 1: Definition of the six Fibonacci sequences.

As can be seen from the following table, the number of elements constituting silver cells is greater than their golden counterpart which becomes clearer when the indicator i increases. To this end, we can say that the main reason for the different dynamical behaviour between the golden and silver structures is the difference in the composition of the elementary cells.

Fibonacci sequences F_i	Golden Mean	Silver Mean	Bronze Mean
F_0	***1***	***1***	***1***
F_1	***1***	***1***	***1***
F_2	***2***	***3***	***4***
F_3	***3***	***7***	***13***
F_4	***5***	***17***	***43***
F_5	***8***	***41***	***142***
F_6	***13***	***99***	***469***
F_7	***21***	***239***	***1549***

Table 2 : Number of elements in the golden, silver, and bronze elementary cells up to Number of elements in the golden, silver, and bronze elementary cells up to F_7.

Chapter 4: Axial waves in one-dimensional generalised Fibonacci Silver Mean rods.

4 Overview

Previous research conducted by (Morini and Gei, 2018) focused on the propagation of axial waves in golden mean phononic rods, which promoted me to conduct research on silver mean phononic rods. The main difference between golden and silver mean sequences is the number of elements that make up each unit cell of each sequences.

In this chapter, I will derive all the equations related to the propagation of axial waves in silver mean phononic rods. The transfer matrix and dispersion relation of the rods will be obtained by applying the Floquet-Bloch theory. Nonlinear map and Kohmoto's invariant for silver mean rods will be derived. Scaling and self-similarity of the frequency spectra of canonical SM rods will be derived and where the scaling is effective in different values of frequency including canonical frequency.

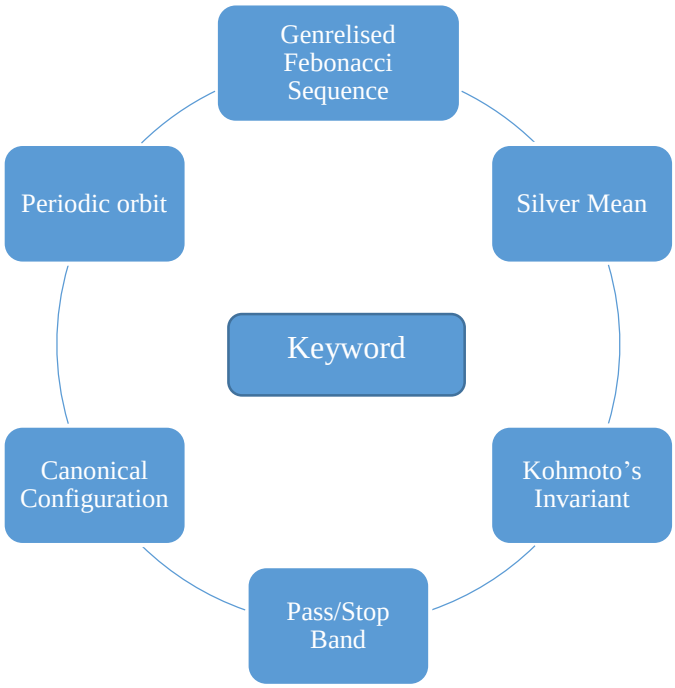

Figure 31: Chapter four keyword

4.1 One-dimensional generalised Fibonacci Silver Mean rods

I introduce a particular class of infinite, one-dimensional, two-component quasiperiodic phononic rods consisting of a repeated elementary cell where two distinct phases, say A and B, are arranged in series according to the so-called *Silver Mean* (SM) sequence as shown in the Figure 32. I will study axial wave propagation in this class of rods in order to understand the behaviour of axial waves in this system to provide wider options for designers of acoustic devices like waveguides and acoustic filters. This will be achieved using tools used in (Morini and Gei, 2018) who studied the propagation of axial waves in golden mean rods.

The repetition of the fundamental cell implies global periodicity along the axis and then the possibility of applying Floquet-Bloch technique to investigate propagation of harmonic elastic

waves in these systems. The two-component SM sequence belongs to the family of patterns commonly known as one-dimensional *generalised Fibonacci tilings* (Kolar and Ali, 1989) and is based on the following substitution rule as follows

A $\rightarrow \delta(A) = A^m\ B^z$, B $\rightarrow \delta(B)$, where in silver mean case $m = 3$ and $z = 1$ as mentioned in the previous chapter.

Or

$$A \rightarrow AAB,\ B \rightarrow A \tag{42}$$

Expression (42) implies that element of $i - th$ order of the sequence (i = 0, 1, 2, . . .), here denoted by F_i , obeys the recursive rule

$$F_i = F_{i-1}^2 F_{i-2}^1, \tag{43}$$

where the initial conditions are F_0 = B and F_1 = A.

In Figure 32, elementary cells representing F_2, F_3 and F_4 are sketched (F_0 = B and F_1 = A are not included because both of them are initial conditions), where the notation F_i will also indicate from now on the elementary cell of the structured rod. The total number of elements of F_i corresponds to the generalised Fibonacci number n_i , given by the recursive relation $n_i = 2n_{i-1} + 1n_{i-2}$with $i \geq 2$ and $n_0 = n_1 = 1$. The limit n_{i+1}/n_i for $i \rightarrow \infty$ corresponds to the silver ratio $\sigma_s = (1 + \sqrt{2}) \cong 2.414$

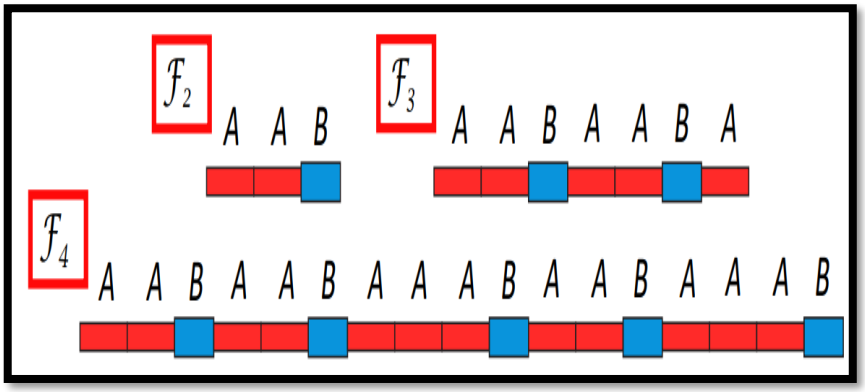

Figure 32: Representative elementary cells for periodic silver-mean phononic rods

Further in the text, we will refer to those structured elements as SM rods. According to the general criterion for the classification of the one-dimensional quasiperiodic patterns proposed by Kolar (1993), the SM arrangement is *quasi-crystalline*. Quasi-crystalline structures possess specific properties that make them an intermediate periodic crystals and random amorphous solids. An example of these interesting and intriguing features is the self-similarity of the distribution of stop and pass bands (regular pattern of the pass and stop band diagram) detected for phononic waveguides arranged according to several generalised Fibonacci sequences

(Morini and Gei, 2018; Gei et al., 2020). In the pass/stop band diagram, the feature of self-similarity is clear where we can note that the number of pass bands in each area of the diagram. The 'match' between patterns improves at increasing index i.

One of the aims of this project is to the analyse the propagation of harmonic axial wave in SM rods. I will show that the spectrum of this class of structures is characterised by specific self-similar properties, different from those pertaining to other quasi-crystalline-generated waveguides. In particular, we will illustrate how these unique features are closely related to the properties of the Floquet-Bloch dispersion relationship, reported in this Section.

Let us introduce the geometrical and physical properties of phases A and B. The lengths of the two elements are indicated respectively with l_A and l_B, while S_X, E_X, and φ_X, X (X ∈ {A, B}) denote cross-section area, Young's modulus and mass density per unit of volume of each element, respectively. For both segments, we define the displacement function along the rod $u(z)$ and the axial force N(z) = $ESu'(z)$, where z is the longitudinal axis. The governing equation of harmonic axial waves in each phase is

$$u''(z) + Q\omega^2 u(z) = 0 \tag{44}$$

where ω is the circular frequency (simply the 'frequency' in the following) and $Q = \varphi/E$ corresponds to the reciprocal of the square of the speed of propagation of longitudinal waves in material X. The general solution for Eq. (44) assumes the form

$$u_X(z) = C_X\, sin(\sqrt{Q_X\, \omega z}\,) + D_X\, cos(\sqrt{Q_X\, \omega z}), \tag{45}$$

where C_X and D_X are integration constants, to be determined by the boundary conditions. To obtain the dispersion diagram of the periodic rod, displacement and axial force at the right-hand boundary of the elementary cell, respectively $u_r$and N_r, have to be identified in terms of those at the left-hand boundary, respectively u_l and N_l.

Since the main differences between the transfer matrix of element A and element B are the geometrical and physical properties of phases A and B, let us only derive the transfer matrix for the phase B as follows

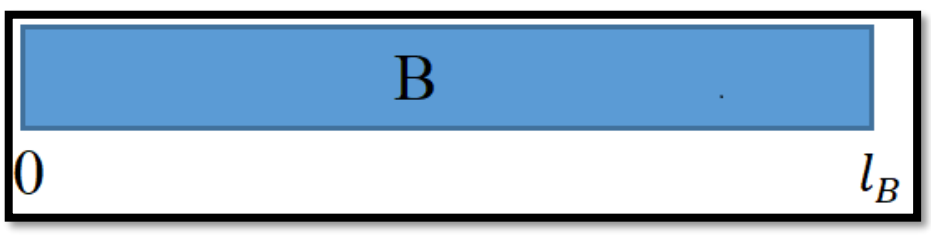

Figure 33: Element B of quasiperiodic phononic rods.

The Eq. (44) can be rewritten for element B as follows

$$u_B(z) = C_B\ sin(\sqrt{Q_B}\ \omega z)\ +\ D_B\ cos(\sqrt{Q_B}\ \omega z), \tag{46}$$

and

$$u'_B(z) = C_B\ \sqrt{Q_B}\,\omega\ cos\left(\sqrt{Q_B}\ \omega z\right) -\ D_B\sqrt{Q_B}\,\omega\ sin(\sqrt{Q_B}\,\omega z), \tag{47}$$

The equation $N(z) = ESu'(z)$ will take the following form

$$N_B(z) = ES\left[C_B\ \sqrt{Q_B}\,\omega\ cos\left(\sqrt{Q_B}\ \omega z\right) -\ D_B\sqrt{Q_B}\,\omega\ sin(\sqrt{Q_B}\,\omega z)\right] \tag{48}$$

The boundary conditions require that at l_B= 0,

$$u_B(0) = D_B, \tag{49}$$

$$N_B(0) = E_B S_B C_B\ \sqrt{Q_B}\,\omega, \tag{50}$$

and at $l = l_B$, we have

$$u_B(l) = \left(\frac{N_B(0)}{E_B S_B \sqrt{Q_B}\,\omega}\right) sin(\sqrt{Q_B}\,\omega l_B + u_B(0)\ cos\left(\sqrt{Q_B}\ \omega l_B\right), \tag{51}$$

$$N_B(l) = E_B S_B\sqrt{Q_B}\,\omega\left[\left(\frac{N_B(0)}{E_B S_B \sqrt{Q_B}\,\omega}\right) cos\left(\sqrt{Q_B}\ \omega l_B\right) - u_B(0)\ sin(\sqrt{Q_B}\,\omega l_B)\right], \tag{52}$$

Now we can have the form of

$$U_r = T_i U_l, \tag{53}$$

$$\begin{bmatrix} u_B(l) \\ N_B(l) \end{bmatrix} = \begin{bmatrix} cos\left(\sqrt{Q_B}\ \omega l_B\right) & \frac{sin(\sqrt{Q_B}\,\omega l_B}{E_B S_B \sqrt{Q_B}\,\omega} \\ -E_B S_B\sqrt{Q_B}\,\omega sin(\sqrt{Q_B}\,\omega l_B & cos\left(\sqrt{Q_B}\ \omega l_B\right) \end{bmatrix} * \begin{bmatrix} u_B(0) \\ N_B(0) \end{bmatrix} \tag{54}$$

where U_r= [u_r N_r] whereas U_l= [u_l N_l], T_i is the transfer (or transmission) matrix of the cell F_i . The latter is the result of the product $T_i = \prod_{p=1}^{n_i} T^X$, where T_X (X ∈ {A, B}) is the transfer matrix relating quantities across a single element, given by

$$T^X = \begin{bmatrix} cos\left(\sqrt{Q_X}\ \omega l_X\right) & \frac{sin(\sqrt{Q_X}\,\omega l_X}{E_X S_X \sqrt{Q_X}\,\omega} \\ -E_X S_X\sqrt{Q_X}\,\omega sin(\sqrt{Q_X}\,\omega l_X) & cos\left(\sqrt{Q_X}\ \omega l_X\right) \end{bmatrix} \tag{55}$$

Transfer matrices are unimodular; a unimodular matrix is a square integer matrix having determinant +1 or −1, here det = 1, which makes the dispersion relation a function only in the trace of the transfer matrix and follows the recursion rule

$$T_{i+1} = T_{i-1} T_i^2 \tag{56}$$

with T_0=T_B and T_1=T_A.

The Floquet-Bloch condition requires that $U_r = exp(iK)\, U_l$, so that, by combining this with Eq. (53), the dispersion equation takes the form det $[T_i - e^{ik} I] = 0$.

Differently, we can study the dispersion properties of this structure by evaluating the eigenvalues of the transfer matrix T_i as follows

$$\det\begin{bmatrix} T_{11}-\lambda & T_{12} \\ T_{21} & T_{22}-\lambda \end{bmatrix} = (T_{11}-\lambda)(T_{22}-\lambda) - (T_{12})(T_{21}) = 0 \qquad (57)$$

where $T_{11} + T_{22} = trT_i$ and $(T_{11}T_{22} - T_{12}T_{21}) = \det T_i = 1$, leading to

$$\lambda^2 - \lambda\, trT_i + \det T_i = 0$$

Or

$$\lambda^2 - \lambda\, trT_i + 1 = 0 \qquad (58)$$

Substituting $e^{ik} = \lambda$ in Eq. (58) and multiplying it by e^{ik} the condition $e^{ik} + e^{-ik} = trT_i$ is achieved leading to

$$k = arccos\frac{trT_i}{2} \qquad (59)$$

The solution of the dispersion relation (59) provides the complete Floquet-Bloch spectrum which allows to obtain the mentioned stop-/pass-band pattern of the waveguides at varying index i. In particular, waves propagate when $|\, trT_i\, | < 2$, stop bands correspond to $|\, trT_i\, | > 2$, whereas $|\, trT_i\, | = 2$ is the condition for standing waves (Morini and Gei, 2018). In finite-size waveguides composed of a finite number of elementary cells, stop bands (pass bands) are the range of frequencies when the reflection (transmission) coefficient approaches one (Lekner, 1994).

4.2 Trace map and Kohmoto's invariant

This section is devoted to the study of the properties of trace trT_i and how these features affect the frequency spectrum of SM rods. A nonlinear recursive relationship connecting traces for consecutive fundamental cells F_i is introduced. An invariant function defining a three-dimensional surface, the so-called Kohmoto's surface, is found for this map. At any frequency, the evolution of the traces corresponds to an orbit on this surface. By means of this analysis, we introduce a special sub-class of structures, characterized by closed periodic orbits on the Kohmoto's surface associated with particular values of the frequency.

4.2.1 Nonlinear map and Kohmoto's invariant

General recursive relations for the traces of unimodular 2×2 transfer matrices of generalised Fibonacci chains have been derived by Kolar and Ali (1989) in terms of Chebyshev polynomials of first and second kind. Specialising these expressions to the case SM, we derive the pair of equations

$$\begin{cases} x_{i+1} = x_i\, t_{i+1} - x_{i-1} & \text{with } i \geq 2 \\ t_{i+1} = x_i x_{i-1} - t_i & \text{with } i \geq 2 \end{cases} \tag{60}$$

where $x_i = tr\, T_i$ and $t_i = tr(T_{i-2}\, T_{i-1})$.Through the new set of variables, we have

$$x_i' = t_{i+2}\,,\ y_i' = x_{i+1}\,,\ \ z_i' = x_i \tag{61}$$

and its substitution into expression (60), the following nonlinear map determining the evolution of x_i and t_i is obtained

$$T_s(x_i', y_i', z_i') = (x_{i+1}', y_{i+1}', z_{i+1}') = (x_i' y_i'^2 - y_i' z_i' - x_i',\ x_i' y_i' - z_i', y_i') \tag{62}$$

with the following specific initial conditions

$$z_0' = x_0 = 2\cos(\sqrt{Q_B}\ \omega\ l_B)$$

$$y_0' = \ x_1 = 2\cos(\sqrt{Q_A}\ \omega\ l_A)$$

$$x_0' = t_2 = 2cos\left(\sqrt{Q_A}\ \omega\ l_A\right) cos\left(\sqrt{Q_B}\ \omega\ l_B\right) - 2\ \beta\ sin\left(\sqrt{Q_A}\ \omega\ l_A\right) sin\left(\sqrt{Q_B}\ \omega\ l_B\right) \tag{63}$$

where the impedance mismatch β takes the form

$$\beta = \frac{S_A^2 E_A^2 Q_A + S_B^2 E_B^2 Q_B}{S_A E_A S_B E_B \sqrt{Q_A Q_B}} \tag{64}$$

Since the nonlinear map (62) is a differentiable map, its jacobian, namely

$$J_s = \frac{\partial(x_{i+1}', y_{i+1}', z_{i+1}')}{\partial(x_i', y_i', z_i')} = \begin{bmatrix} y_i'^2 - 1 & 2y_i' x_i' - z_i' & -y_i' \\ y_i' & x_i' & -1 \\ 0 & 1 & 0 \end{bmatrix} \tag{65}$$

can be evaluated showing that for all the three maps det $J_s = -1$. The main use of jacobian matrix is found in the transformation of the coordinates. It deals with the concept of differentiation with coordinate transformation.

Through a little algebra we can also demonstrate that, similarly to all precious mean sequences (Morini and Gei, 2018), the quantity

$$\mathrm{I}(\omega) = \mathrm{x}_i'^2 + \mathrm{y}_i'^2 + \mathrm{z}_i'^2 - \mathrm{x}_i' \mathrm{y}_i' \mathrm{z}_i' - 4 = (\beta^2 - 4)\ sin^2\left(\sqrt{Q_B}\ \ \omega\ l_B\right) sin^2\left(\sqrt{Q_A}\ \ \omega\ l_A\right) \tag{66}$$

is an invariant of the map illustrated in (62).

This means that at a given frequency ω, the value I(ω) is independent of the order i of the sequence F_i . In the three-dimensional space spanned by the cartesian coordinate system $O\ x'y'z'$, the cubic $x_i'^2 + y_i'^2 + z_i'^2 - x_i'y_i'z_i' - 4 = I(\omega)$ is the equation of a two-dimensional manifold that was named by the authors Kohmoto's surface.

In the case of Golden Mean Structures (GMs), at any value of frequency ω, all the coordinates x_i', y_i' and z_i' represent the values of three consecutive traces obtained by three successive sequences. Differently, for Silver Mean Structures (SMs), only $y_i' = x_{i+1}\ and\ z_i' = x_i$ represent the traces of transfer matrices while $x_i' = t_{i+2}$ is an auxiliary variable produced by the recurrence relationship (60). For a given frequency ω, all points detected by the triad $R_i(x_i', y_i', z_i')$ and generated through (62) can be mapped onto the surface defined by Eq. (66).

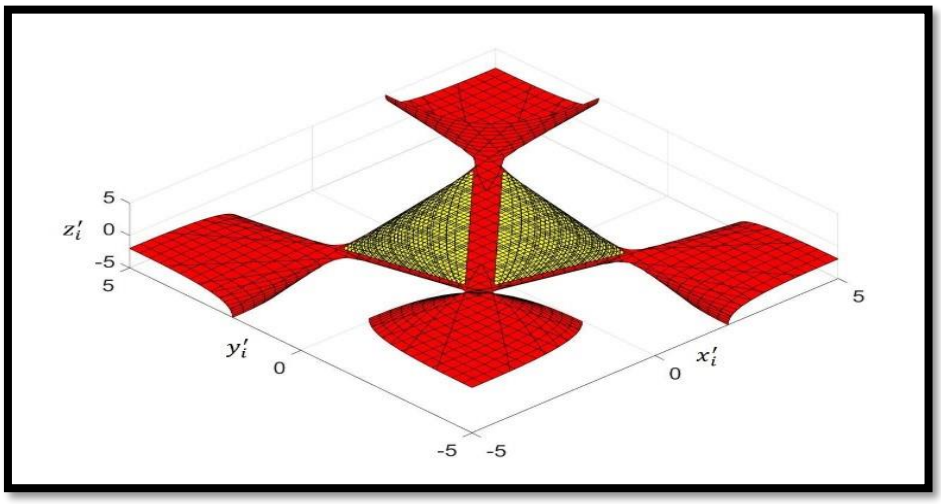

Figure 34 Shape of Kohmoto's surface.

Visibly, there are two different colours on the surface. The yellow region expresses that all ($|y_i'|$,$|z_i'|$) <2 . This means that $R_i(x_i', y_i', z_i')$ will be on pass band and waves will propagate at this frequency along the rods produced by the elementary cells F_{i+1} and F_i. On the other hand, if at least one of two elementary cells F_{i+1} and F_i ($|y_i'|$,$|z_i'|$)>2, the waves will not propagate (stop band) and this what the red region represents.

By taking into account that y_i', z_i' correspond to real traces (see Eq. (61)), the position of point $R_i(x_i', y_i', z_i')$ may reveal if, at a given ω, both F_i and $F_{i+1}$are in a pass band, namely if {$|x_i|$, $|x_{i+1}|$} < 2, both F_i and F_{i+1} in a stop band if {$|x_i|$, $|x_{i+1}|$} > 2.

The four plots in Figure 35 refer to a prototype SM rod whose parameters belong to $Q_B/Q_A = 1$, $E_B/E_A = 1$, $S_B/S_A = 1/2$, l_B/l_A = 5 will be further described in the next section, at a dimensionless frequency $\sqrt{Q_A}\ \omega\ l_A$= 1.548.

In Figure 35(a), the Kohmoto's surface in the 3-dimensional space $O\ x'y'z'$is represented; the yellow domain corresponds to {$|x_i|$, $|x_{i+1}|$} < 2 (traces of the transfer matrix) and three out of

the six saddle points possessed by the surface are indicated with a green dot. In Figures 35(b, c, d), the same surface is sketched in the subspace $O\,y'z'$, where the white squares in the center of the three panels match, in projection, the yellow sub-surface in part a). Therefore, a point $R_i(\omega) = (y_i', z_i') = (x_{i+1}\ (\omega),\ x_i\ (\omega))$ belonging to these squares indicates that the circular frequency ω for both F_i and F_{i+1}lies in a pass band.

The trajectories sketched in the three plots of the same figure have parametric equations (x_2 (ω), x_1 (ω))(b), (x_3 (ω), x_2 (ω)); (c) and (x_4 (ω), x_3 (ω)); (d). All trajectories start at the corner of coordinates (2, 2) that corresponds to ω = 0, then the red line covers the range $\bar{\omega} = \sqrt{Q_A}\ \omega\ l_A \in [0, \pi/2]$ after which the green line follows, reaching $\bar{\omega} = \pi$. The trajectory then continues with a pattern that the reader can easily envisage. In b) the represented trajectory describes all frequencies $\bar{\omega}$ [0, +∞] as the continuation for $\bar{\omega} \in [\pi, 2\,\pi]$ corresponds to the same path, but travelling in the opposite direction, and so on. Moreover, as expected, $|x_1| \leq 2$, $\forall\omega$, as F_1 is a homogeneous waveguide with any stop band in its spectrum. In the same part b), the first three low-frequency stop bands (SB) for F_2 are indicated. Parts c) and d) can be similarly interpreted, in particular the location of stop bands can be spotted following the curved lines, however the complexity increases at increasing index i of the sequence. Note, for instance, where is the point of transition between red and green lines (i.e., $\bar{\omega} = \pi/2$) in Figure 35(d).

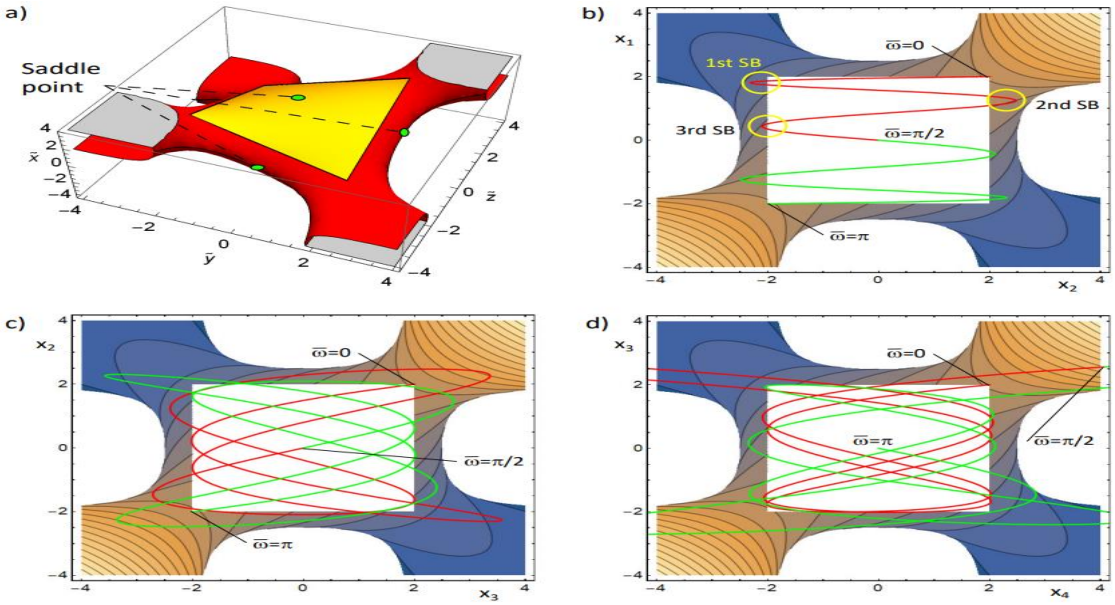

Figure 35 Kohmoto's surface for a SM rod whose parameters are $Q_B/Q_A = 1$, $E_B/E_A = 1$, $S_B/S_A = 1/2$, l_B/l_A = 5. a) 3-dimensional representation where three out of six saddle points are indicated. b), c), d) sketches in the plane (y', z'), where the reported trajectories have parametric equations: b) (x_2 (ω), x_1 (ω)); c) (x_3 (ω), x_2 (ω)); d) (x_4 (ω), x_3 (ω)). In all plots

of b), c), d) the red line is for $\bar{\omega} = \sqrt{Q_A}\,\omega\, l_A \in [0, \pi/2]$, the green one is for $\bar{\omega} \in [\pi/2, \pi]$. SB stands for 'stop band': (Farhat et al, 2022).

4.3 Periodic orbits on Kohmoto's surface and canonical configurations

By recalling the analyses performed by Morini and Gei (2018) and Gei et al. (2020), there are essentially three kinds of orbits which can be followed by points R_i as a consequence of the iteration map (62): (i) periodic orbits, (ii) non-periodic bounded orbits and (iii) escaping orbits. At any frequency ω, corresponding to a determinate Kohmoto's surface (66), the type of orbit is uniquely determined by the initial point $R_0(x_0', y_0', z_0')$whose coordinates are given by expressions (63).

The main difference between the two first kinds (i) and (ii) is that in the case orbit is periodic (i) after a specific number N of repetitions the triple (x_i', y_i', z_i') will assume the values of the initial point $R_0(x_0', y_0', z_0')$ again which lead to repeat the sequence of stop and pass band at every N iterations. In contrast, non-periodic bounded orbits (ii) belong to cases where $R_i$never assumes the initial position again at increasing index. That means that the trajectory defined by the successive points will be open. Morini and Gei (2018) in their study illustrated the relationship between orbits on the Kohmoto's surfaces produced by iterating map (66) and the stop/pass band diagrams.

It is worthy to point out that there is a clear difference in terms of using of Kohmoto's surfaces to illustrate the pass/stop band areas between Golden and Silver Mean structures. In the case of SM, the coordinate x_i' does not indicate to the trace of a transfer matrix as written in the Eq.(61). This means that only $y_i'$and z_i' represent the traces of a transfer matrix, and thus the condition $|x_i'| \geq 2$ does not belong to the bandgap of a structure whereas in the case of GM all three coordinates are traces of a transfer matrix and thus the conditions $|x'| \geq 2$, $|y'| \geq 2$ and $|z'| \geq 2$ are belong to stop band.

According to Morini and Gei (2018), there are two types of orbits can be described as perturbations of the periodic orbit on the Kohmoto's surface which are (ii) non-periodic bounded orbits and (iii) escaping orbits at any ω .This means that the periodic orbit is a reference orbit to those orbits noted in the (ii) and (iii) notations. Now we focus our attention on periodic orbits and in particular to the investigation of specific configurations for SM periodic rods. Guided by the previous work on standard, golden mean (GM) rods, we indicate with P_j (j = 1, . . . , 6) the six saddle points of the manifold (66) whose coordinates are $P_{1,4}$ = $(0, 0, \pm\beta_1)$, $P_{3,6} = (0, \mp\beta_2, 0)$, $P_{2,5} = (\pm\beta_3, 0, 0)$, where the top sign is associated with the lowest index. As anticipated, in Figure 35(a) three out of six saddle points are sketched. We then

wonder if any periodic orbit joining those points might exist. The answer can be found by imposing, at some frequencies,

$$y_0' = z_0' = 0. \tag{67}$$

and

$$x_0' = y_0' = 0, \text{or} \quad x_0' = z_0' \tag{68}$$

The requirements (67) and (68) can be fulfilled only for particular classes of layouts, namely the canonical (SM) layouts, in analogy to the definition proposed by Gei et al (2020) for GM sequences. By substituting expressions (63) into condition (67), the following relationship between physical and geometrical properties of phases A and B are derived as follows

$$2\cos(\sqrt{Q_B}\,\omega\, L_B) = \; 2\cos\left(\sqrt{Q_A}\,\omega\, L_A\right) = 0$$

$$cos\sqrt{Q_B}\,\omega\, l_B = 0 \overset{IF}{\Rightarrow} \sqrt{Q_B}\,\omega\, l_B = (\,\frac{\pi}{2}\,,\frac{3\pi}{2},\frac{5\pi}{2},,,,,) \text{ or } \sqrt{Q_B}\,\omega\, l_B = \frac{\pi}{2}(2n+1), \tag{69}$$

and

$$cos\sqrt{Q_A}\,\omega\, l_A = 0 \overset{IF}{\Rightarrow} \sqrt{Q_A}\,\omega\, l_A = (\,\frac{\pi}{2}\,,\frac{3\pi}{2},\frac{5\pi}{2},,,,,) \text{ or } \sqrt{Q_A}\,\omega\, l_A = \frac{\pi}{2}(2m+1). \tag{70}$$

This leads to

-*Family no.1* for canonical structures is $C_1 = \frac{l_B}{l_A}\frac{\sqrt{Q_B}}{\sqrt{Q}_A} = \frac{(2n+1)}{(2m+1)}$: C_1 = (1,5 ,7,1/3). (71)

By applying the same procedures for the expressions (68), family no.2 and 3 for canonical structures will be obtained as follows

-*Family no.2* for canonical structures is

$$C_2 = \frac{l_B}{l_A}\frac{\sqrt{Q_B}}{\sqrt{Q}_A} = \frac{(2n+1)}{(2q)} : C_2 = (\frac{1}{2},\frac{3}{2},\frac{5}{6}). \tag{72}$$

-*Family no.3* for canonical structures is

$$C_3 = \frac{l_B}{l_A}\frac{\sqrt{Q_B}}{\sqrt{Q}_A} = \frac{(2q)}{(2m+1)}: C_3 = (\frac{2}{3}, 2,4) \tag{73}$$

where $(m\,, n, q \in N)$.

respectively. C_1, C_2 and C_3 are the canonical ratios. Each of them identifies a family of canonical SM rods (no. 1, no. 2, and no. 3, respectively). In turn, the canonical frequencies are given by

$$\omega_{c_{rn}} = \omega_{c_r}(1+2n), \quad \text{with } (n \in N),\ r = 1,2,3 \tag{74}$$

$$\omega_{c_1} = \omega_{c_3} = \frac{\pi}{2l_A\sqrt{Q_A}}(1+2m), \quad \text{with } (m \in N) \tag{75}$$

$$\omega_{c_2} = \frac{\pi}{l_A\sqrt{Q_A}}q \text{ with } (q \in N) \tag{76}$$

Any arbitrary canonical SM waveguide F_i displays a periodic stop/pass-band layout whose period depends only on the value of the canonical frequency. In particular, periodicity is enforced by requirements (67) and (68). The least frequency interval where all traces are periodic is [0, $4\omega_{c_r}$] (r = 1, 2, 3), as an inspection of the first two equalities in (63) may reveal.

As mentioned earlier that for SM only y_i and z_i are traces of transfer matrix (T_i) while x_i is a variable produced by recurrence relation (60), the equation (61), can be written as follows

$$t_{i+2} = tr(T_iT_{i+1}), y_i' = trT_{i+1}, z_i' = trT_i \tag{77}$$

an example of this sequence considering

$$i = 0\,; \quad t_2 = tr(T_0T_1), y_i' = trT_1, z_i' = trT_0.$$

Thus the initial point is $\mathrm{R}_0(\mathrm{x}_0', \mathrm{y}_0', \mathrm{z}_0') = (t_2, trT_1, trT_0)$.

To identify the periodic orbits of the canonical SM rods that characterize each family, the three coordinates of each point detected by the triad $R_i(x_i', y_i', z_i')$ are displayed in the following figures in next section for two prototype examples belonging to Family no.1 ($\boldsymbol{C_1} = 5$) and Family no.3 ($\boldsymbol{C_3}$ =2/3), respectively. In all cases displayed in these figures, $\frac{Q_B}{Q_A} = 1$, $\frac{E_B}{Q_A} = 1$, $\frac{S_B}{S_A} = 1/2$, so that β = 2.5. Therefore, the chosen length ratio l_B/l_A corresponds to $\boldsymbol{C}$.

4.3.1 Family one periodic orbits

Since the pass/stop band layout is periodic for all families, the periodic orbits can be found. This can help in optimizing the spectrum for this particular class of structures, we do not need to evaluate the band gap for a large frequency range but only for one period. Periodic orbit is a result of coordinates x_i (trace of the transfer matrix) and t_i (an auxiliary variable produced by the recurrence relationship (60)) that their evolution can be determined by the nonlinear map (63) and therefore explains the behaviour of these coordinates in the form of points that can be represented on Kohmoto's surface.

Elements of Family no. 1 possess features that differ from those characterizing the other two families that can be studied together.

$$C_1 = 5, \ \therefore \frac{L_B}{L_A} = 5, \quad \frac{s_A}{s_B} = 0.5$$

The normalized canonical frequency $\omega_{c_1} = \pi/2$ and $\omega_{c_3} = 3\pi/2$ are represented by a red vertical line in all figures.

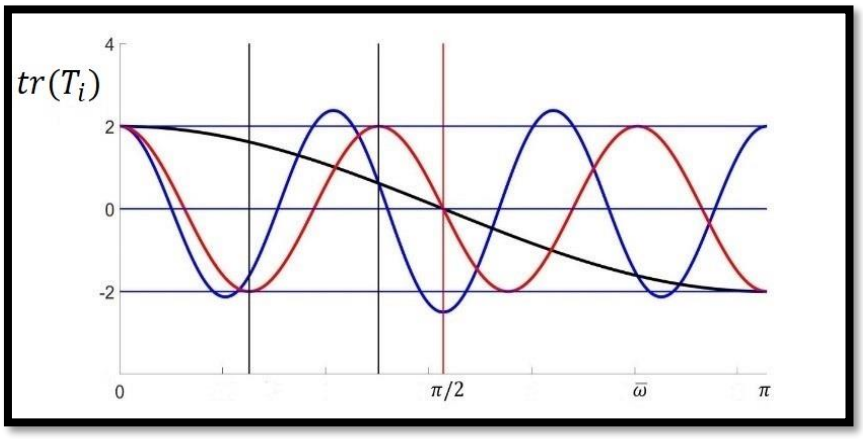

Figure 36: Description of the three coordinates $R_0\ (x_0', y_0', z_0')$: $R_0\ (trT_0T_1: blue, trT_1: black, trT_0: red)$ for SM rods assuming family one $C_1 = 5$, $E_A = E_B$, $\frac{Q_B}{Q_A} = 1$, $S_B/S_A = 1/2$ .The red vertical line is the canonical frequency.

In Figure 36, the coordinate y_0' (blue curve) intersects the canonical frequency at the value of $\beta = -2.5$ while both trT_1 and trT_0 intersect the canonical frequency at zero. This means that the first saddle point (starting point) is $P_2(-\beta\ , 0, 0)$= $(-2.5, 0, 0)$.

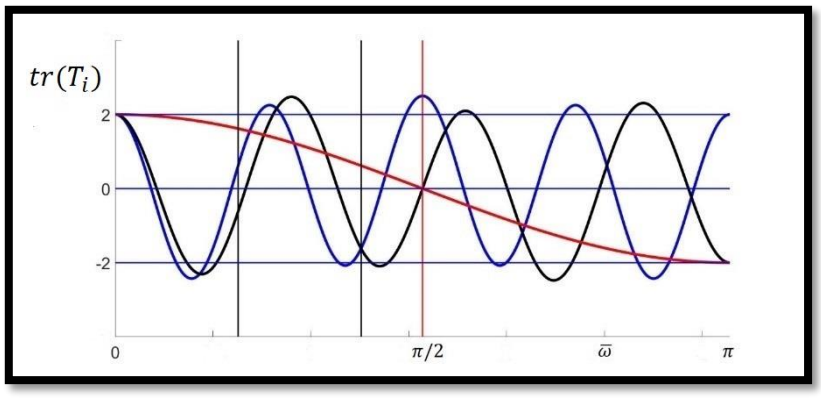

Figure 37: Description of the three coordinates $R_1(x_1', y_1', z_1')$: $R_1(trT_1T_2: blue, trT_2: black, trT_1: red)$ for SM rods assuming family one $C_1 = 5$, $E_A = E_B$, $\frac{Q_B}{Q_A} = 1$, $S_B/S_A = 1/2$ .The red vertical line is the canonical frequency.

In Figure 37, the second saddle point is $P_5(\beta, 0, 0)$= (2.5, 0, 0). The third saddle point is $(-2.5, 0, 0)$ which is the same as the initial point P_2= $(-2.5, 0, 0)$.

Due to rule (60) and Eq. (67), it turns out that, for Family no. 1, x_2 = x_1t_2-x_0, an expression which leads to x_2= 0 at the canonical frequencies. Therefore, x_i $(\omega_{c_{1n}})$ = 0, $\forall_i$, implying that at these frequencies a waveguide belonging to Family no. 1 always displays a pass band. Moreover, a two-point periodic orbit is achieved at ω_{c1n} , namely

$P_2(-2.5, 0, 0) \xrightarrow{\mathcal{T}} P_5(2.5, 0, 0) \xrightarrow{\mathcal{T}} P_5$, where $\mathcal{T}$ indecate to the cycle transformation (78)

or, equivalently, $T_2^S(P_{2,5}) = P_{2,5}$. The orbit (78) will be denoted henceforth as T_2^S.

Note that I (ω_{c1}) = I $(\omega_{c_{1n}}) = \beta^2 - 4 > 0$. (78.1)

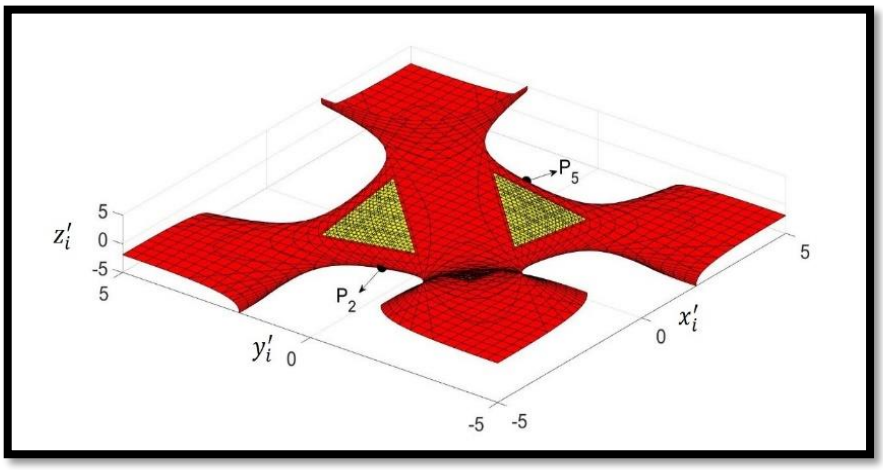

Figure 38 Representation of the two saddle points on the Kohmoto's surface at canonical frequency $\omega = \omega_{c1}$.

4.3.2 Family three periodic orbit

Since family two and three can be studied together (they shows same properties), I will focus only on family three.

$C_3 = 2/3, \ \therefore \frac{L_B}{L_A} = 2/3, \ \ \frac{s_A}{s_B} = 0.5, \omega_{c_3} = 3\pi/2.$

For Families no. 2 and 3, the invariant evaluated at a canonical frequency always vanishes, i.e., $I(\omega_{c_{rn}}) = 0$ $(r = 2, 3)$. The recursive rule (60) provides a four-point periodic orbit encompassing the four saddle points not involved in T_2^S.

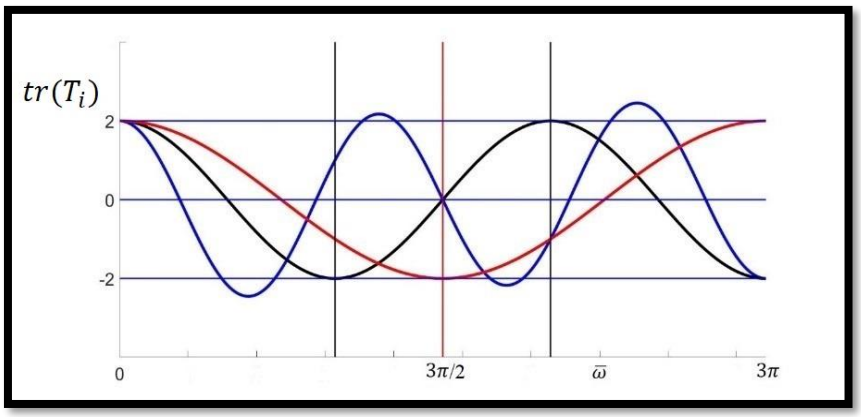

Figure 39: Description of the three coordinates (x_0', y_0', z_0') $(trT_0T_1: blue, trT_1: black, trT_0: red)$ for SM rods assuming family three $C_3 = \frac{2}{3}, E_A = E_B \ , \frac{Q_B}{Q_A} = 1, \ S_B/S_A = 1/2$ .The red vertical line is the canonical frequency. The black vertical lines at π and 2π are the locus of a 4-point periodic orbit.

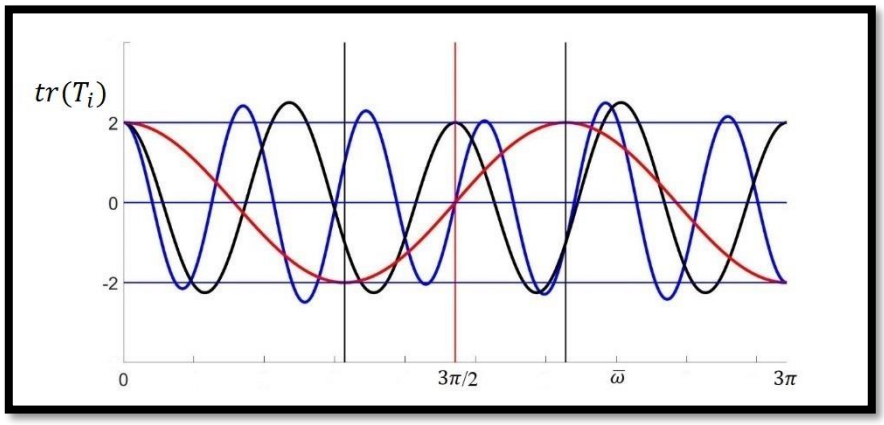

Figure 40: Description of the three coordinates (x_1', y_1', z_1') $(trT_1T_2: blue, trT_2: black, trT_1: red)$ *for SM rods assuming family three* $C_3 = 2/3,\ E_A = E_B\ , \frac{Q_B}{Q_A} = 1,\ S_B/S_A = 1/2$ *.The red vertical line is the canonical frequency. The black vertical lines at* π *and* 2π *are the locus of a 4-point periodic orbit.*

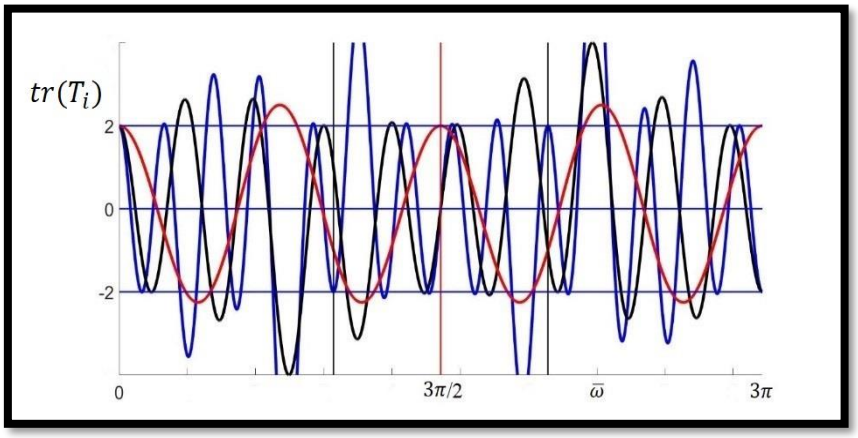

Figure 41: Description of the three coordinates (x_2', y_2', z_2') $(trT_2T_3: blue, trT_3: black, trT_2: red)$ *for SM rods assuming family three* $C_3 = 2/3,\ E_A = E_B\ , \frac{Q_B}{Q_A} = 1,\ S_B/S_A = 1/2$ *.The red vertical line is the canonical frequency. The black vertical lines at* π *and* 2π *are the locus of a 4-point periodic orbit.*

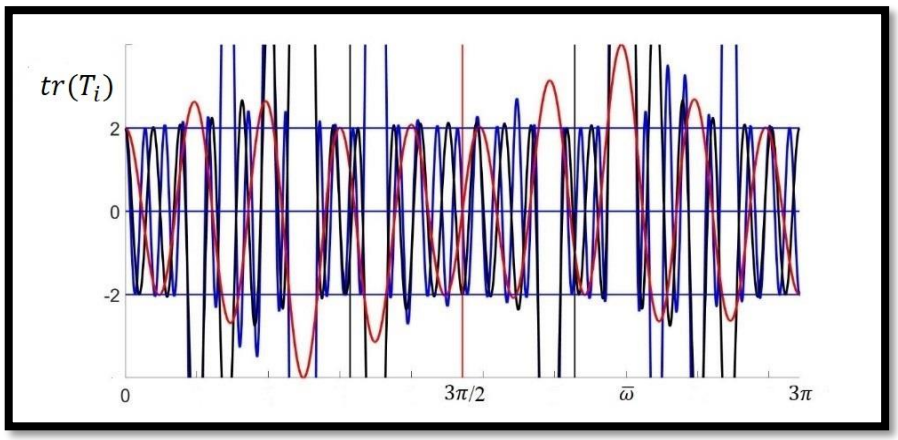

Figure 42: Description of the three coordinates (x_3', y_3', z_3') $(trT_3T_4: blue, trT_4: black, trT_3: red)$ *for SM rods assuming family three* $C_3 = 2/3,\ E_A = E_B\ , \frac{Q_B}{Q_A} = 1,\ S_B/S_A = 1/2$ *.The red vertical line is the canonical frequency. The black vertical lines at* π *and* 2π *are the locus of a 4-point periodic orbit.*

in Figure 39, the coordinate z_0' (red curve) intersects the canonical frequency at the value of $\beta = -2$ while both coordinates x_0' and y_0' intersect the canonical frequency at zero. This leads to the first saddle point which is $P_3(0, 0, -\beta)$= (0, 0, −2). The second, third, and fourth saddle points can be extracted from the Figures 40,41, and 42 respectively.

These four points are connected to periodic orbit through the four-cycle transformations T_s^4as follows:

$$P_4(0, 0, -2) \xrightarrow{\mathcal{T}} P_6(0, 2, 0) \xrightarrow{\mathcal{T}} P_1\ (0, 0, 2) \xrightarrow{\mathcal{T}} P_3(0, -2, 0). \qquad (79)$$

This orbit (79) will be referred from now on as T_4^s.

The Eq. (78.1) shows how Kohmoto's invariant relates to pass and stop bands, where the coordinate β produced by the traces y_i' and z_i' depends on this invariant.

Note that at higher index i, the dispersion diagrams became unclear as can be seen in the figure 42.

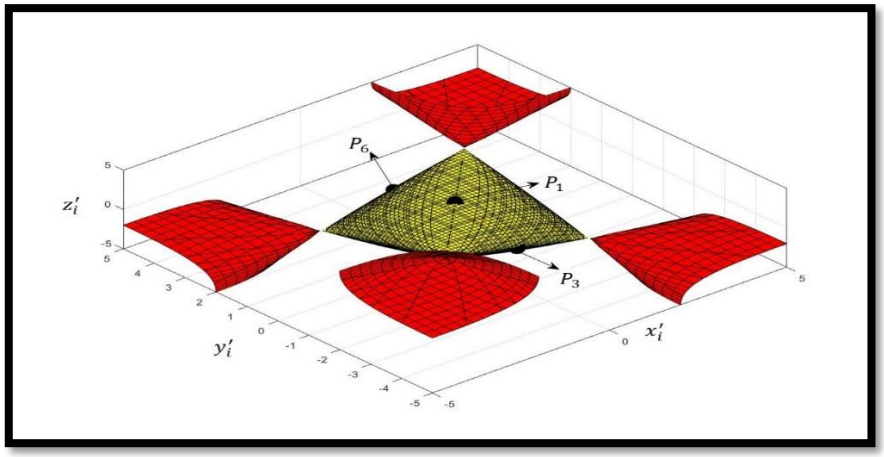

Figure 43: Representation of the saddle points on the Kohmoto's surface at canonical frequency $\omega = \omega_{c3}$. P_4 is on the hidden part.

Here the situation is different, as all four points are located in the yellow region. This means that the investigated frequency lies on a pass band where the frequency band can propagate.

Generally, these points (P_2, P_5) and (P_4, P_6, P_1, P_3) are periodic points of the map (62). Since it is a closed and periodic orbit, the starting point in (78) and (79) can be any saddle point. The table below gives a comparison between Family no. 1 and Family no. 3 around the canonical frequency.

Feature	Family one : C_1 =5	Family three: C_3 =2/3
Variable of x_i'	Always not zero	Always zero
Traces y_i' and z_i'	Always vanishes	$\pm\beta$ or zero
Kohmoto's invariant $I(\omega_c)$	$I(\omega_{c_1}) = 2.25$	$I(\omega_{c_3}) = 0$
Periodic points	$P_2(-\beta,0,0) \xrightarrow{T_s} P_5(\beta,0,0)$ Where $\beta = 2.5$	$P_4(0, 0, -\beta) \xrightarrow{T_s} P_6(0, \beta, 0) \xrightarrow{T_s} P_1(0, 0, \beta) \xrightarrow{T_s} P_3(0, -\beta, 0)$.
Scaling k	$k = -8.127$	$k = 33.971$

Table 3: comparison between Family no. 1 and Family no. 3 around the canonical frequency.

Additional periodic orbits can be found at non-canonical frequencies ω such that $I(\omega) = 0$.This may occur in a large variety of cases depending on the value of C that are however not classified here. Nevertheless, the following cases are universal. (i.e., valid for all three Families of canonical rods):

(i) the pair $x_0 = x_1 = 2$ can be found at the endpoints of the interval where traces are periodic, namely at $\omega = 0, 4\ \omega_c$; therefore, $R_i = (2, 2, 2)$, $\forall_i$, corresponding to a fixed-point orbit, i.e. $T_{s1}(R_i) = R_i$; (i.e., valid for all three Families of canonical rods)

(ii) In Family no. 1 at $\omega = 2\omega_c$, $x_0 = x_1 = -2$, then $R_i = (2, -2, -2)$ = the general rule for this frequency is that the orbit is fixed-point periodic, i.e., $T_{s1}(R_i) = R_i$. In Family no .2 and 3 at $\omega = 2\omega_c$, $x_0 = -x_1 = -2$, then $R_0 = (-2, -2, 2) = R_2 = R_K$, with K even, whereas $R_1 = (-2, 2, -2) = R_3 = R_m$, with m odd; the general rule for this frequency is that the orbit is two-point periodic, i.e. $T_{s2}(R_{k,m}) = R_{k,m}$.

To illustrate the features of the dispersion diagram for canonical SM rods, the pass/stop-band layouts are displayed in the bottom of Figure 44 and 45.

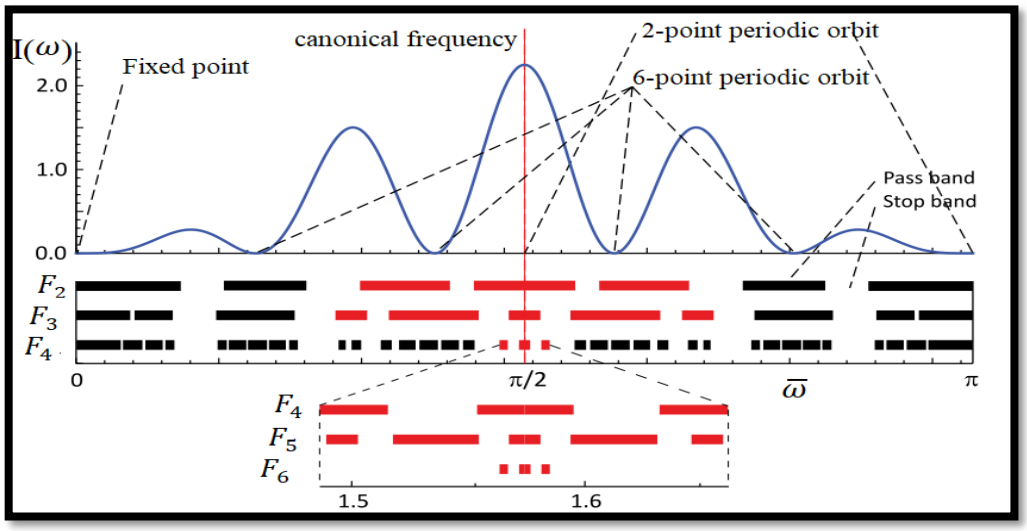

Figure 44: Canonical SM rod with $C_1 = 5$ (Family no. 1). Top: sketch of the invariant I(ω) in the interval $[0, 2l_A\sqrt{Q_A}\,\omega_{c1}]$ the frequencies at which periodic orbits occur are indicated; bottom: stop/pass-band layout in the same interval for sequences F_2 to F_4. The dimensionless canonical frequency (red vertical line) is π/2.

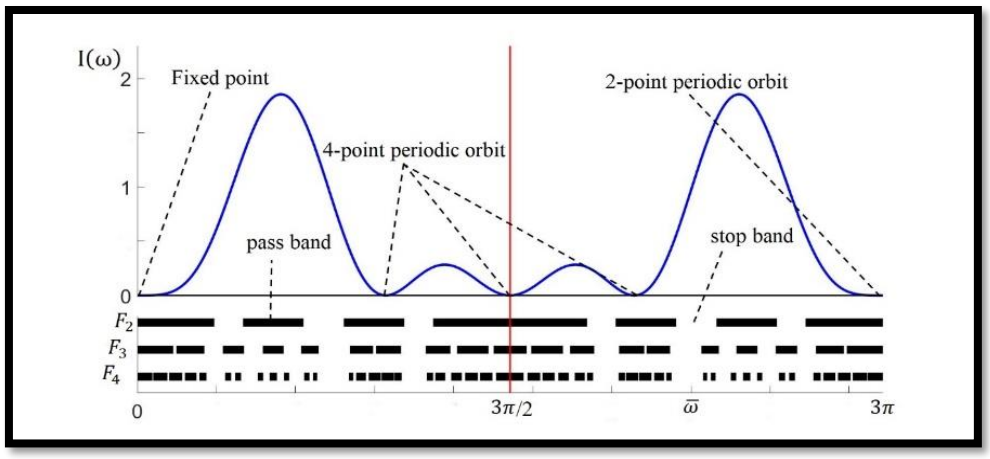

Figure 45: Canonical SM rod with $C_3 = 2/3$ (Family no. 3). interval $[0, 2l_A\sqrt{Q_A}\,\omega_{c1}]$ the frequencies at which periodic orbits occur are indicated; bottom: stop/pass-band layout in the same interval for sequences F_2 to F_4. The dimensionless canonical frequency (red vertical line) is 3π/2.

In the top part of Figure 44, the invariant I(ω) is sketched in the interval in which the function itself , see above – is periodic, namely $[0, 2l_A\sqrt{Q_A}\omega_{c_1}]$. While, on the one hand, it is confirmed that, as predicted, $I(\omega_{c_1})$> 0 (its value is 2.25), on the other hand, in addition to cases classified as (i) and (ii) just above, at $\bar{\omega} = l_A\sqrt{Q_A}\omega = p\,\pi$ /5(p = 1, . . . , 4) the function vanishes. There, periodic orbits may be found which are all 6-point periodic. However, the orbits produced at p = (1, 4) have the same values of $x_i' = tr(T_iT_{i+1})$ and opposite values of both $y_i' = trT_{i+1}$ *and* $z_i' = trT_i$.This similarity also occurs for values of p = (2, 3).

For $\bar{\omega} = \pi/5$, 6-point periodic orbit is

$R_1(-\phi, \phi, -2) \xrightarrow{T} R_2(1/\phi, -1/\phi, \phi) \xrightarrow{T} R_3\ (1/\phi, -2, -1/\ \phi) \xrightarrow{T} R_4(1/\phi, -1/\phi, -2) \xrightarrow{T} R_5(-\phi, \phi, -1/\ \phi) \xrightarrow{T} R_6\ (-\phi, -2, \phi)$.

where ϕ is the golden ratio ($\phi = (\sqrt{5} + 1)/2$).

For $\bar{\omega} = 4\pi/5$, 6-point periodic orbit is

$R_1(-\phi, -\phi, 2) \xrightarrow{T} R_2(1/\phi, 1/\phi, -\phi) \xrightarrow{T} R_3\ (1/\phi, 2, 1/\ \phi) \xrightarrow{T} R_4(1/\phi, 1/\phi, 2) \xrightarrow{T} R_5(-\phi, -\phi, 1/\ \phi) \xrightarrow{T} R_6\ (-\phi, 2, -\phi)$.

For $\bar{\omega} = 2\pi/5$, 6-point periodic orbit is

$R_1(1/\phi, 1/\phi, 2) \xrightarrow{T} R_2(-\phi, -\phi, 1/\phi) \xrightarrow{T} R_3\ (-\phi, 2, -\phi) \xrightarrow{T} R_4(-\phi, -\phi, 2) \xrightarrow{T} R_5(1/\phi\ ,1/\phi, -\ \phi) \xrightarrow{T} R_6\ (1/\phi, 2, 1/\phi)$.

For $\bar{\omega} = 3\pi/5$, 6-point periodic orbit is

$R_1(1/\phi, -1/\phi, -2) \xrightarrow{T} R_2(-\phi, \phi, -1/\phi) \xrightarrow{T} R_3\ (-\phi, -\ 2, \phi) \xrightarrow{T} R_4(-\phi, \phi, -\ 2) \xrightarrow{T} R_5(1/\phi, -1/\phi, \phi) \xrightarrow{T} R_6\ (1/\phi, -2, -1/\phi)$.

In the bottom part of the Figure 44, the layout of stop/pass bands is sketched for sequences F_2 to F_4. A higher index i could have been studied for the whole interval, but the increasing smallness of the widths of the bands in certain frequency ranges would have made the diagram illegible. However, a close-up view of the layout for F_4 to F_6 in the neighbourhood of the canonical frequency is included to highlight the local self-similar pattern of the spectra, where the number of pass bands in each area of the pass/stop diagram is the same.

It is evident that in the scaled domain, F_4 –F_5 –F_6 show a sequence of pass bands very similar to that pertaining to F_2 –F_3 –F_4 (sketched in red) in the whole domain. The 'match' between patterns improves at increasing index i; the value of the scaling factor will be determined with the method developed in section (4.3).

In Figure 45, the function $I(\omega)$ in the same interval (i.e. $[0,\ 2l_A\sqrt{Q_A}\omega_{c_3}]$) is reported. Differently than Figure 44, at the canonical frequency the invariant vanishes, namely $I\ (\omega_{c_3}\ ) = 0$, and this also occurs for $\bar{\omega} = \pi$ and 2π. All the three frequencies are loci where 4-point periodic orbits are present with initial point being equal to $R_0 = (1, -2, -1)$ for $\bar{\omega} = \pi$ and $R_0 = (-1, 2, -1)$ for $\bar{\omega} = 2\pi$.

The 4-point periodic orbit for $\bar{\omega} = \pi$

$R_1(1, -2, -1) \xrightarrow{T} R_2(1, -1, -2) \xrightarrow{T} R_3\ (-2, 1, -1) \xrightarrow{T} R_4(1, -1, 1).$

And for $\bar{\omega} = 2\pi$

$R_1\ (-1, 2, -1) \xrightarrow{T} R_2(-1, -1, 2) \xrightarrow{T} R_3\ (2, -1, -1) \xrightarrow{T} R_4(-1, -1, -1).$

In order to give the reader an insight into the diagrams illustrated in Figures 44 and 45, we consider two finite waveguides composed of six elementary cells F_2 and F_4, respectively, belonging to Family no. 1. They join two semi-infinite, identical outer media whose elastic properties match those of phase A (Figure 46 (a)). We expect the system to be able to transmit (reflect) a signal whose frequency belongs to a pass band (stop band). To this end, transmission coefficient T_C and reflection coefficient $R_C = 1 - T_C$ can be calculated following the method presented in (Lekner, 1994). The reflection coefficients for the two problems at hand are displayed in Figure 46. For F_2, the whole domain $[0, 2l_A\sqrt{Q_A}\omega_{c_1}]$ represented in Figure 44 is analyzed in Figure 46 (b), whereas for the elementary cell F_4, the range $l_A\sqrt{Q_A}\ \omega \in [1.376, 1.764]$ is analyzed in Figure 46 (d). In both diagrams, it is evident that R_C approaches 1 in the stop bands, thus confirming that the model of infinite, periodic waveguide provides an excellent estimation of the range of frequencies at which waves cannot propagate. For cell F_2, the reflection coefficient for a domain three times wider than that in Figure 46 (b) is reported in Figure 46 (c) to show the periodicity of the response of the finite-size device, confirming once again the prediction of the theory of canonical phononic waveguides.

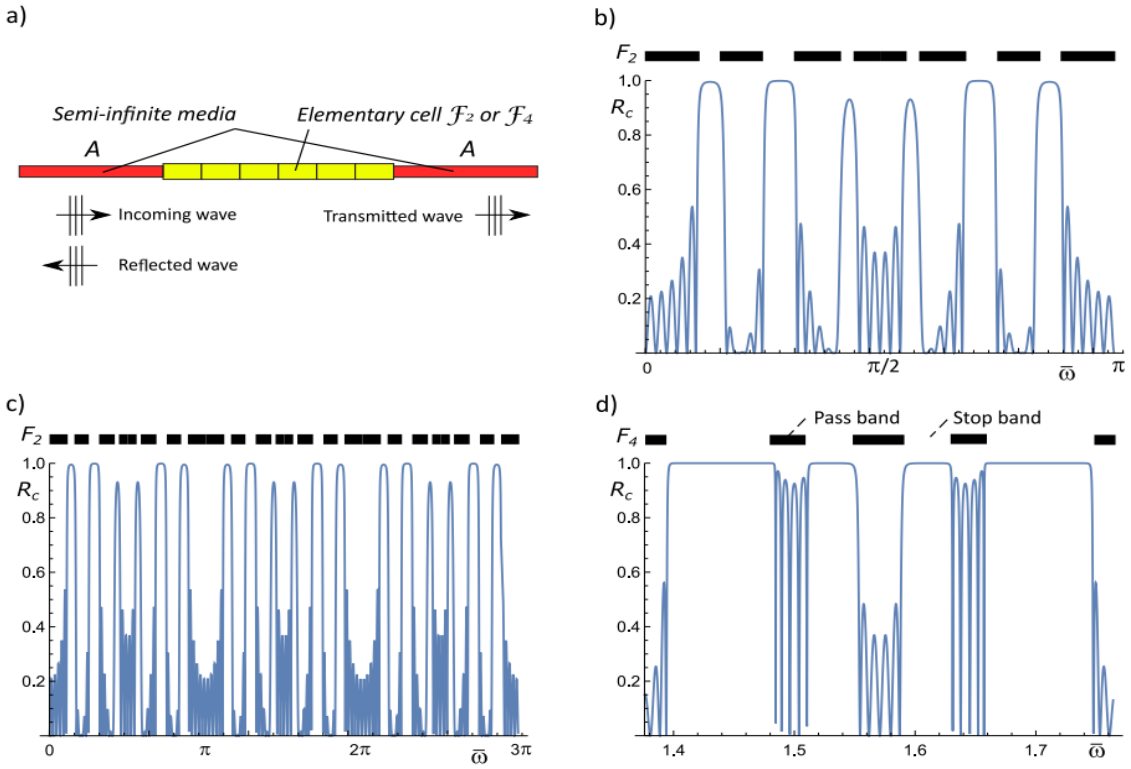

Figure 46: Canonical SM rod with $C_1 = 5$ (Family no. 1). (a) Schematic of the finite-size waveguide; (b) plot of the reflection coefficient R_C for elementary cell F_2 for a dimensionless frequency in the interval $[0, 2l_A\sqrt{Q_A}\omega_{c_1}]$; (c) same as in (b), but in the domain $[0, 6l_A\sqrt{Q_A}\omega_{c_1}]$; (d) plot of the reflection coefficient R_C for elementary cell F_4 in the domain [1.376, 1.764] : (Farhat et al, 2022).

4.4 Scaling and self-similarity of the frequency spectra of canonical SM rods

In this section, analytical scaling factors which govern the self-similar pattern of stop and pass-band layouts of canonical SM rods are obtained through the linearization of the map (62) about the relevant periodic orbits mentioned in the expressions (78) and (79).

Let us see what happen around the canonical frequency in each family.

- Family no. 1, since this family is characterised by two-cycle transformation T_s^2, the ratio of pass band width around the canonical frequency called scaling ratio is $\frac{\omega_i}{\omega_{i+2}} = 8.1$. This ratio can be comparable with the absolute result of k_{s+2}^{+} which will derive in next section.

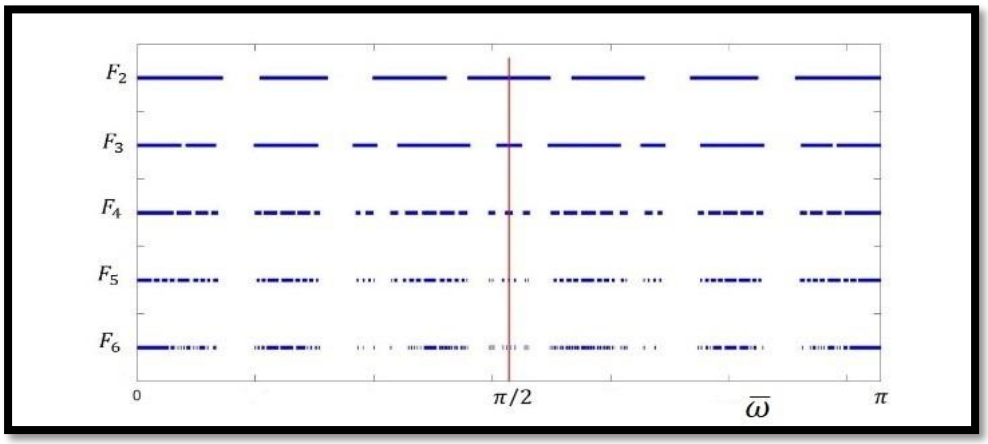

Figure 47: Stop/pass-band layout for canonical SM rod corresponding to elementary cells F_2 to F_6 with $C_1 = 5$ (Family no. 1) in the interval $[0, 2l_A\sqrt{Q_A}\,\omega_{c1}]$. The dimensionless canonical frequency is π/2.

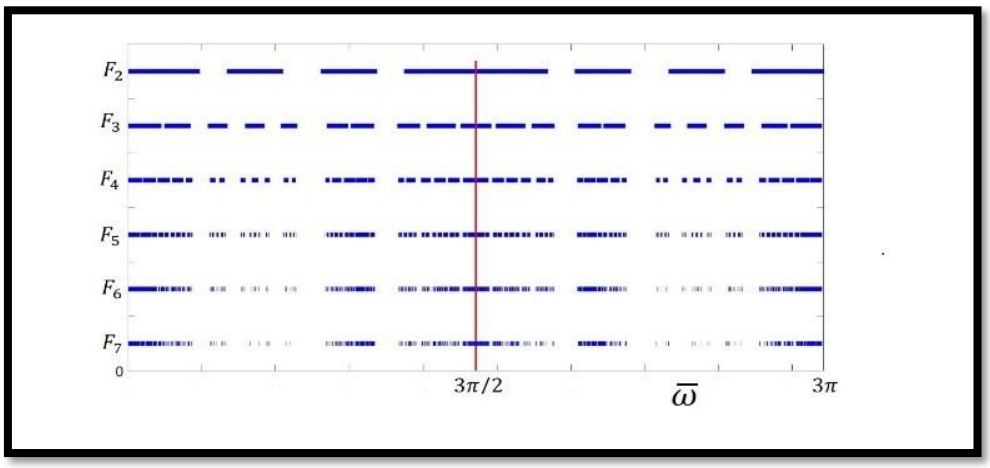

Figure 48:stop/pass-band layout for canonical SM rod corresponding to elementary cells F_2 to F_7 with $C_3 = 2/3$ (Family no. 3) in the interval $[0, 2l_A\sqrt{Q_A}\,\omega_{c3}]$ .The dimensionless canonical frequency is 3π/2.

.

- In Family no. 3, The scaling ratio $\frac{\omega_i}{\omega_{i+4}}$ 33.97 shows a great converge to the eigenvalue k_{s+4}^{+} = 33.971 which will derive in next section especially at high sequences.

4.4.1 Linearization of the trace map about saddle points

As mentioned earlier, non-periodic bounded and escaping orbits can be studied as a perturbation of the periodic trajectory on Kohmoto's surface given by the two and four-cycle transformations defined by Eq. (78) and (79).

Following the approach proposed by Morini and Gei (2018) and Gei et al (2020), we can study non-periodic bounded orbits on the Kohmoto's surface as linear perturbations of the periodic orbits defined in the previous section. Consider a saddle point $P_{\bar{j}}$ as a point of a p−periodic orbit. Let us assume, for a 'small' δ, that $\bar{R}_i = R_i(\omega + \delta\omega)$, where $R_i\,(\omega) = P_{\bar{j}}$. We can then say

that $\bar{R}_i$ is in the neighbourhood of $P_{\bar{j}}$, therefore the modulus of the vector $\delta r_i\ (\delta\omega) = \bar{R}_i - P_{\bar{j}}$ is small with respect to the value of the non-vanishing coordinate of $P_{\bar{j}}$. On the one hand, by applying P times the transformation T , the exact position of $\bar{R}_{i+P} = T^P(\bar{R}_i)$ can be established. On the other, due to the smallness of $|\,\delta r_i\,|$, a linearisation of the nonlinear map can be performed such that the position of point $\bar{R}_{i+P}$ can be approximated by $P_{\bar{j}} + \delta\acute{r}_{i+P}$. From above we can say that

$$\delta\acute{r}_{i+P} = \bar{A}_P\ \delta r_i. \tag{80}$$

For Family no.1 we have

$$\bar{R}_{i+2} = T_s^2\ (\bar{R}_i)$$

$$\delta\acute{r}_{i+P} = \bar{A}_2\ \delta r_i. \tag{81}$$

For Family no. 2 and 3, we have

$$\bar{R}_{i+4} = T_s^4\ (\bar{R}_i)$$

$$\delta\acute{r}_{i+4} = \bar{A}_4\ \delta r_i. \tag{82}$$

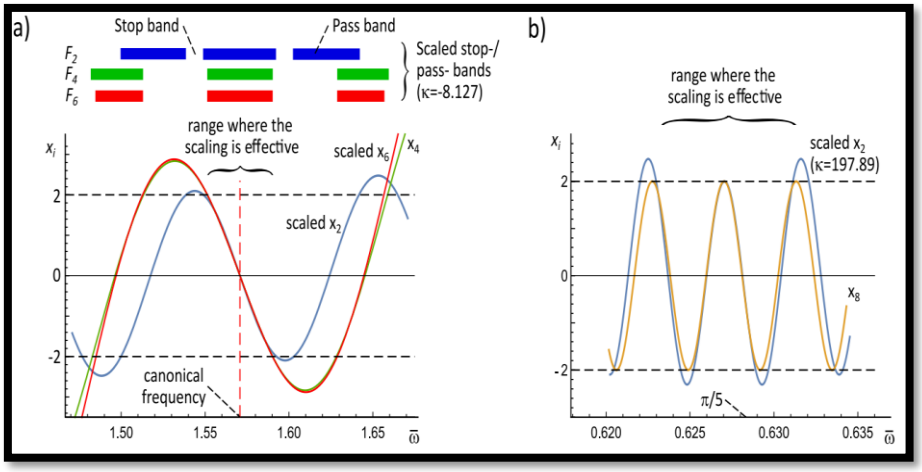

Figure 49: Canonical SM rod with $C_1 = 5$ (Family no. 1). (a) Plot of traces $x_2\ (k\omega)$, $x_4(\omega)$, $x_6\ (\omega/k)$ $(\kappa = -8.127)$ in the neighborhood of the canonical frequency $(l_A\sqrt{Q_A}\ \omega_{c3} = \pi/2)$; (b) plot of traces $x_2(k\omega)$ and $x_8(\omega)$ $(\kappa = 197.89)$ in the neighborhood of the point $\bar{\omega} = = l_A\sqrt{Q_A}\ \omega = \pi/5$ where a 6-point periodic orbit is detected (see Figure. 35): (Farhat et al, 2022).

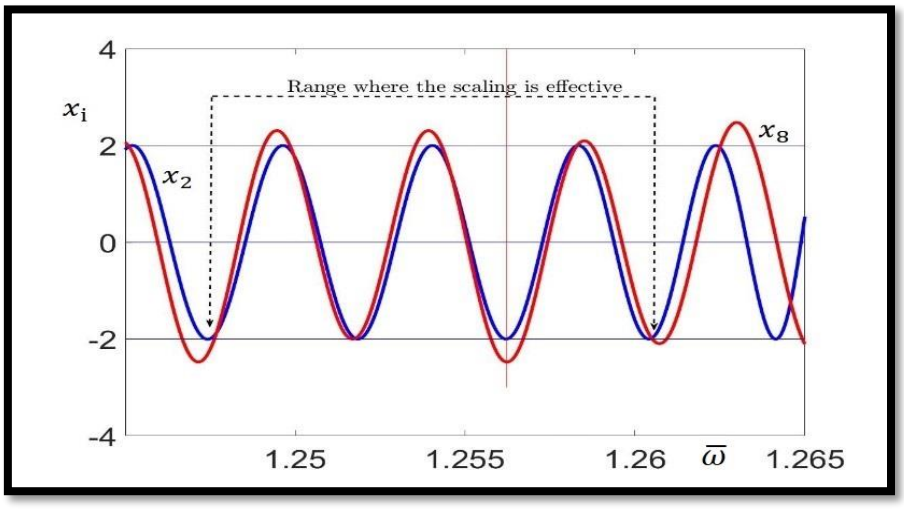

Figure 50: Figure 50: plot of traces $x_2(k\omega)$ and $x_8(\omega)$ (κ = 197.89) in the neighborhood of the point $\bar{\omega} = l_A\sqrt{Q_A}\,\omega = 2\pi/5$ where a 6-point periodic orbit is detected (see Figure. 37).

The operator $\bar{A}_P$ depends on the orbit and examples in this thesis include

$$\bar{A}_2 = J_s(P_5)J_s(P_2) \tag{83}$$

for T_2^S [Eq. (78)]

and

$$\bar{A}_4 = J_s(P_4)J_s(P_6)\,J_s(P_1)J_s(P_3) \tag{84}$$

for T_4^S [Eq. (79)]

where $J_s(P_J)$ is the jacobian matrix (15) evaluated at the saddle point (P_J). The jacobian matrix can deal with the concept of differentiation with coordinate transformation. In other words, if the function is differentiable at a point, its differential is given in coordinates by the jacobian matrix.

Since this class of structures is characterised by two-cycle and four-cycle transformation, we will suffice to derive the Jacobian matrix for two-cycle transformation assuming P_2 is the starting point, taking advantages from the expression (65).

$$A_1 = J_s P_2(-\beta, 0, 0) = \begin{bmatrix} y_i'^2 - 1 & 2y_i'x_i' - z_i' & -y_i' \\ y_i' & x_i' & -1 \\ 0 & 1 & 0 \end{bmatrix} = \begin{bmatrix} -1 & 0 & 0 \\ 0 & -\beta & -1 \\ 0 & 1 & 0 \end{bmatrix}$$

And

$$A_2 = J_s P_5(\beta, 0, 0) = \begin{bmatrix} y_i'^2 - 1 & 2y_i'x_i' - z_i' & -y_i' \\ y_i' & x_i' & -1 \\ 0 & 1 & 0 \end{bmatrix} = \begin{bmatrix} -1 & 0 & 0 \\ 0 & \beta & -1 \\ 0 & 1 & 0 \end{bmatrix}$$

By applying Eq. (83) ,the matrix $\bar{A}_2$ calculated at P_2 as a reference saddle point is

$$\bar{A}_2 = A_2 * A_1 = \begin{bmatrix} 1 & 0 & 0 \\ 0 & -\beta^2 - 1 & -a \\ 0 & -\beta & -1 \end{bmatrix}$$

The matrix of $\bar{A}_2$ can be changed if the reference saddle point changed. However, if we consider P_5 was as the reference saddle point, the matrix $\bar{A}_2$ will be written as

$$\bar{A}_2 = A_1 * A_2 = \begin{bmatrix} 1 & 0 & 0 \\ 0 & -\beta^2 - 1 & a \\ 0 & \beta & -1 \end{bmatrix}.$$

To proceed further, let us focus on the spectral representations of $\bar{A}_2$ and $\bar{A}_4$ that are matrices whose determinants are both unitary. They both share an eigenvalue equal to one that is associated with a unit eigenvector, say g^*. The linearized transformation (83) possess two additional pairs of eigenvalues as illustrated below.

$$k_2^{\pm} = \mp\frac{1}{2}\left[\sqrt{(4 + I(\omega)) * (8 + I(\omega))} + (4 + I(\omega)) + 2\right]. \quad (85)$$

Since $I(\omega) = \beta^2 - 4$, Eq. (85) can be written as follows

$$k_2^{\pm} = -1/2[2 + \beta^2 \pm \beta\sqrt{4 + \beta^2}\,] \quad (86)$$

Similarly, the linearized transformation (84) possesses the following eigenvalues

$$k_4^{\pm} = \left[\sqrt{(3 + I(\omega))^2 - 1} \pm (3 + I(\omega))\right]^2 \quad (87)$$

Since the $I(\omega)$ evaluated at a canonical frequency always vanishes i.e. $I(\omega_{c_{rn}}) = 0$ ($r = 2, 3$).

$$k_4^{\pm} = (2\sqrt{2} \pm 3)^2 \quad (88)$$

It is worthy to point out that the scaling factor $k_2^{\pm}$or $k_4^{\pm}$ can be negative.

In the next section we will see how the scaling κ can be changed at non canonical frequency and still govern the self-similar pattern of stop and pass-band layouts but in certain area as illustrated in Figures 49 and 50. The criterion used to determine the area in which the scaling is effective is the extent to which the behavior of the three consecutive traces is similar in that area.

The scaling factor can predict pass and band gab width for different families of canonical structures. In silver structure family no.1, we can compare the pass (stop) bands width of sequence F_i and F_{i+2} using the scaling factor. For family no. 2,3, which are characterised by four-cycle transformations, the comparison will be between F_i and F_{i+4}.

It has to be noted that $k_P^+ = 1/k_P^-$ (P = 2, 4) and $k_4^+ = \sigma_s^4$. We indicate the unit eigenvector related to k_P^+ (resp. k_P^-) as g^+ (resp. g^-). k_P^+ is usually much larger than the other two eigenvalues and its value will be also indicated from now as k_P, or simply k, as there is no risk of confusing it with another quantity. Imagine now to decompose δr_i with respect to the basis $\{g^+, g^-, g^*\}$ as $\delta r_i = \xi^+ g^+ + \xi^- g^- + \xi^* g^*$.

Therefore, by applying Eq. (80), it turns out that:

$$\acute{r}_{i+P} = \bar{A}_P \, \delta r_i = k_P \xi^+ g^+ + \xi^- g^- / k_P + \xi^* g^*. \tag{89}$$

Due to the dominance of the highest eigenvalue, we can ignore some parts from the above equation and rewrite it as follows

$$\delta\acute{r}_{i+P} \approx k_P \xi^+ g^+ \approx k_P \delta r_i \tag{90}$$

Note that, due to the fact that we are analysing a saddle point, eigenvector $g^*$is orthogonal to the tangent plane at $P_{\bar{j}}$ whereas the other two eigenvectors span the tangent plane. Therefore, vector $k_P \xi^+ g^+$ belongs to the tangent plane itself. For periodic orbits other than those originating in the neighbourhood of a saddle point, the methodology is similar and based on the linearisation about one of the point of the orbit.

Examples of the interpretation of the linearization of the trace map as a method to explain scaling of the frequency spectra of canonical SM rods are reported in Figures 49 and 53, which analyse self-similar portions of the stop-/pass-band layouts displayed in Figures 44 and 45, respectively. In detail, in Figure 49(a) the neighbourhood of the canonical frequency ($2 l_A \sqrt{Q_A}\, \omega_{c1} = \pi/2$), at which a 2-point periodic orbit occurs, is investigated. With reference to the linearisation procedure, the involved saddle point is here $P_{\bar{j}} = P_2$, where the two vanishing coordinates correspond to x_2 and x_3 . To the first order, vector $\delta r_2(\delta\omega) = \bar{R}_2 - P_2$ can be written as

$$\delta r_2(\delta\omega) = \gamma(\delta\omega), \tag{91}$$

where $\gamma = grad\ \delta r_2$. Approximation (91) lies in the tangent plane spanned by coordinates x_2 and x_3 , therefore, we can say that, in the neighbourhood of the canonical frequency,

$x_2 \approx \gamma_2\, \delta\omega$ and $x_3 \approx \gamma_3\, \delta\omega$, where γ_k (k = 2, 3) are the projections of vector γ onto axes x_k (k = 2, 3).

Focusing on x_2 , it is clear that after a 2-point cycle, Eq.(90) leads to $x_4 \approx k\gamma_2\, \delta\omega$ and, by repeating the cycle, $x_6 \approx k^2 \gamma_2$. This is exactly what is reported in Figure 49(a) where traces x_2 , x_4 , x_6 are scaled accordingly by using the factor $k_2^+ = -8.127$ evaluated for β = 2.5); the

only difference is that the frequency range reported on the horizontal axis pertains strictly to x_4 , therefore x_2 is scaled and plotted as $x_2\ (k\omega)$, whereas x_6 is plotted as $x_6\ (\omega/k)$. It is evident that within the range comprised within the brace in the Figure 49, the scaling of traces explains quantitatively very well their behaviour about the canonical frequency. As a consequence, the stop-/pass-band layout can be predicted through scaling about the canonical frequency, as shown on top of Figure 49(a). Note that in this case, and for all canonical SM rods belonging to Family no. 1, the scaling factor can be negative. For Figure 49(b), similar comments can be made, here the focus is the neighborhood of frequency $\bar{\omega} = \pi/5$, where a 6-point periodic orbit is detected. Therefore, the two represented traces are $x_8\ (\omega)$ and the scaled $x_2\ (k\omega)$, where this time the multiplicative factor is $k_2^+ = \sigma_s^6 = 197.89$.

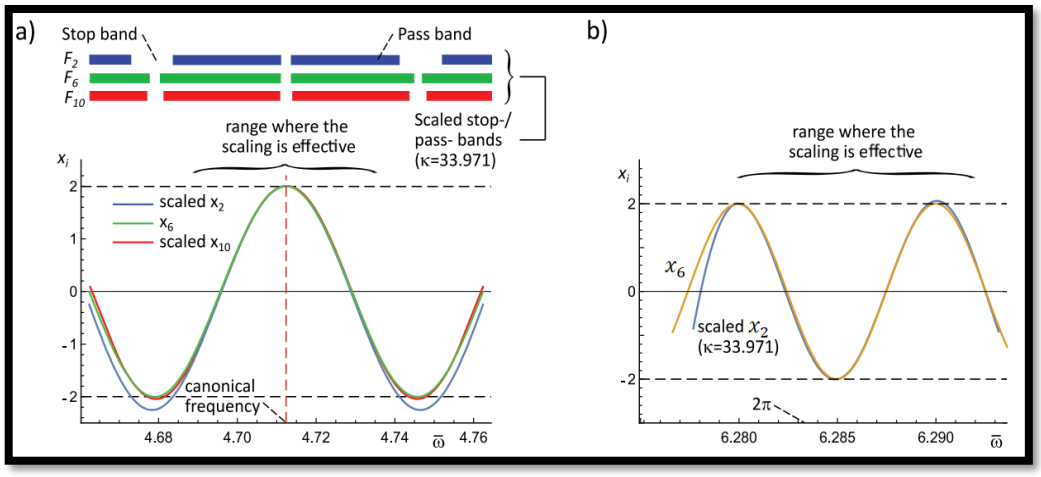

Figure 51: Canonical SM rod with $C_3 = 2/3$ (Family no. 3). (a) Plot of traces $x_2\ (k\omega)$, $x_6\ (\omega)$, $x_{10}\ (\omega/k)$ (κ = 33.971) in the neighbourhood of the canonical frequency [$2l_A\sqrt{Q_A}\,\omega_{c3} = 3\pi/2$] (b) plot of traces $x_2\ (k\omega)$ and $x_6\ (\omega)$ (κ = 33.971) in the neighbourhood of the point $\bar{\omega} = = 2l_A\sqrt{Q_A}\,\omega = 2\pi$ where a 4-point periodic orbit is detected (see Figure 36): (Farhat et al, 2022).

The Figures 52 and 53 below show the behaviour of the traces without and with the scaling factor. It is clear that the scaling is effective in the period $\bar{\omega}$ from 0 to 2.9.

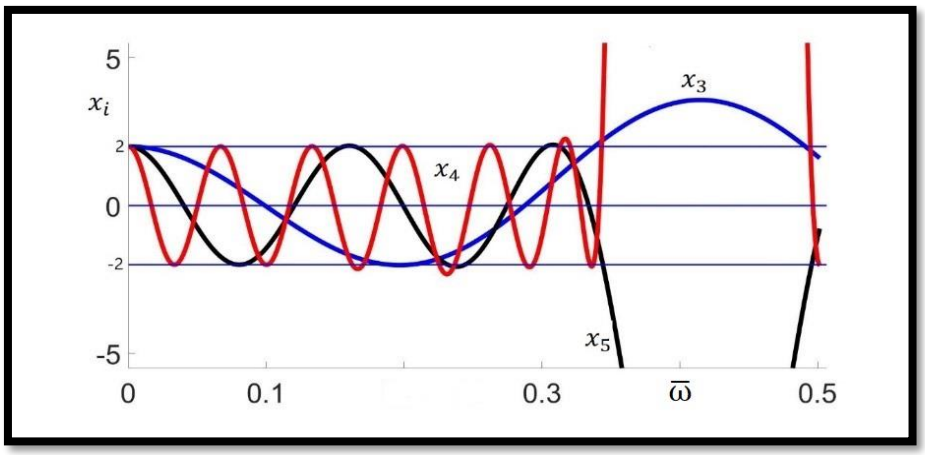

Figure 52: Canonical SM rod with $C_1 = 5$ (Family no. 1): plot of traces $x_3\ (\omega), x_4(\omega), x_5\ (\omega)$,and $x_6(\omega)$ in the neighbourhood of ω =0 where a fixed-point orbit, R_0 = (2, 2, 2) is present. plots of x_5 and x_6 are almost indistinguishable.

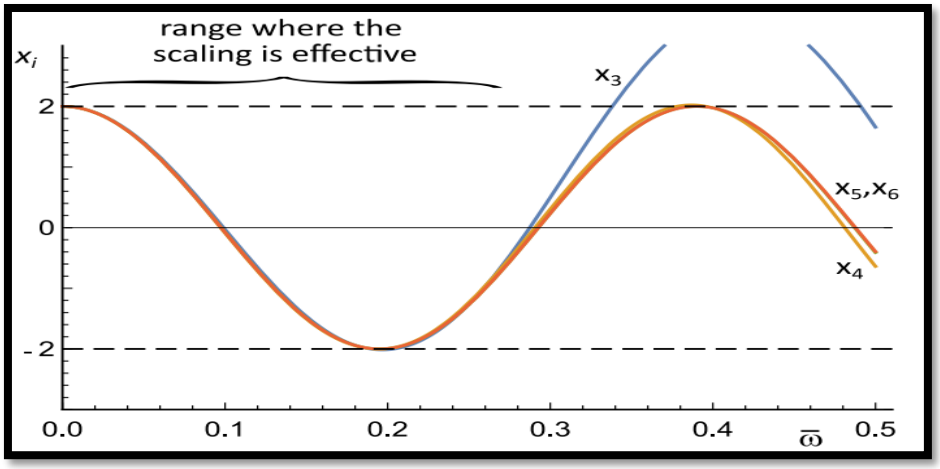

Figure 53: Canonical SM rod with $C_1 = 5$ (Family no. 1): plot of traces $x_3\ (\omega), x_4(\omega/k), x_5(\omega/k^2), x_6(\omega/k^3)$ $(k = \sigma_s)$ in the neighborhood of $\omega = 0$ where a fixed-point orbit, $R_0 = (2, 2, 2)$ is present. The plots of x_5 and x_6 are almost indistinguishable: (Farhat et al, 2022).

Figure 51(a) covers the case belonging to Family no. 3 reported in Figure 45, where the canonical frequency ($2l_A\sqrt{Q_A}\ \omega_{c3} = 3\pi/2$) is the locus of a 4-point periodic orbit. Therefore, the represented traces are $x_6\ (\omega)$, $x_2\ (k\omega)$ and $x_{10}\ (\omega/k)$ with $k = \sigma_s^4$ = 33.971 (Eq. (88)). The feature that distinguishes this example from that in Figure 49(a) is that the function x_2 evaluated at ω_{c3} is not null. I will show however that the scaling factor between the chosen three traces is still κ despite the fact that they are not linear functions of circular frequency in the vicinity of ω_{c3}. The involved saddle point is now P_1 that should be better seen as the point of Kohmoto's surface whose coordinates are $(t_4\ , x_3\ , x_2\ )_{|\omega=\omega_{c3}}$ = (0, 0, 2). On the one hand, following the argument presented before, about the canonical frequency, t_4 and x_3 are linear in the frequency, then $t_4 = \eta_4\ \delta\omega$ and $x_3 = \gamma_3\ \delta\omega$; on the other hand, at the lowest order, x_2 can be approximated as $x_2 \approx 2 - \zeta_2\delta\omega^2$ and the invariant as $I \approx \delta\omega^2$ as it can be easy inferred with a Taylor expansion of (66).

The use of the above approximations still in (66) yields, to the leading (second) order,

$$\delta\omega^2 = (\eta_4\ \delta\omega)^2 + (\gamma_3\ \delta\omega)^2 - 4\zeta_2\delta\omega^2 - 2\eta_4\gamma_3\delta\omega^2, \qquad (92)$$

and, finally,

$$4\zeta_2 = (\eta_4 - \gamma_3)^2 - 1\ , \qquad (93)$$

which is a consequence of the recursive relationships between adjacent traces.

Let us turn now our attention to the same saddle point, but evaluated after a cycle of four applications of the trace map, i.e. $(t_8, x_7, x_6)_{|\omega=\omega_{c3}}$ = (0, 0, 2). By following the same argument, we can write

$t_8 = \eta_8\, \delta\omega$, $x_7 = \gamma_7\, \delta\omega$ and $x_6 \approx 2 - \zeta_6 \delta\omega^2$

where

$$\eta_8 = k\eta_4 \text{ and } \gamma_7 = k\gamma_3 \tag{94}$$

and the overbar will be added to the independent variable because we need to consider a scaled domain. Our goal is to find the connection between ζ_2 and ζ_6 through the factor κ.

In particular, note that in analogy to the case illustrated in Figure 49(a), x_7 (resp. t_8) matches x_3 (resp. $t4$) if $\delta\omega = \delta\omega/k$. Therefore, we can again consider Eq. (92) and substitute the terms of the r.h.s. with those expressed as a function of $\overline{\delta\omega}$, i.e.

$$\overline{\delta\omega}^2 = (\eta_8\overline{\delta\omega})^2 + (\gamma_7\overline{\delta\omega})^2 - 4\zeta_6\overline{\delta\omega}^2 - 2\eta_8\zeta_7\overline{\delta\omega}^2. \tag{95}$$

Updating the l.h.s. of Eq. (95) using $\delta\omega = k\overline{\delta\omega}$ and employing (94) yields

$$k^2\,[(\eta_4 - \gamma_3)^2]/4 = \zeta_6, \tag{96}$$

which transforms to $k^2\zeta_2 = \zeta_6$ with the help of Eq. (93). Therefore, we have proofed our conjecture; k enters as a square as it is associated with a second-order term in the Taylor expansion. Note that for the parameters selected in Fig. (51a), ζ_6 = 8867.11 and ζ_2 = 7.778 whose ratio has square root equal to 33.76, a value very close to k. In Fig (51b), the neighbourhood of $\bar{\omega} = 2\pi$ is analysed. As at this frequency a 4-point periodic orbit takes place, trace x_6 (ω) and the scaled one x_2 $(k\omega)$ are sketched where k = 33.971 is still the scaling factor obtained from the linearisation of the trace map.

Figure 53 illustrates the effectiveness of the presented method to explain scaling by sketching the plots of the functions of four scaled traces (x_3 to x_6, the represented domain is that of the function x_3 (ω)) at the origin (ω = 0) where a fixed-point orbit is present (see case i) in section 4.3. The scaling factor is now $k = \sigma_s$.

4.5 Summary

I investigated propagation of harmonic axial waves in particular class of periodic two-phase phononic rods whose elementary cells are generated adopting the quasi-crystalline silver mean Fibonacci substitution rule. The stop-/pass-band spectra of this family are studied with the aid of a trace map formalism which provides a geometrical interpretation of the recursive rule governing traces of the relevant transfer matrices: the traces of two consecutive elementary cells can be represented as a point on a surface defined by an invariant function of the circular frequency, and the recursivity implies the description of an orbit on the surface. I illustrated that, for a sub-class of silver mean-generated waveguides, the orbits predicted by the trace map at specific frequencies are periodic for all families. The configurations for which this occurs, called canonical, are also associated with periodic stop-/pass-band diagrams along the frequency domain. Several types of periodic orbits can be found and each corresponds to a self-similar portion of the dynamic spectra whose scaling law can be studied by linearising the trace map in the neighbourhood of the orbit. The scaling factor can be negative and changed at non canonical frequency and still govern the self-similar pattern of stop and pass-band layouts but in certain area.

Chapter 5: Comparative analysis between Golden and Silver mean rods.

5.1 Overview

In this chapter, I will compare the propagation of harmonic axial waves in a class of periodic two-phase phononic rods whose elementary cells are built adopting the Fibonacci golden sequence with their silver counterpart for *canonical structure* using the same tools used in Chapter Four, related to the propagation of waves in silver rods, which were also used by Morini and Gei in their research related to the propagation of waves in golden rods. The stop/pass band spectra of these structures are studied with the aid of a trace-map formalism which provides a geometrical interpretation of the recursive rule governing traces of the relevant transfer matrices. I will show that silver mean rods show a greater number of band gabs than golden mean rods.

5.2 One-dimensional generalised Fibonacci Golden (Silver) Mean rods

The elementary cells of Fibonacci golden mean sequence obey to the general substitution rule $F_i = F_{i-1}F_{i-2}$.

F_2=AB, F_3=ABA F_4=ABAAB

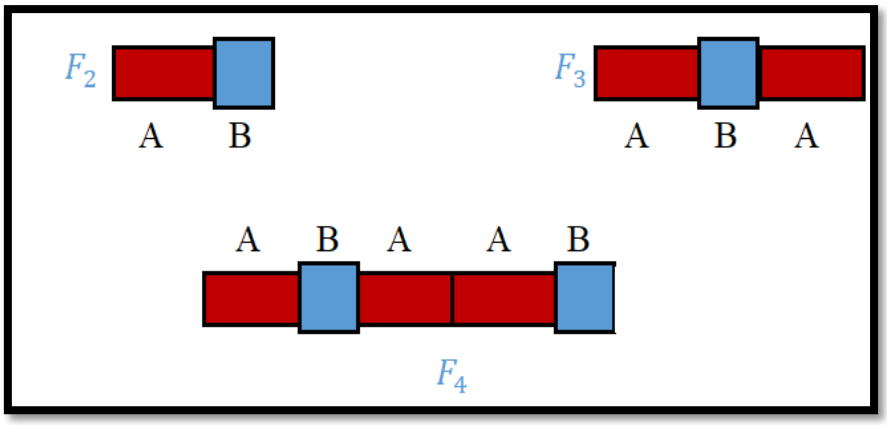

Figure 54: Representative elementary cells for periodic Golden-mean phononic rods.

In contrast, the elementary cells of Fibonacci silver mean sequence obey to the general substitution rule: $F_i = F^2{}_{i-1}F_{i-2}$.

F_2=AAB, F_3=AABAABA, F_4= AABAABAAABAABAAAB.

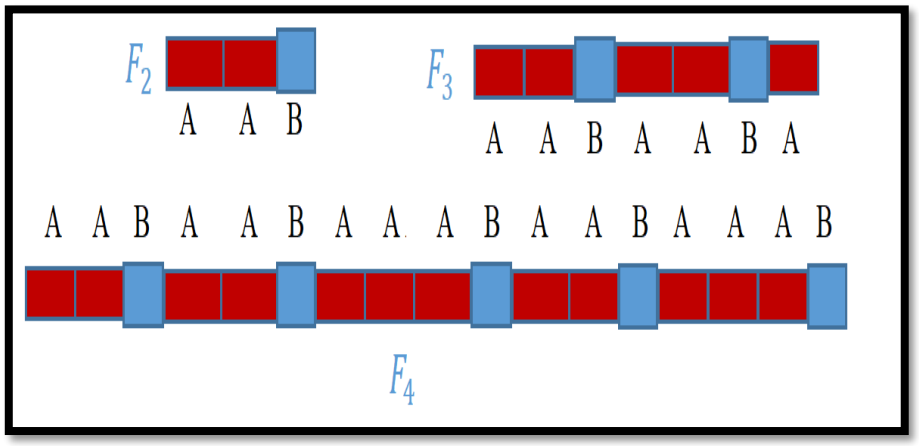

Figure 55:Representative elementary cells for periodic silver-mean phononic rods.

The following Figures refer to the traces of the transfer matrix obtained for both GM and SM rods whose parameters belong to $Q_B/Q_A = 1$, $E_B/E_A = 1$, $S_B/S_A = 1/2$, $l_B/l_A = C_1$ ($C_1 = 1{,}3$)

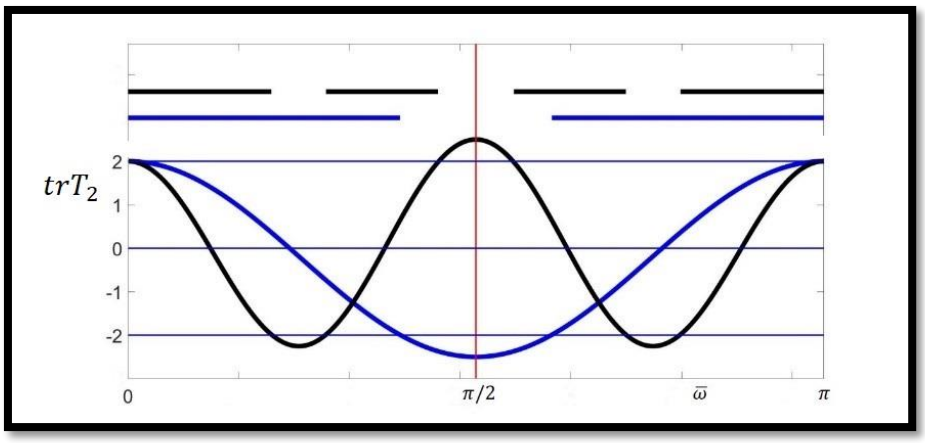

Figure 56: Traces (curves) and pass/ stop band(dashed lines)of the sequence F_2 *for GM rods assuming family one (* $C_1 = 1$, *blue colour,* $C_1 = 3$ *black colour)* $E_A = E_B$, $\frac{Q_B}{Q_A} = 1$, $S_B/S_A = 1/2$ *.The red vertical line is the canonical frequency.*

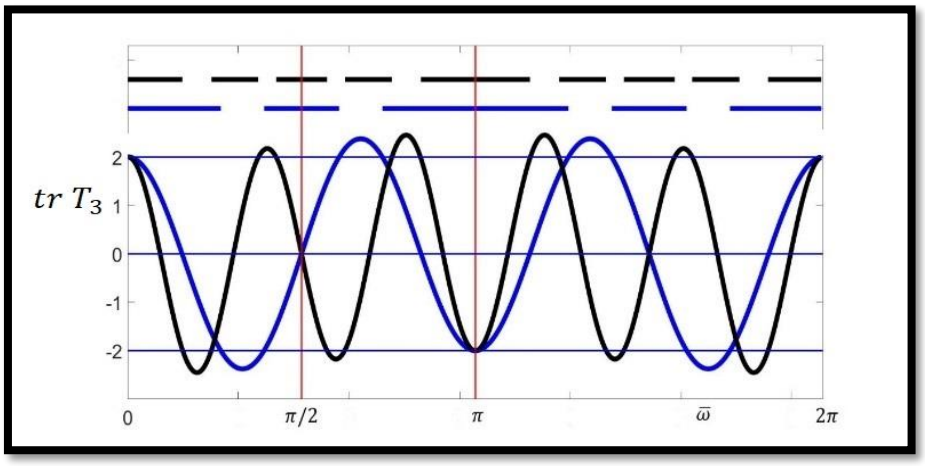

Figure 57: Traces (curves) and pass/ stop band(dashed lines) of sequence F_3 for GM rods assuming family one ($C_1 = 1$, blue colour, $C_1 = 3$ black colour) $E_A = E_B$, $\frac{Q_B}{Q_A} = 1$, $S_B/S_A = 1/2$ .The red vertical line at $\bar{\omega} = \pi/2$ is the canonical frequency and the red vertical line at $\bar{\omega} = \pi$ indicates the half interval.

For GMSs and SMSs, the analysed sequences in Figure 58 are F_2 to F_6. Here, we show that the group of stop/pass band diagrams exhibit a self-similar pattern for all sequences, where the pattern of the spectra is similar for each area of pass stop diagram. In other words, the number of pass bands in each area of the diagram is equal, for example the number of pass bands for Golden or Silver around the canonical frequency is the same number of pass band in area left or right the canonical frequency. However, the 'match' between patterns improves at increasing index i. In addition, the distribution of pass/ stop band is divided into two equal halves at the canonical frequency which is located in the middle of the interval (have interval) for the sequences $F_{2,5,8}$ ($F_{3,4,6,7}$). Moreover, not all GM sequences have the same periodicity, as we find that the sequences $F_{2,5,8}$ that are characterized by stop band around the canonical frequency have a periodicity ends at π, while the sequences $F_{3,4,6,7}$ that are characterized by pass band around the canonical frequency have a periodicity ends at 2π.

In addition, each pass band will split into a number of smaller pass bands in the subsequent row to create additional stop band that obey the recursive rule of Fibonacci numbers, n_i, i.e. 1, 1, 2, 3, 5,8, . . . for golden and n_i, i.e. 1, 1, 3, 7, 17,41,. . . for silver as illustrated in table (4). Moreover, the number of pass bands for a generic sequence F_i is equal to n_i, and the number of band gaps equals $n_i - 1$. Note that the value of $I(\omega)$= 2.25.

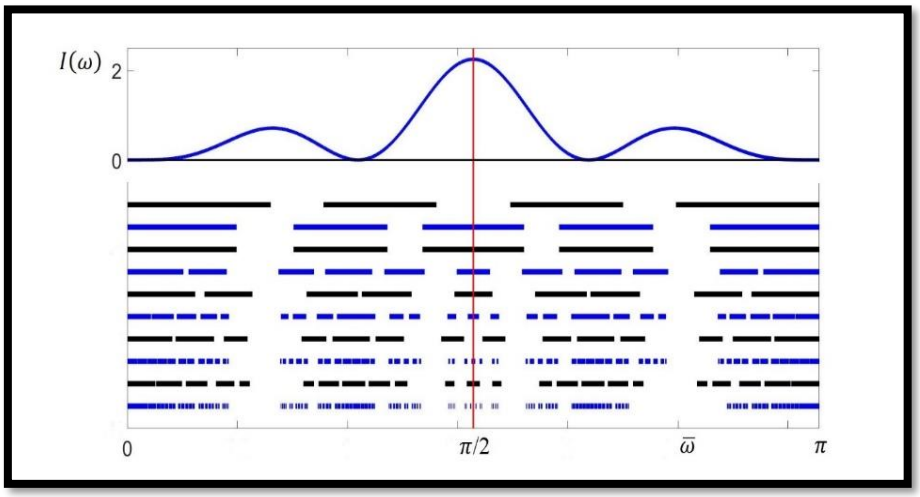

Figure 58: Kohmoto's invariant (top sketch) and Pass/Stop band diagram corresponding to elementary cells F_2 to F_6 for golden sequences (black horizontal cut-off lines) and silver sequences (blue horizontal cut-off lines) assuming family one C_1 =3, $E_A = E_B$, $\rho_A = \rho_B$, $A_A/A_B = 0.5$, the red vertical line is the canonical frequency.

The table below shows the regular number of pass band in each area of the pass stop band diagram obtained in Figure 58. The regular pattern of pass/stop diagram can be explained by the regular number of the pass band. However, this regular patter is clear for GM sequences, but for Silver Mean sequences, it will be also clear at increasing index i with very small interval of ω to allow very small pass/stop bands to be seen.

F_i	*Golden: (Pass band number)*	*Silver: (Pass band number)*
F_2	*1*	*1*
F_3	*1*	*1*
F_4	*2*	*3*
F_5	*3*	*7*
F_6	*5*	*17*

Table 4: The number of Pass band in Golden and Silver mean structures assuming family one C_1 =3, $E_A = E_B$, $\rho_A = \rho_B$, $A_A/A_B = 0.5$.

5.3 Scaling and self-similarity of the frequency spectra of canonical GM (SM) rods and periodic orbit

The scaling factor is useful in predicting the width of pass and stop band for different families of canonical structures. For golden structures, we can compare the pass or band gab width of sequence F_i with sequence F_{i+6} using the scaling factor. In silver structure, the comparison is between F_i and F_{i+2} (family no.1) as illustrated in the table (5). This comparison can be at any frequency range not only at the canonical frequency. In other words, for high sequence F_i, we can predict the width of pass or stop band using the scaling factor.

Here we will compare the accuracy of the scaling of the frequency spectra of GM rods against SM counterpart assuming family one C_1 =3.

According to Farhat et al (2021) and Morini and Gei (2018), the scaling factor of GM

$$k_g^{\pm} = \frac{1}{4}\left[\sqrt{4 + (4 + I(\omega))^2} \pm (4 + I(\omega))\right]^2$$

Or

$$k_g^{+} = \frac{1}{4}\left[\sqrt{4 + (4 + I(\omega))^2} + (4 + I(\omega))\right]^2 = 41$$

And for SM rods is

$$k_s^{\pm} = \mp\frac{1}{2}\left[\sqrt{(4 + I(\omega)) * (8 + I(\omega))} + (4 + I(\omega)) + 2\right]$$

Or

$$k_s^{+} = -\frac{1}{2}\left[\sqrt{\left(4 + I(\omega)\right) * \left(8 + I(\omega)\right)} + \left(4 + I(\omega)\right) + 2\right] = -8.127$$

GM scaling ratio: $\frac{\Delta\omega_i^g}{\Delta\omega_{i+6}^g}$	*SM scaling ratio:* $\frac{\Delta\omega_i^s}{\Delta\omega_{i+2}^s}$	$Error(\Delta^s) = \lvert k_s^+ \rvert - \frac{\Delta\omega_i^s}{\Delta\omega_{i+2}^s}$
$\frac{\Delta\omega_3^g}{\Delta\omega_9^g} = 45$	$\frac{\Delta\omega_2^s}{\Delta\omega_4^s} = 8.8$	*0.67*
$\frac{\Delta\omega_4^g}{\Delta\omega_{10}^g} = 42.9$	$\frac{\Delta\omega_3^s}{\Delta\omega_5^s} = 8.4$	0.273
$\frac{\Delta\omega_6^g}{\Delta\omega_{12}^g} = 42.2$	$\frac{\Delta\omega_4^s}{\Delta\omega_6^s} = 8.1$	0.027

Table 5: The scaling ratios of GM and SM sequences at the canonical frequency assuming family one $C_1 = 3$, $E_A = E_B$, $\frac{Q_B}{Q_A} = 1$, $S_B/S_A = 1/2$.

As we mentioned earlier that GM rods are characterized by six-cycle transformation and SM rods (Family no.1) are characterized by two-cycle transformation, the table above gives a comparison of the accuracy of the scaling ratio for pass band lengths at the canonical frequency between GM and SM rods. In addition, the scaling ratio of GM sequences which is $\frac{\Delta\omega_i^G}{\Delta\omega_{i+6}^G}$ is very close to the eigenvalue $k_g^+ = 41$ especially at high indices of i, while the scaling ratio of SM sequences which is $\frac{\Delta\omega_i^s}{\Delta\omega_{i+2}^s}$ is also very close to the absolute value $|k_s^+|$.

In contrast, the scaling ratios of SM rods gave high accuracy as the index i increases, for instance the scaling ratio at the third cycle $\frac{\Delta\omega_4^s}{\Delta\omega_6^s} = 8.1$, which is 99.7% of 8.127, while the scaling ratios of GM rods shown less accuracy which is 97% at the same cycle. The reason for this, as mentioned previously, is that the number of elements in silver sequences is greater than their golden counterparts which makes that the third sequence, for example, in silver almost

represents an advanced sequence in its golden counterpart. However, both structures give high accuracy in terms of scaling ratios compared to the eigenvalues.

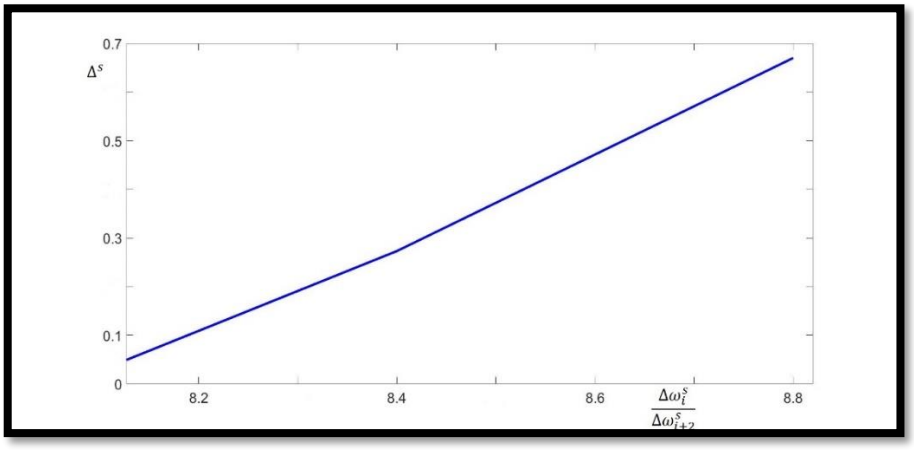

Figure 59: Silver mean scaling ratios VS. Error.

5.3.1Periodic orbits

In this section, we will show the periodic orbits of Golden and Silver mean rods separately, then we will mention the common orbits between them.

i. Golden mean rods periodic orbits

At the canonical frequency, 6-point periodic orbit is

$P_5(0,\ 0,\ 2.5) \xrightarrow{T_s} P_6(0,\ 2.5,\ 0) \xrightarrow{T_s} P_1\ (0,\ 0,\ 2.5) \xrightarrow{T_s} P_2(\ -2.5,\ 0,\ 0) \xrightarrow{T_s} P_3\ (\ 0,\ -2.5,\ 0) \xrightarrow{T_s} P_4(0,\ 0,\ -2.5)$.

At non-canonical frequencies ω such that $I(\omega) = 0$, there are additional periodic orbits can be found. This may occur in a large variety of cases depending on the value of C that are however not classified here.

At $\bar{\omega} = 2\pi/3$, 4-point periodic orbit is

$R_1(-1,\ -1,\ 2) \xrightarrow{T} R_2(-1,\ -1,\ -1) \xrightarrow{T} R_3\ (2,\ -1,\ -1) \xrightarrow{T} R_4(-1,\ 2,\ -1)$.

ii. Silver mean rods periodic orbits

At the canonical frequency, 6-point periodic orbit is

$P_2(-2.5,\ 0,\ 0) \xrightarrow{T_s} P_5(2.5,\ 0,\ 0) \xrightarrow{T_s} P_5$.

Additional periodic orbit for SM rods were classified in the chapter 4, at $\bar{\omega} = p\ \pi\ /5$: ($p$ = 1, . . . , 4) as the function $I(\omega_{c_1})$=0 which are all 6-point periodic

The following cases are universal (valid for GM and SM rods).

the pair $x_0 = x_1 = 2$ can be found at the endpoints of the interval where traces are periodic, namely at $\omega = 0, 4\ \omega_c$; therefore, $R_i = (2, 2, 2), \forall_i$, corresponding to a fixed-point orbit, i.e. $T_{g,s1}(R_i) = R_i$; (i.e., valid for all three Families of canonical GM (SM) rods)

Other periodic orbits can be found for family .1 at $\omega = 2\omega_c$, $x_0 = x_1 = -2$, then $R_i = (2, -2, -2)$ corresponding to a fixed-point which is fixed-point orbit, i.e., $T_{g,s1}(R_i) = R_i$.

5.4 Summery

Comparative analysis between Golden and Silver mean rods for axial waves has been done.

The number of band gabs in silver mean rods is greater than its golden counterpart, which can be useful in several applications such as wave filters.

I have shown the distribution of pass bands follows a self-similar law when the index i of the generation sequence F_i increases. This property can be recognized at the area around the canonical frequency and other areas left or right the canonical frequency. Since the number of elements in SM sequences is greater than their GM counterpart, the scaling ratios of SM rods gave high accuracy as the index i increases than its GM counterpart. This Comparative analysis between Golden and Silver mean rods gives the designers of acoustic devices boarder options in choosing the best sequence that achieve the desired results.

Chapter 6: Effects of pre-stress on dispersive properties of flexural waves in multi-supported beam

6.1 Overview

The widespread use of phononic systems with periodic structures such as rods, plates and beams is due to the filtrations properties presented by these materials that can be exploited in many applications such as design of filters, waveguides and resonators (Brun et al, 2010; Shmuel and Band, 2016; Trainiti et al, 2019). The feature of stop band or so called band gap in periodic structures has been studied and exploited by many researchers starting from Cremer and Leilich in the year of 1953.

Mead in his work focused mainly on methods developed at the University of Southampton to analyse and predict the free and forced wave propagation in continuous periodic engineering structures (Mead,1996). Research conducted recently by (Morini and Gei, 2018) studied the features of self-similarity of the distribution of stop/pass bands in periodic structures.

According to previous studies on the effect of pre-stress on the dispersion properties of Bloch–Floquet elastic waves in the periodic structures, including (Gei et al, 2009; Gei, 2010), the presence of pre-stress has a noticeable effect, especially on the dynamic properties. One of these affected properties is the changes in the width of band gaps. However, the effect of pre-stress on the filtering properties for both pass and band gaps need to be studied deeply. In this chapter, we will focus in more details on the effect of pre-stress on the dispersion diagram, taking the advantages of the preliminary results achieved by Gei (2010).

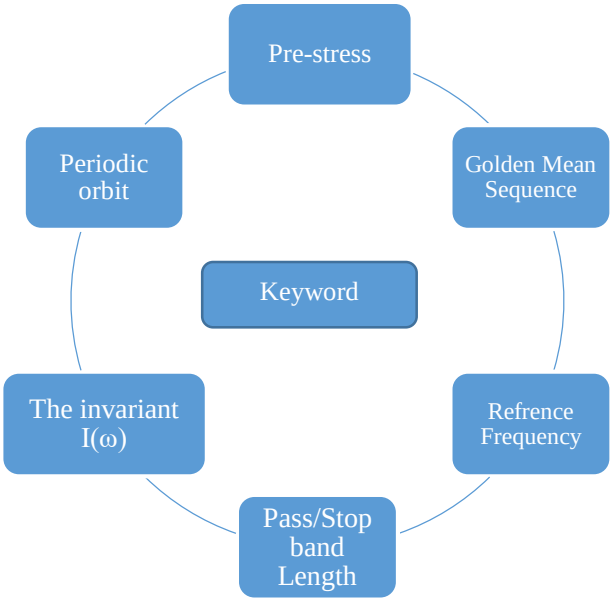

Figure 60: Chapter five keyword..

6.2 Multi-supported beam generated according to Fibonacci Golden Mean rule

I now investigate the role of the pre-stress in changing the dispersion diagrams for flexural waves of quasiperiodic Multi-supported beam. The structure is created by the repetition of the elementary cell produced adopting the Fibonacci sequence, based on the primary sequence commonly known as Golden mean. In this section, we will focus in details on the effect of pre-stress on the width of pass/stop band by assuming a different value of pre-stress (tensile, null, compressive).

6.3 Mathematical Model of the quasiperiodic beam

Consider a particular class of infinite, one-dimensional, two-component quasiperiodic phononic beam consisting of a repeated elementary cell based on a particular position of supports as illustrated in the Figure 61 where two distinct phases, say *A* and *B*, are arranged in series according to the so-called Golden Mean (GM) sequence. We can also create this structure using Silver Mean (SM) sequence.

Based on the following substitution rule, the prototype structure represented in Figure 61 has been obtained and its elements are as mentioned above *A* and *B*.

$$A \rightarrow AB,\ B \rightarrow A. \tag{97}$$

Expression (97) implies that element of $i-th$ order of the sequence (i = 0, 1, 2, . . .), here denoted by F_i, obeys the recursive rule

$$F_i = F^1{}_{i-1} F^1_{i-2} \tag{98}$$

with initial conditions $F_0 = B$ and $F_1 = A$. This means that for any index (i), the corresponding Fibonacci cell will be easy formed. An example is:

$F_2 = AB$, $F_3 = ABA$.

where the notation F_i will also indicate from now on the elementary cell of the structured beam. The total number of elements of F_i corresponds to the generalised Fibonacci number n_i given by the recursive relation $n_i = n_{i-1} + n_{i-2}$, with $i \geq 2$ and $n_0 = n_1 = 1$. The limit $\sigma = lim_{i\to\infty} \frac{n_{i+1}}{n_i}$ corresponds to the Golden mean ratio $\sigma_g = \frac{1+\sqrt{5}}{2}$ that is corresponding to the golden ratio σ_g=1. 618.

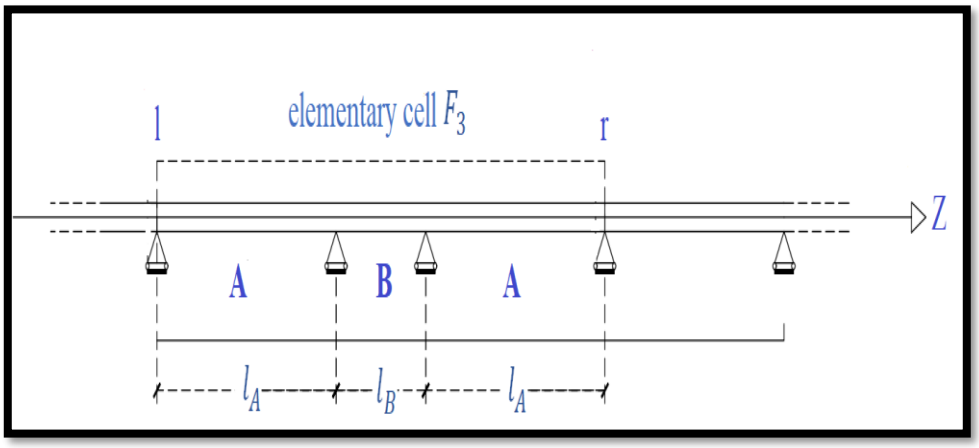

Figure 61: flexural vibrations of a quasiperiodic beam: elementary cell for the sequence F_3. Symbols r and l denote right and left-hand boundaries of the elementary cell.

The structure which is a homogeneous beam is subjected to pre-stress and bending stiffness donated by *N* and *S* respectively where the variations in these important parameters affect the dispersion diagrams. The pre-stress is associated with the switch of the spectrum and an initial band gap. If the pre-stress is compressive the spectrum will move in one direction whereas the tensile load will move the spectrum in the opposite direction. The quasi-periodicity is given now by the specific position of supports along the beam axis. The two-component GM sequence belongs to the family of patterns commonly known as one dimensional generalized Fibonacci tilings (Kolar and Ali, 1989).

The physical and geometrical properties of phases *A* and *B* are l_A and l_B represent the lengths of the elements *A* and *B* respectively while mass density per unit length of each element for beam segments is donated by ρ. The variation of the mass density of the two phases will affect the pass stop band diagram.

The governing equation of flexural waves along the longitudinal axis $\mathcal{Z}$ in each phase of beam is as follows:

$$Sv'''' - Nv'' - \rho\omega^2 v = 0 \qquad (99)$$

where ω is the circular frequency and v is the vertical displacement while r is the radius of gyration of the cross section of the beam and thus the following dimensionless parameters can be written as follows

$$\bar{N} = \frac{Nr^2}{S}, \; P = \frac{\rho r^4}{S} \qquad (100)$$

The general solution for Eq. (99) yields the form

$$(kr)^4 - \bar{N}(kr)^2 - P\omega^2 = 0 \qquad (101)$$

Four solution can be derived for the variable k from the Eq. (101) as follows

$$k_{1,2} = \pm\frac{1}{r}\left[-\frac{\bar{N}}{2}+\sqrt{\frac{\bar{N}^2}{4}+P\omega^2}\,\right]^{1/2}$$

$$k_{3,4} = \pm\frac{1}{r}\left[-\frac{\bar{N}}{2}-\sqrt{\frac{\bar{N}^2}{4}+P\omega^2}\,\right]^{1/2} \quad (102)$$

I will follow the same procedure as (Gei, 2010) to obtain the dispersion diagram of the flexural beam. To this end, the transmission matrix M_i of the cell of the sequence F_i can be derived if rotation $\phi(\mathcal{Z})$ and its derivative $\phi'(\mathcal{Z})$ at each constrained point are known.

Now we have

$$\phi_l' = k_1^2\mathrm{A}+k_1^2\mathrm{B}+k_3^2\mathrm{C}+k_3^2\mathrm{D} \quad (103)$$

$$\phi_r' = k_1^2\, e^{\,ik_1^2}\,\mathrm{A}+k_1^2\, e^{\,-ik_1^2}\,\mathrm{B}+k_3^2 e^{\,ik_3^2}\,\mathrm{C}+k_3^2\, e^{\,-ik_3^2}\,\mathrm{D} \quad (104)$$

By substituting A, B, C and D and applying Floquet-Bloch theory, we will have

$$\begin{bmatrix}\phi_l'\\ \phi_r'\end{bmatrix} = M\begin{bmatrix}\phi_l\\ \phi_r\end{bmatrix} \quad (105)$$

$$\begin{bmatrix}\phi_l\\ \phi_r\end{bmatrix} = \Psi\begin{bmatrix}\phi_l'\\ \phi_r'\end{bmatrix} \text{ where } \Psi = M^{-1} = \begin{bmatrix}\Psi_{AA} & \Psi_{AB}\\ \Psi_{BA} & \Psi_{BB}\end{bmatrix} \quad (106)$$

The following quantities depends on the circular frequency and pre-stress through k_1 and k_3 that are given by Eq. (102) through the sign + as follows.

$$\Psi_{AA}^X = \frac{\boldsymbol{k_1}\cot(\boldsymbol{k_1 l_X})-\boldsymbol{k_1}\cot(\boldsymbol{k_3 l_X})}{K_3^2-K_1^2}$$

$$\Psi_{BB}^X = \frac{\boldsymbol{k_1}\cot(\boldsymbol{k_1 l_X})-\boldsymbol{k_3}\cot(\boldsymbol{k_3 l_X})}{K_1^2-K_3^2}$$

$$\Psi_{AB}^X = \frac{\boldsymbol{k_1}\csc(\boldsymbol{k_1 l_X})-\boldsymbol{k_1}\csc(\boldsymbol{k_3 l_X})}{K_1^2-K_3^2}$$

$$\Psi_{BA}^X = \frac{\boldsymbol{k_1}\csc(\boldsymbol{k_1 l_X})-\boldsymbol{k_1}\csc(\boldsymbol{k_3 l_X})}{K_3^2-K_1^2} \quad (107)$$

and then

$$\phi_l = \Psi_{AA}^X * \phi_l' + \Psi_{AB}^X * \phi_r' \Rightarrow \phi_r' = \frac{\phi_l}{\Psi_{AB}^X} - \frac{\Psi_{AA}^X}{\Psi_{AB}^X}\,\phi_l'$$

$$\phi_0 = \Psi_{BA}^X * \phi_l' + \Psi_{BB}^X * \phi_r'$$

$$\phi_r' * \Psi_{AB}^X = \phi_l - \Psi_{AA}^X * \phi_l' \Rightarrow \phi_r = \frac{\Psi_{BB}^X}{\Psi_{AB}^X}\phi_l + (\Psi_{BA}^X - \frac{\Psi_{BB}^X \Psi_{AA}^X}{\Psi_{AB}^X})\phi_r'$$

From all above we can write the following equations as follows

$$\phi_l = \frac{\Psi_{BB}^X}{\Psi_{AB}^X}\phi_0 + (\Psi_{BA}^X - \frac{\Psi_{BB}^X \Psi_{AA}^X}{\Psi_{AB}^X})\phi_l'$$

$$\phi_r' = \frac{1}{\Psi_{AB}^X}\phi_l - \frac{\Psi_{AA}^X}{\Psi_{AB}^X}\phi_l'$$

Now we can write

$$\begin{bmatrix}\phi_r \\ \phi_r'\end{bmatrix} = \begin{bmatrix}\frac{\Psi_{BB}^X}{\Psi_{AB}^X} & \Psi_{BA} - \frac{\Psi_{BB}^X \Psi_{AA}^X}{\Psi_{AB}^X} \\ \frac{1}{\Psi_{AB}^X} & \frac{\Psi_{AA}^X}{\Psi_{AB}^X}\end{bmatrix}\begin{bmatrix}\phi_l \\ \phi_l'\end{bmatrix} \Rightarrow \begin{bmatrix}\phi_r \\ \phi_r'\end{bmatrix} = M^X \begin{bmatrix}\phi_l \\ \phi_l'\end{bmatrix} \quad (108)$$

where $M^X = \begin{bmatrix}\frac{\Psi_{BB}^X}{\Psi_{AB}^X} & \Psi_{BA}^X - \frac{\Psi_{BB}^X \Psi_{AA}^X}{\Psi_{AB}^X} \\ \frac{1}{\Psi_{AB}^X} & -\frac{\Psi_{AA}^X}{\Psi_{AB}^X}\end{bmatrix}$

$$U_l = M_i U_0 \quad (109)$$

Where $U_j = [\phi_j \ \ \phi_j']^T$ and the matrix M_i which is the result of the product

$M_i = \prod_{p=1}^{n_i} M^X$ where M^X: $X \in (A\,, B)$ is the receptances matrix of a simply supported beam of each element in the cell.

The matrix M_i is unimodular where the det M_i =1, and obey the following recursion rule

$M_{i+1} = M_{i-1}\, M_i$, with initial conditions $M_0 = M_B$ and $M_1 = M_A$

An example to this relation $M_2 = BA$, $M_3 = ABA$

det $[M_i - e^{ik} I\ ]$ = 0,

or

$$k = \frac{\arccos(\text{tr}\, M_i)}{2}. \quad (110)$$

The solution of Eq. (110) presents the complete Floquet-Bloch spectrum and allows to obtain the mentioned stop-/pass-band pattern of the waveguides at varying index i. In particular, waves propagate when $|\text{tr}\, M_i| < 2$ is satisfied. Conversely, whereas stop bands comply with $|\text{tr}\, M_i| > 2$,

It is worthy to point out that Floquet-Bloch spectrum is not periodic as we had in the axial waves reported in the chapter. 4. In other words, in this case we are dealing with flexural waves

assuming pre-stress and bending stiffness as illustrated in the fourth order equation numbered which has two parts, periodic part and non-periodic part. This mean that we can not have periodicity as in the case of axial rods but we can still apply the Fibonacci recursion rule and Kohmoto's invariant.

6.4 Cyclic transformation of Golden Mean beams and Kohmoto's invariant

General recursive relations for the traces of unimodular 2 × 2 receptance matrices of GM generalised Fibonacci chains in terms of Chebyshev polynomialsh have been derived by Kolar and Ali (1989) as follows

$$x_{i+1} = x_{i-1}x_i - x_{i-2} \quad \text{with } i \geq 2 \tag{111}$$

where $x_i = tr\ M_i$ with initial conditions;

$$x_0 = trM_B = \frac{M_{bb}^B}{M_{ab}^B} - \frac{M_{aa}^B}{M_{ab}^B} \qquad \text{(element B}$$

$$x_1 = trM_A = \frac{M_{bb}^A}{M_{ab}^A} - \frac{M_{aa}^A}{M_{ab}^A}$$

$$x_2 = tr(M_B M_A). \tag{112}$$

Let us introduce the set of new variables

$$x_i' = t_{i+2}\ , y_i' = x_{i+1}\ ,\ \ z_i' = x_i\ . \tag{113}$$

By substituting coordinates (112) into Eq.(111), a nonlinear trace map for Golden Mean Structures (SMSs), defining the evolution of x_i can be obtained

$$T_G(x_i', y_i', z_i') = (x_{i+}', y_{i+1}', z_{i+1}') = (x_i'y_i' - z_i',\ x_i', y_i'). \tag{114}$$

The nonlinear map determined by the Eq. (10) is differentiable map, its Jacobian as follows;

$$J_s = \frac{\partial(x_{i+1}', y_{i+1}', z_{i+1}')}{\partial(x_i', y_i', z_i')} = \begin{bmatrix} y_i'^2 - 1 & 2y_i'x_i' - z_i' & -y_i' \\ y_i' & x_i' & -1 \\ 0 & 1 & 0 \end{bmatrix} \tag{115}$$

From all above, an invariant *Kohmoto's invariant* I(ω) can be written as follow

$$\mathrm{I}(\omega) = \mathrm{x}_i'^2 + \mathrm{y}_i'^2 + \mathrm{z}_i'^2 - \mathrm{x}_i'\mathrm{y}_i'\mathrm{z}_i' - 4. \tag{116}$$

This invariant is independent of the order (i) of the sequence F_i and depends only on the frequency (ω). This means that this invariant is valid for all precious mean structures GMSs, SMSs and BMSs.

In the case of Golden Mean structures (GMs), at any value of frequency ω, all the coordinates x_i', y_i' and z_i' represent the values of three consecutive traces obtained by three successive sequences can be can be mapped onto the surface defined by Eq.(116). Differently, for Silver Mean structures (SMs), only $y_i' = x_{i+1}$ *and* $z_i' = x_i$ represent the values traces of transfer matrices whereas $x_i' = tr(M_i M_{i+1})$ is an auxiliary variable produced by the recurrence relationship corresponding to the SMSs, see (Morini and Gei, 2018).

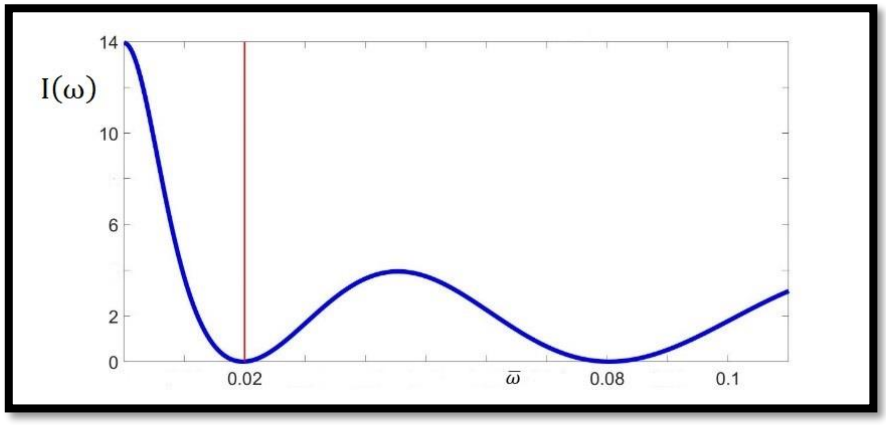

Figure 62: Kohmoto's invariant for a GM beam assuming family.1 whose parameters are $L_A/L_B = 0.5555$, $\bar{N} = 0$. *The normalized circular frequency* $\bar{\omega} = \sqrt{P_a} * \omega$.

All points singled out by the three coordinates $R_i(x_i', y_i', z_i')$ produced by the map (114) are confined on the surface obtained by representing equation (116) in the three-dimensional space $Ox_i'\ y_i'\ z_i'$ and can be mapped on this surface. Visibly, there are two different colours on the surface. The yellow region expresses that all $(|x_i'|,|y_i'|,|z_i'|) \leq 2$. This means that $R_i(x_i', y_i', z_i')$ will be on pass band and waves will propagate at this frequency along the two rods produced by the elementary cells F_{i+2}, F_{i+1} and F_i. On the other hand, if at least one of two elementary cells F_{i+2}, F_{i+1} and F_i $|x_i'|,|y_i'|,|z_i'|) \geq 2$, the waves therefore will not propagate (stop band) and this what the red region represents.

6.5 Configuration of GM beams (ratios and frequency) and Periodic orbits

The sets of points generated by the iterating map represented by Eq. (114) define confined orbit on surface determined by the Eq. (113). As mentioned in the previous chapter, Kohmoto and Oono (1984) were the first who introduced this surface and thus we will name this surface as Kohmoto's surface.

According to Morini and Gei (2018), each surface I(ω) = 0 has six saddle points ($P1$, $P2$. . ., $P6$). In Golden Mean maps (GMMs), these six saddle points are connected to the periodic orbit through the six-cycle transformations.

$$P_1(0,0,\mathrm{a}) \overset{T_g}{\rightarrow} P_2\ (-\mathrm{a},0,0) \overset{T_g}{\rightarrow} P_3(0,-\mathrm{a},0) \overset{T_g}{\rightarrow} P_4\ (,0,0,-\mathrm{a}) \overset{T_g}{\rightarrow} P_5\ (\mathrm{a},0,0) \overset{T_g}{\rightarrow} P_6(0,\mathrm{a},0) \overset{T_g}{\rightarrow} P_1 \qquad (117)$$

The orbit (14) will be denoted henceforth as T_g^6 where a = $\sqrt{4 + I(\omega)}$. Since it is a closed and periodic orbit, the starting point in (117) can be any saddle point. In real structures, in order to follow six-cycle transformations introduced by Eq. (117), three conditions must be satisfied at any value of ω.

$$x_0\,' = 0,\ y_0\,' = 0 \tag{118}$$

$$x_0\,' = \text{a},\ y_0\,' = 0, \text{ or } x_0\,' = 0,\ y_0\,' = \text{a}. \tag{119}$$

The requirements (118) and (119) can be fulfilled only for particular classes of layouts, namely $C = l_B/l_A$. By substituting expressions (113) into conditions (118) and (119), the following relationships are derived, i.e. $C = l_B/l_A$ respectively. C_1 , C_2 and C_3 which are non-canonical ratios.

Each of the three ratios C_1 , C_2 and C_3 identifies a family of GM beams but not canonical (no. 1, no. 2 and no. 3, respectively) as follows

$$C_1 = \frac{l_B}{l_A} = 0.5555$$

$$C_2 = \frac{l_B}{l_A} = 0.7755$$

$$C_3 = \frac{l_B}{l_A} = 0.8178$$

Family no. 1 possesses different properties from the Families no. 2 and 3, which can be studied together. These ratios are calculated at normalized frequency $\bar{\omega}_{r_n} = 0.02$ with $n = 1, 2, 3$. The main difference between canonical and non-canonical frequencies is that canonical frequency repeats itself in each period of the spectrum, while non-canonical frequency is not related to the periodicity of the spectrum.

Henceforth, we will call this frequency the reference frequency.

The results obtained in the following figures belong to family no.1 (C_1) and family no.3 (C_3) for sequence F_3 are obtained at different value of pre-stress $\bar{N}$ (0, 0.002, -0.002).

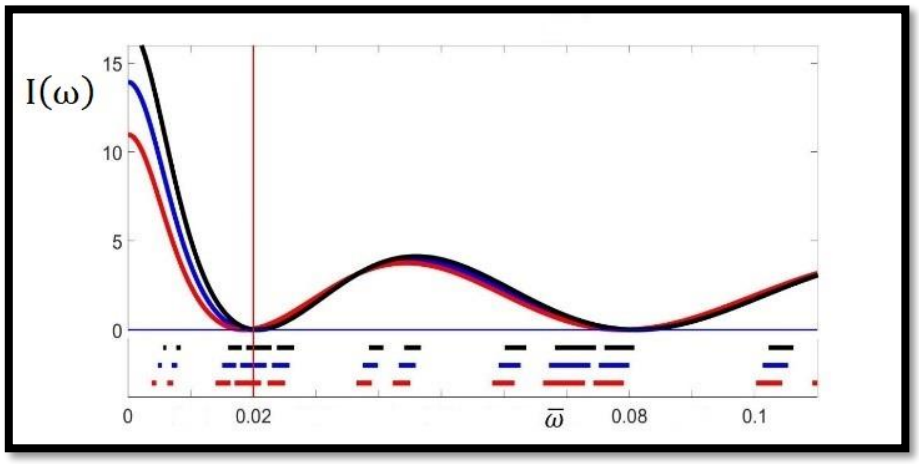

Figure 63: GM beams with $C_1 = \frac{L_B}{L_A} = 0.5555$ *(Family no. 1). Top: sketch of the invariant* $I(\omega)$ *in the interval* $[0, 1.11]$ *for different values of pre-stress* ($\bar{N} = 0$ *blue curve*, $\bar{N} = 0.002$ *black curve*, $\bar{N} = -0.002$ *red curve*) *(; bottom: stop/pass-band layout in the same values of pre-stress for sequence* F_3*. The dimensionless reference frequency is 0.02 (red vertical line).*

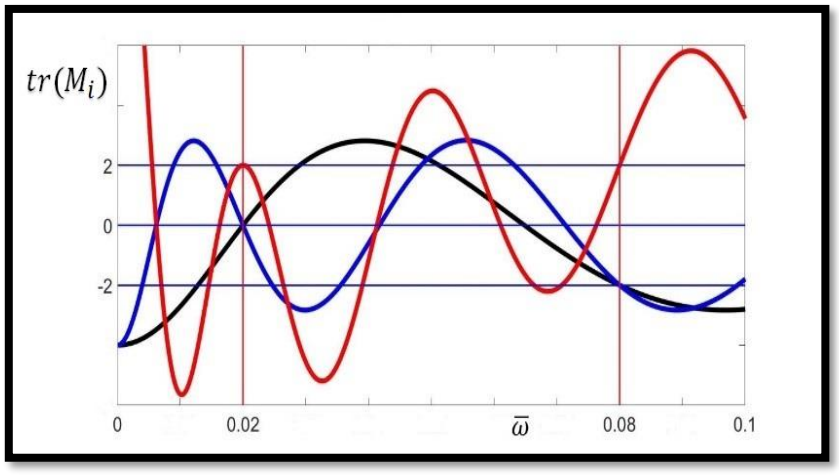

Figure 64: Description of the three coordinates (x_0', y_0', z_0') $(trM_2: red, trM_1: blue, trM_0: black)$ *for GM beam whose parameters* $C_1 = \frac{L_A}{L_B} = 0.5555, \bar{N} = 0$.

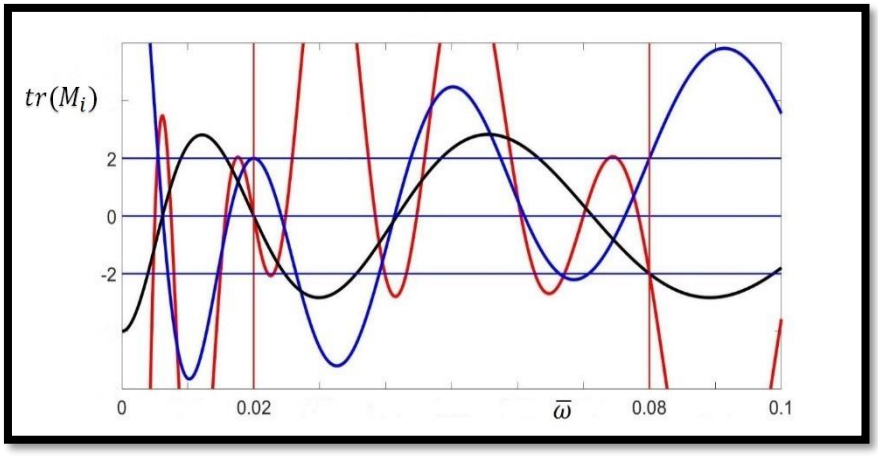

Figure 65: Description of the three coordinates (x_1', y_1', z_1') $(trM_3: red, trM_2: blue, trM_1: black)$ *for GM beam whose parameter* $C_1 = \frac{L_A}{L_B} = 0.5555, \bar{N} = 0$.

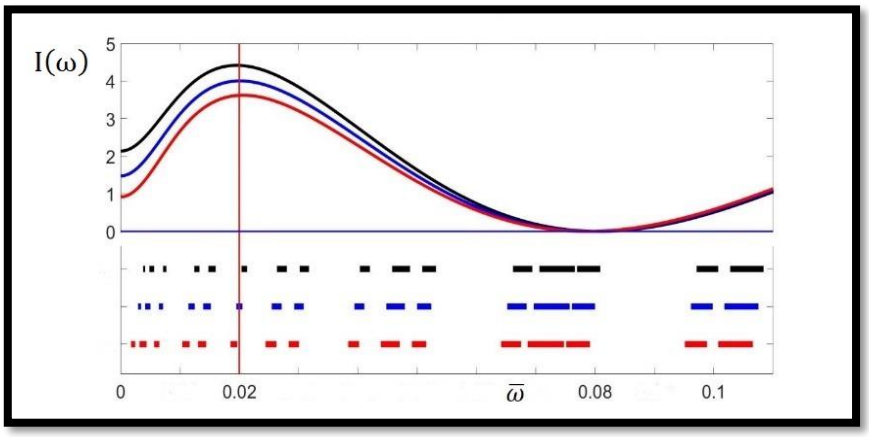

Figure 66: GM beams with $C_3 = \frac{L_B}{L_A} = 0.8178$ (Family no. 3). Top: sketch of the invariant $I(\omega)$ in the interval $[0, 1.11]$ for different values of pre-stress ($\bar{N} = 0$ blue curve, $\bar{N} = 0.002$ black curve, $\bar{N} = -0.002$ red curve); bottom: stop/pass-band layout in the same values of pre-stress for sequence F_3. The dimensionless reference frequency is 0.02 (red vertical line).

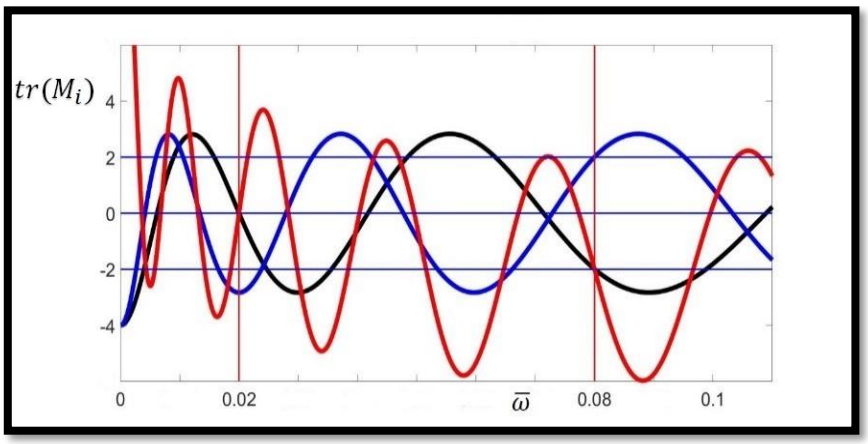

Figure 67: Description of the three coordinates (x_0', y_0', z_0') (trM_2: red , trM_1: blue, trM_0: black) for GM beam assuming family no .3 whose parameters $C_3 = \frac{L_A}{L_B} = 0.8178, \bar{N} = 0$. The red vertical line at 0.02 is the dimensionless reference frequency.

The invariant I(ω) and the stop/pass band distribution of a GM beam generated by sequence F_3 as functions of the axial pre-stress $\bar{N}$ (Null ($\bar{N} = 0$), Tensile($\bar{N} = +$) , Compressive ($\bar{N} = -$) is reported. It is clear that a tensile stress pushes the band (pass/stop) towards higher frequencies almost in a linear fashion (note that $\bar{N} = 0$ is the reference case between tensile and compressive load) as shown in Figure 69. In contrast, the compression stress shifts the band towards lower frequencies. The reason for that is that tensile load tends to increase the length of the material, while compressive load causes a decrease in the length of the material. The effect of the axial per-stress on the pass and stop band is calculated in the tables below.

For family no.1, at the reference frequency $\bar{\omega}_{r_1} = 0.02$, the invariant vanishes for all values of pre-stress, namely $I(\omega_{C_1}) = 0$. The significant effect of the pre-stress on $I(\omega_{C_1})$ can be clearly

observed in the period between $\bar{\omega} = 0$ and 0.02, while the effect of the pre-stress is almost non-existent in the interval after $\bar{\omega}$ =0.02 to the end of interval.

In details, around the reference frequency $\bar{\omega}_{r_1}$ where the band is characterized by pass band, the length of the pass band is 0.0042 for the cases of the pre-stress $\bar{N} = (0, -0.002)$, but at $\bar{N} = +0.002$, a decrease in the length was recorded which is 0.0041. The significant influence of the pre-stress is very clear between $\bar{\omega} = 0$ and 0.02 where the width of first pass band at $\bar{N} = 0$ is 0.000636 while at $\bar{N} = (0.002, -0.002)$ is 0.000477 and 0.000716 respectively. This means that the negative pre-stress (compressive stress) increases the width of the pass band whereas the positive pre-stress (tensile stress) decreases it. The stop band was also effected by the pre-stress where the width of the stop band immediately before and after $\bar{\omega}_{r_1} = 0.02$ was effected by the difference in the applied pre-stress, as the width of the stop band immediately before $\bar{\omega}_{r_1} = 0.02$ was not affected by the compressive stress, but its width increased by the tensile stress. In addition, the width of the stop band immediately after the reference frequency $\bar{\omega}_{r_1} = 0.02$ was increased by the compressive stress from 0.000875 at $\bar{N} = 0$ to 0.001035 and was not affected by the tensile stress.

The following readings in the width of the stop band for the first and second ultra wide stop band at $\bar{N} = (0, 0.002, -0.002)$ are (0.011698 ,0.11937, 0.011381) and (0.01321, 0.01337, 0.01305) respectively.

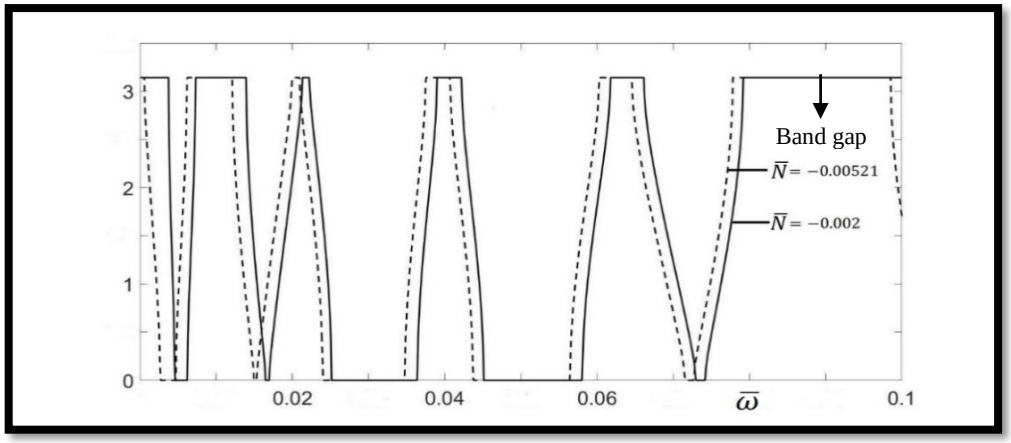

Figure 68: Family no. 3 (C1 = LB LA = 0.5555):Effect of compressive stresses on dispersion diagrams close to buckling , $\bar{N}_b = -0.00285$ for flexural waves of a multi-supported quasiperiodic beam generated by sequence F_3.

F_i	$\bar{N}_b$	Family no.1 Pass band width		
		$\bar{N}_0$(Reference)	$\bar{N}_C = -0.002$	$\bar{N}_T = 0.002$
F_0	-0.01282			
F_1	-0.00395			
F_2	-0.00655	0.00883	0.00891	0.00867
F_3	-0.00528	0.00350	0.00358	0.00342
F_4	-0.00557	0.00262	0.00270	0.00254
F_5	-0.00543	0.001191	0.00127	0.00119

Table 6: Family no. 1 ($C_1 = \frac{L_B}{L_A} = 0.5555$):Effect of pre-stress on the pass band for flexural waves of a multi-supported quasiperiodic beam generated by sequences F_2 to F_5.

F_i	$\bar{N}_b$	Family no. 1 Stop band width		
		$\bar{N}_0$(Reference)	$\bar{N}_C = -0.002$	$\bar{N}_T = 0.002$
F_0	-0.01282			
F_1	-0.00395			
F_2	-0.00655	0.1368	0.01360	0.01392
F_3	-0.00529	0.01321	0.01305	0.01337
F_4	-0.00557	0.01297	0.01289	0.01321
F_5	-0.00543	0.01297	0.01289	0.01313

Table 7 :Family no. 1 ($C_1 = \frac{L_B}{L_A} = 0.5555$):effect of the pre-stress on the stop band for flexural waves of a multi-supported quasiperiodic beam generated by sequences F_2 to F_5.

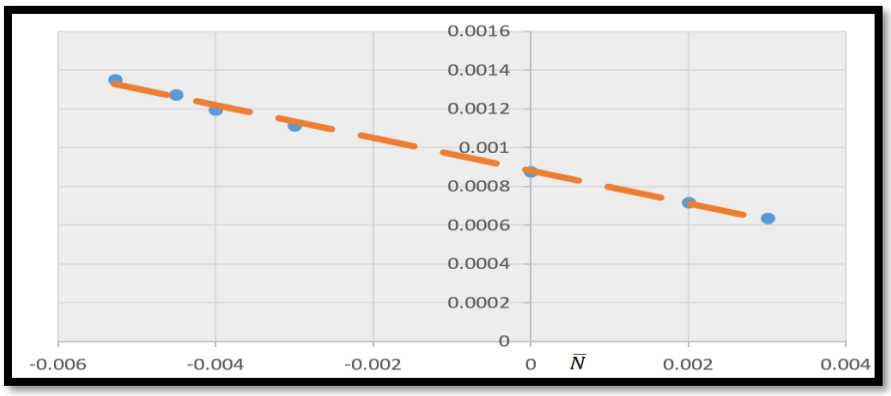

Figure 69: Family no. 1 ($C_1 = \frac{L_B}{L_A} = 0.5555$):influence of $\bar{N}$ on pass-band width. The orange dashed line is the trend line.

For the ultra-wide stop band, the width of the stop band is slightly affected due to the pre-stress, as the width increased with the tensile load and decreased with the compressive load. If we consider that the case of non-pre-stress is the reference between tensile and compressive load, as illustrated in Figure 70 below, Ultra-wide stop band is important for some applications; for

instance, semiconductors with ultra-wide bandgap permit devices to operate at much higher voltages, frequencies, and temperatures than conventional semiconductor materials.

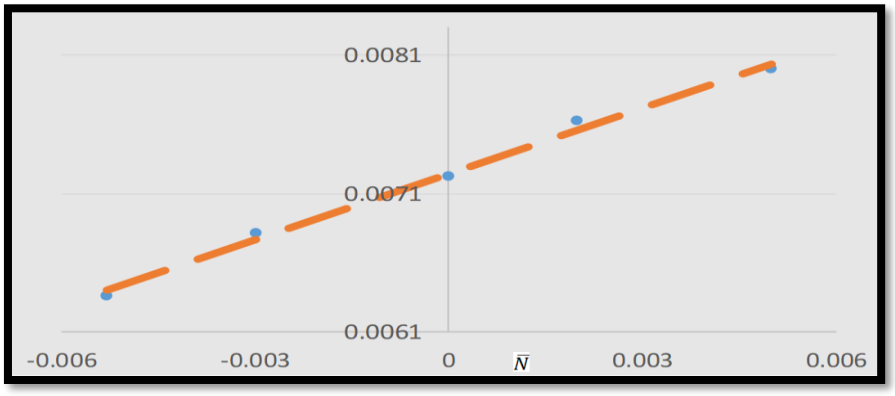

Figure 70: Family no. 1 ($C_1 = \frac{L_B}{L_A} = 0.5555$):influence of $\bar{N}$ on ultra wide stop-band width . The orange dashed line is the trend line.

For Family no. 3, at the reference frequency $\bar{\omega}_{r_3} = 0.02, I(\omega_{c_3}) > 0$ for all values of pre-stress. The significant effect of the pre-stress on $I(\omega_{c_3})$ can be clearly observed in the period between $\bar{\omega} = 0$ and 0.04, while the effect of the pre-stress is almost non-existent in the interval from 0.04 to the end of interval.

Generally, the widths of the pass (stop) band close to the reference frequency $\bar{\omega}_{r_3} = 0.02$ for the three cases of pre-stress (null , tensile , compressive) influenced by the inclusion of the pre-stress. The tensile stress reduces the width of the pass band while the compressive stress increases their width. The widths of the stop bands increase (reduce) their widths when a tensile (compressive) stress is applied. The tables below show the changes in the widths of the pass/stop bands at frequency far from the reference frequency.

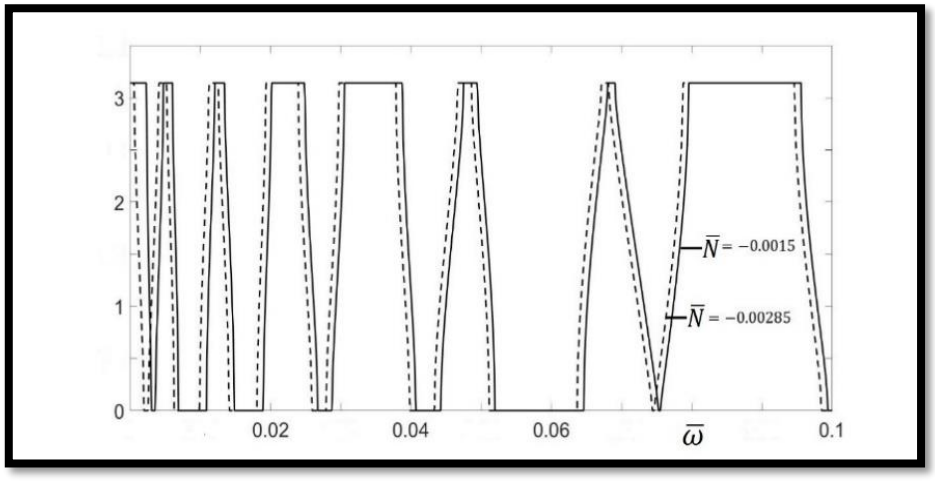

Figure 71: Family no. 3 ($C_3 = \frac{L_B}{L_A} = 0.8178$):Effect of compressive stresses on dispersion diagrams close to buckling $\bar{N}_b = -0.00285$ for flexural waves of a multi-supported quasiperiodic beam generated by sequence F_3.

F_i	$\bar{N}_b$	Family no. 3 Pass band width		
		$\bar{N}_0$(Reference)	$\bar{N}_C = -0.002$	$\bar{N}_T = 0.002$
F_0	-0.00394			
F_1	-0.00263			
F_2	-0.00317	0.00421	0.00437	0.00413
F_3	-0.00296	0.00310	0.00318	0.00302
F_4	-0.00304	0.00127	0.00135	0.00119
F_5	-0.00302	0.00063	0.00063	0.00055

Table 8: Family no. 3 ($C_3 = \frac{L_B}{L_A} = 0.8178$):Effect of the pre-stress on the pass band for flexural waves of a multi-supported quasiperiodic beam generated by sequences F_2 to F_5.

F_i	$\bar{N}_b$	Family no. 3 Stop band width		
		$\bar{N}_0$(Reference)	$\bar{N}_C = -0.002$	$\bar{N}_T = 0.002$
F_0	-0.00394			
F_1	-0.00263			
F_2	-0.00317	0.00875	0.00851	0.00883
F_3	-0.00296	0.00374	0.00366	0.00374
F_4	-0.00304	0.00358	0.00350	0.00366
F_5	-0.00302	0.00350	0.00342	0.00358

Table 9: Family no. 3 ($C_3 = \frac{L_B}{L_A} = 0.8178$):Effect of the pre-stress on the stop band for flexural waves of a multi-supported quasiperiodic beam generated by sequences F_2 to F_5.

Now we turn to the periodic orbit obtained from these families. For Family no. 1, at the reference frequency 0.02 implying that at this frequency a waveguide belonging to Family no. 1 always displays a pass band. Moreover, a six-point periodic orbit is obtained at $\bar{\omega}_{r_1} = 0.02$.

As shown in the Figures 64 and 65, the coordinate x_0' (red curve) intersects the normalized reference frequency at 2 which is the value of "a" while both coordinates $y_0' = trT_1$ and $z_0' = trT_0$ intersect the canonical frequency at zero. This leads to the first saddle point (starting point) namely $P_5(\mathrm{a}, 0,0)$= (2,0,0). In the same way the rest of the points of the periodic orbit can be identified.

For Family no.1, the six-point periodic orbit is

$$P_5(2,0,0) \xrightarrow{T_g} P_6\ (0,2,0) \xrightarrow{T_g} P_1(0,0,2) \xrightarrow{T_g} P_2\ (-2,0,0) \xrightarrow{T_g} P_3\ (0,-2,0) \xrightarrow{T_g} P_4(0,0,-2) \xrightarrow{T_g} P_5 \qquad (120)$$

However, for family no. 3, at the reference frequency, $I(\omega_{c_3}) > 0$, and therefore we find that $x_{\mathrm{i}} > |2|$. This means that Family no. 3 always displays a stop band. Moreover, a six-point periodic orbit is obtained at $\bar{\omega}_{C_3}$ as family no. 1 with different starting point namely.

$P_3(0,-2.82,0) \xrightarrow{T_g} P_4(0,0,-2.82)\ P_5(2.82,0,0) \xrightarrow{T_g} P_6(0,2.82,0) P_1(0,0,2.82) \xrightarrow{T_g} P_2(-2.82,0,0) \xrightarrow{T_g} P_3$ (121)

The orbits (120) and (121) will be denoted henceforth T_g^6.

Additional periodic orbits can be found at non-reference frequency such that $I(\omega) = 0$. This may occur in different values of ω.

- In family no .1 at $\omega = 4\bar{\omega}_{r_1}$, 3-point periodic orbits are present as follows

  $R_1(2, -2, -2) \xrightarrow{T} R_2(-2, 2, -2) \xrightarrow{T} R_3(-2, -2, 2)$

- For family no .2 and 3 at $\omega = 4\bar{\omega}_{r_{2,3}}$, the periodic orbits are also 3-point periodic orbit with different starting point

  $R_2(-2, 2, -2) \xrightarrow{T} R_3(-2, -2, 2) \xrightarrow{T} R_1(2, -2, -2)$.

Nevertheless, following case is universal (i.e., valid for all three families GM beams):

- at $\omega = 16\ \bar{\omega}_{C_{1,2,3}}$, 3-point periodic orbits are as follows

$R_1(2, -2, -2) \xrightarrow{T} R_2(-2, 2, -2) \xrightarrow{T} R_3(-2, -2, 2)$.

6.6 summery

The filtering properties of a multi-supported quasiperiodic beam with elementary cells generated according to Fibonacci golden sequence have been investigated for three non-canonical families namely, C_1, C_2, and C_3 by determining the position of pass/stop bands in the relevant dispersion diagrams. This system does not give us a periodicity as we had in the axial waves reported in the chapter no. 4. I have shown that, for cells generated by different Fibonacci golden sequences that the pre-stress can be applied to tune the properties of these systems for flexural waves. The pass/stop bands can be shifted towards higher (lower) frequencies when tensile (compressive) stress is applied. The widths of pass (stop) band are also influenced by the pre-stress. In other words, tensile stress reduces the width of the pass band but increases the stop band width. On the other hand, compressive stress increases the width of the pass band but reduces the stop band width. It has to be noted that the effect of the pre-stress in some frequencies bands is weak, especially in the short stop (pass) bands. The main result from above is that the pre-stress can be applied to modify and tune the dynamic properties of a periodic beam and other structures.

Six point periodic orbit for all three families can be found at the reference frequency $\bar{\omega}_{r_{1,2,3}} = 0.02$ with different starting point. Other periodic orbits can be found at non-reference frequencies $\dot{\omega}$ such that $I(\omega) = 0$. This occurred at $\dot{\omega} = 4\bar{\omega}_{r_{1,2,3}}$ and $\dot{\omega} = 16\ \bar{\omega}_{r_{1,2,3}}$.

Chapter7: Conclusion and future work.

7.1 Conclusion

This thesis focused on three core aims, the first of which is how to control harmonic axial wave propagation in Fibonacci Silver mean phononic rods, and the second is the comparison between golden and silver mean rods for axial waves, and finally I studied the effect of the pre-stress on the position of pass and stop band in multi-supported beams constructed according to Fibonacci golden mean sequence. The contribution made by this thesis is to give broader options to designers of acoustic devices like waveguides and acoustic filters.

7.1.1 Axial waves in Silver mean phononic rods

I studied the propagation of harmonic axial waves in silver mean phononic rods constructed by collecting a two-face elementary cells. I detect a self-similar behaviour depends on Kohmoto's invariant, that is an invariant of the set and depends only on the wave frequency and obtained analytical scaling factor to control the self-similar behaviour. The rational values between the geometrical and physical properties of the phases *A* and *B* in order to have periodic spectrum have been obtained.

One of the goals of this thesis is to find the existence of similar canonical arrangements for silver-mean Fibonacci phononic waveguides that are based on one of the possible generalisation of the standard Fibonacci chain. I give a positive answer to the initial objective and the outcomes of the present research can be listed as follows:

- The dispersive properties of harmonic axial waves in SM rods are fully determined by studying the variation of the traces of the transmission matrices as a function of the angular frequency. For any value of the frequency, the traces corresponding to three arbitrary subsequent elementary cells are related through a recursive relationship that is different from that ruling standard, or golden-mean, structures, but characterised by the same Kohmoto's invariant. This allows us to represent geometrically the traces as coordinates of points which describe orbits on the 3D surface defined by the invariant;
- We found ratios between the geometrical and the physical properties of the two faces *A* and *B* which correspondence to periodic spectrum and we call this type of structure canonical structure. These ratios represented three families. However, Family no. 1 displays a two-point periodic orbit on the Kohmoto's surface, whereas for Families no. 2 and 3 periodic orbits involve four saddle points;

- In general, there exist some frequencies at which additional periodic orbits are present. For all these frequencies ω, the Kohmoto's invariant vanishes. This could be detected in several cases depending on the value of the ratio C which determines the modulation of the invariant with respect to ω.
- A self-similar layout of the stop-/pass-band diagram is observed for canonical SM rods. Analytical scaling factors capturing this pattern are derived through the linearisation of the trace map about the relevant periodic orbits. Depending on the number of points p composing the orbits, portions of the spectra corresponding to elementary cells of the order i and $i+p$ are related by means of these factors. A detailed analysis of the frequency ranges where the scaling is effective is performed;

- I finally propose a different way to represent the sequence of pass bands and stop bands by following the trajectories of points at varying frequency on a 2D projection of the Kohmoto's surface. The exceptional self-similar properties of the spectrum of two-phase canonical silver-mean rods here illustrated could be applied to realize phononic waveguides possessing stop and pass bands of tuneable width centered at a selected frequency. The filtering properties of these devices can be predicted and optimised by means of the novel analytical approach introduced in the project.

7.1.2 Comparison between golden and silver mean rods for axial waves

A comparative analysis between golden and silver mean rods has been done for axial waves. This comparison clearly showed the differences between the two structures in some aspects as follows:

- The number of pass/stop bands in silver mean rods is greater than their golden counterpart, and this is because the number of elements in Fibonacci silver mean sequence is greater than golden counterparts.
- The analytical scaling ratios of GM and SM sequences is very close to the eigenvalues. However, according to our numerical calculations, silver mean scaling is more accurate than golden mean scaling which lead to better accuracy of pass and stop band width at higher Fibonacci sequences.

7.1.3 Flexural waves in multi-supported quasiperiodic beam

I studied a different system which is a multi-supported beam where the distances between the supports are modulated according to the lengths of the elements A and B which provide a band gap effect. I studied the band gap effect where we detect the same band gap structure, self-similar behaviour, and scaling factor. This system has a different type of dispersion relation which is not periodic because the receptances matrix has non-periodic parts in its components. In addition, this system does not give a periodicity for the spectrum but we still have the Kohmoto's invariant, scaling factor, and self-similarity behaviour.

The filtering properties of a multi-supported quasiperiodic beam with elementary cells generated according to Fibonacci golden sequence have been investigated for three non-canonical families namely by determining the positions of pass/stop bands in the relevant dispersion diagrams. We have shown that, for cells generated by different Fibonacci golden sequences that the pre-stress can be applied to tune the properties of these systems for flexural waves. The pass/stop bands can be shifted towards higher (lower) frequencies when tensile (compressive) stress is applied. The width of pass (stop) band are also influenced by the pre-stress. In other words, tensile stress reduces the length of the pass band but increases the stop band length. On the other hand, compressive stress increases the length of the pass band but reduces the stop band length. It has to be noted that the effect of the pre-stress in some frequencies bands is weak, especially in the short stop (pass) bands. This means the pre-stress can be used to tune the properties of these structures for flexural waves.

The periodic orbit can be found in various frequencies, for example, six point periodic orbit for all three families can be found at the reference frequency $\bar{\omega}_{r_{1,2,3}}$ with different starting point. Other periodic orbits can be found at non-reference frequencies $\dot{\omega}$.

7.2 limitations

The first limitation is that at higher index *i,* the dispersion diagrams are illegible, which is why I considered the primary sequences in the thesis. In addition, the layout of stop/pass bands could have been studied for the whole interval, but the increasing smallness of the widths of the bands in certain frequency ranges would have made the diagram illegible.

In the case of pre-stress, if the elastic limit is exceeded or we apply a load higher than the buckling load, the results will be inaccurate because in the plastic region, permanent deformation of the material occurs.

7.3 Future work

- These general mathematical tools we have used in this thesis can be useful in order to design smart waveguides which are able to provide a very thin and localized band gap depends on the desired application such as narrow–band filter by choosing the proper sequence among all Fibonacci sequences. These tools can be also used to control sounds and vibrations propagating in the structures.

- Two materials with different density can be used to provide a very accurate band gap. The changes in contrast between the two martials of the structure can be useful to tune the width of the band gap because the position of the pass/stop band depends only on the ratio between the geometrical and physical properties of the phases *A* and *B*.
- The pre-stress can be used to shift the position of a certain band gap at a given frequency.
- The experiments can be designed in order to provide waveguides which give us a very narrow band gap.
- These results can be extended not only to mechanics but also to eclectic and electronics fields.

The findings achieved in this thesis provide the necessary insight to start a research programme in quasicrystalline meta-materials. The established methodology could be extended to investigate the dynamics of quasicrystalline plates and composite materials.

References

Ando, T., 1989. Numerical study of symmetry effects on localization in two dimensions. Physical Review B, 40(8), p.5325.

Armenise, M.N., Campanella, C.E., Ciminelli, C., Dell'Olio, F. and Passaro, V.M., 2010. Phononic and photonic band gap structures: modelling and applications. Physics Procedia, 3(1), pp.357-364.

Assouar, B., Oudich, M. and Zhou, X., 2015, March. Sound insulation and energy harvesting based on acoustic metamaterial plate. In Health Monitoring of Structural and Biological Systems 2015 (Vol. 9438, pp. 218-226). SPIE.

Aynaou, H., El Boudouti, E.H., Djafari-Rouhani, B., Akjouj, A. and Velasco, V.R., 2005. Propagation and localization of acoustic waves in Fibonacci phononic circuits. Journal of Physics: Condensed Matter, 17(27), p.4245.

Azbel, M.Y., 1964. Energy spectrum of a conduction electron in a magnetic field. Sov. Phys. JETP, 19, p.634.

Becker, J.N. and Becher, C., 2017. Coherence properties and quantum control of silicon vacancy color centers in diamond. physica status solidi (a), 214(11), p.1700586.

Beenakker, C.W., 1997. Random-matrix theory of quantum transport. Reviews of modern physics, 69(3), p.731.

Benchabane, S., Khelif, A., Rauch, J.Y., Robert, L. and Laude, V., 2006. Evidence for complete surface wave band gap in a piezoelectric phononic crystal. Physical Review E, 73(6), p.065601.

Bloch, F., 1928. ber die Quantenmechanik der Electron in Kristallgittern. Zeitschrift fr Physik, 52, pp.550-600.

Boechler, N., Theocharis, G. and Daraio, C., 2011. Bifurcation-based acoustic switching and rectification. Nature materials, 10(9), pp.665-668.

Bolat, C. and Köse, H., 2010. On the properties of k-Fibonacci numbers. Int. J. Contemp. Math. Sciences, 5(22), pp.1097-1105.

Boussora, K. and Mazouz, S., 2004. The use of the Golden Section in the Great Mosque at Kairouan. Nexus Network Journal, 6(1), pp.7-16.

Brillouin, L., 1953. Wave propagation in periodic structures: electric filters and crystal lattices.

Brillouin, L., 1953. Wave propagation in periodic structures: electric filters and crystal lattices (Vol. 2). Dover publications.

Brillouin, L., 1946, Wave Propagation in Periodic Structures, Dover, New York

Bringuier, S., Swinteck, N., Vasseur, J.O., Robillard, J.F., Runge, K., Muralidharan, K. and Deymier, P.A., 2011. Phase-controlling phononic crystals: Realization of acoustic Boolean logic gates. The Journal of the Acoustical Society of America, 130(4), pp.1919-1925.

Castiñeira-Ibáñez, S., Romero-García, V., Sánchez-Pérez, J.V. and Garcia-Raffi, L.M., 2010. Overlapping of acoustic bandgaps using fractal geometries. EPL (Europhysics Letters), 92(2), p.24007.

Cervera, F., Sanchis, L., Sánchez-Pérez, J.V., Martinez-Sala, R., Rubio, C., Meseguer, F., López, C., Caballero, D. and Sánchez-Dehesa, J., 2001. Refractive acoustic devices for airborne sound. physical review letters, 88(2), p.023902.

Chen, A.L. and Wang, Y.S., 2007. Study on band gaps of elastic waves propagating in one-dimensional disordered phononic crystals. Physica B: Condensed Matter, 392(1-2), pp.369-378.

Chen, A.L., Wang, Y.S., Guo, Y.F. and Wang, Z.D., 2008. Band structures of Fibonacci phononic quasicrystals. Solid State Communications, 145(3), pp.103-108.

Chen, L.S., Kuo, C.H. and Ye, Z., 2004. Acoustic imaging and collimating by slabs of sonic crystalsmade from arrays of rigid cylinders in air. Applied physics letters, 85(6), pp.1072-1074.

Christensen, J., Fernandez-Dominguez, A.I., de Leon-Perez, F., Martin-Moreno, L. and Garcia-Vidal, F.J., 2007. Collimation of sound assisted by acoustic surface waves. Nature Physics, 3(12), pp.851-852.

Collet, M., Ouisse, M., Ruzzene, M. and Ichchou, M.N., 2011. Floquet–Bloch decomposition for the computation of dispersion of two-dimensional periodic, damped mechanical systems. International Journal of Solids and Structures, 48(20), pp.2837-2848.

Conference September (pp. 4-7). 22. Velasco, V.R. and Zarate, J.E., 2001. Elastic waves in quasiperiodic structures. Progress in Surface Science, 67(1-8), pp.383-402.

Cremer, L., and Leilich, H. O., 1953, "Zur theorie der biegekettenleiter," (On Theory of Flexural Periodic Systems), Arch. Elektr. Uebertrag, 7, pp. 261–270

De Espinosa, F.M., Jimenez, E. and Torres, M., 1998. Ultrasonic band gap in a periodic two-dimensional composite. Physical Review Letters, 80(6), p.1208.

de Spinadel, V.W., 1999. The family of metallic means. Vis. Math, 1(3), pp.1-16.

Duhamel, D., Mace, B.R. and Brennan, M.J., 2006. Finite element analysis of the vibrations of waveguides and periodic structures. Journal of sound and vibration, 294(1-2), pp.205-220.

Economou, E.N. and Sigalas, M.M., 1993. Classical wave propagation in periodic structures: Cermet versus network topology. Physical Review B, 48(18), p.13434.

El Boudouti, E.H., El Hassouani, Y., Aynaou, H., Djafari-Rouhani, B., Akjouj, A. and Velasco, V.R., 2007. Electromagnetic wave propagation in quasi-periodic photonic circuits. Journal of Physics: Condensed Matter, 19(24), p.246217.

Elachi, C., 1976. Waves in active and passive periodic structures: A review. Proceedings of the IEEE, 64(12), pp.1666-1698.

El-Kady, I., Olsson III, R.H. and Fleming, J.G., 2008. Phononic band-gap crystals for radio frequency communications. Applied Physics Letters, 92(23), p.233504.

Espinosa, V., Sánchez-Morcillo, V.J., Staliunas, K., Pérez-Arjona, I. and Redondo, J., 2007. Subdiffractive propagation of ultrasound in sonic crystals. Physical Review B, 76(14), p.140302.

Falcón, S. and Plaza, Á., 2007. On the Fibonacci k-numbers. Chaos, Solitons & Fractals, 32(5), pp.1615-1624.

Farhat, A.K.M., Morini, L. and Gei, M., 2022. Silver-mean canonical quasicrystalline-generated phononic waveguides. Journal of Sound and Vibration, 523, p.116679.

Farzbod, F., 2010. Analysis of Bloch formalism in undamped and damped periodic structures (Doctoral dissertation, Georgia Institute of Technology).

Floquet, G., 1883. Sur les équations différentielles linéaires à coefficients périodiques. In Annales scientifiques de l'École normale supérieure (Vol. 12, pp. 47-88).

Fokker, P.A., Dijkhuis, J.I. and De Wijn, H.W., 1997. Stimulated emission of phonons in an acoustical cavity. Physical Review B, 55(5), p.2925.

Frazier, M.J., 2015. Dissipative wave propagation in phononic crystals and metamaterials: Models and analysis (Doctoral dissertation, University of Colorado at Boulder).

Gei, M., 2010. Wave propagation in quasiperiodic structures: stop/pass band distribution and prestress effects. International Journal of Solids and Structures, 47(22-23), pp.3067-3075.

Gei, M., Bigoni, D. and Franceschni, G., 2004. Thermoelastic small-amplitude wave propagation in nonlinear elastic multilayers. Mathematics and mechanics of solids, 9(5), pp.555-568.

Gei, M., Chen, Z., Bosi, F. and Morini, L., 2020. Phononic canonical quasicrystalline waveguides. Applied Physics Letters, 116(24), p.241903.

Gei, M., Movchan, A.B. and Bigoni, D., 2009. Band-gap shift and defect-induced annihilation in prestressed elastic structures. Journal of Applied Physics, 105(6), p.063507.

Gellermann, W., Kohmoto, M., Sutherland, B. and Taylor, P.C., 1994. Localization of light waves in Fibonacci dielectric multilayers. Physical review letters, 72(5), p.633.

Ghulinyan, M., Oton, C.J., Dal Negro, L., Pavesi, L., Sapienza, R., Colocci, M. and Wiersma, D.S., 2005. Light-pulse propagation in Fibonacci quasicrystals. Physical Review B, 71(9), p.094204.

Hirsekorn, M., Delsanto, P.P., Batra, N.K. and Matic, P., 2004. Modelling and simulation of acoustic wave propagation in locally resonant sonic materials. Ultrasonics, 42(1-9), pp.231-235.

Hou, Z., Wu, F. and Liu, Y., 2004. Acoustic wave propagating in one-dimensional Fibonacci binary composite systems. Physica B: Condensed Matter, 344(1-4), pp.391-397.

Hussein, M.I., Leamy, M.J. and Ruzzene, M., 2014. Dynamics of phononic materials and structures: Historical origins, recent progress, and future outlook. Applied Mechanics Reviews, 66(4).

Hvatov, A. and Sorokin, S., 2015. Free vibrations of finite periodic structures in pass-and stop-bands of the counterpart infinite waveguides. Journal of Sound and Vibration, 347, pp.200-217.

Gibson, L.J. and Ashby, M.F., 1999. Cellular Solids: Structure and Properties. Cambridge Univ Press. Cambridge, UK.

Gomez Garcia, P. and Fernández-Álvarez, J.P., 2015. Floquet-Bloch theory and its application to the dispersion curves of nonperiodic layered systems. Mathematical Problems in Engineering, 2015.

Guillén-Gallegos, C., Alva-Medrano, H., Pérez-Aguilar, H., Mendoza-Suárez, A. and Villa-Villa, F., 2019. Phononic band structure of an acoustic waveguide that behaves as a phononic crystal. Results in Physics, 12, pp.1111-1118.

Gupta, B.C. and Ye, Z., 2003. Theoretical analysis of the focusing of acoustic waves by two-dimensional sonic crystals. Physical Review E, 67(3), p.036603.

Gupta, G.S., 1970. Natural flexural waves and the normal modes of periodically-supported beams and plates. Journal of Sound and Vibration, 13(1), pp.89-101.Journal of the Acoustical Society of America, 39(5A), pp.887-894.

Gupta, G.S., 1971. Dynamics of Periodically Stiffened Structures Using a Wave Approach. SOUTHAMPTON UNIV (ENGLAND) INST OF SOUND AND VIBRATION RESEARCH.

Gurtin, M.E. and Murdoch, A.I., 1975. A continuum theory of elastic material surfaces. Archive for rational mechanics and analysis, 57(4), pp.291-323.

Hladky-Hennion, A.C., Allan, G. and de Billy, M., 2005. Localized modes in a one-dimensional diatomic chain of coupled spheres. Journal of applied physics, 98(5), p.054909.

Holzer, M., 1988. Nonlinear dynamics of localization in a class of one-dimensional quasicrystals. Physical Review B, 38(8), p.5756.

Hretcanu, C.E. and Crasmareanu, M., 2013. Metallic structures on Riemannian manifolds. Rev. Un. Mat. Argentina, 54(2), pp.15-27.

Hsu, J.C. and Wu, T.T., 2006. Efficient formulation for band-structure calculations of two-dimensional phononic-crystal plates. Physical review B, 74(14), p.144303.

Huang, J., Ruzzene, M. and Chen, S., 2017. Analysis of in-plane wave propagation in periodic structures with Sierpinski-carpet unit cells. Journal of Sound and Vibration, 395, pp.127-141.

Hussein, M.I., Hulbert, G.M. and Scott, R.A., 2005, January. Hierarchical design of phononic materials and structures. In ASME International Mechanical Engineering Congress and Exposition (Vol. 42258, pp. 163-172).

Hussein, M.I., Hulbert, G.M. and Scott, R.A., 2006. Dispersive elastodynamics of 1D banded materials and structures: analysis. Journal of sound and vibration, 289(4-5), pp.779-806.

Hussein, M.I., Hulbert, G.M. and Scott, R.A., 2007. Dispersive elastodynamics of 1D banded materials and structures: design. Journal of Sound and Vibration, 307(3-5), pp.865-893.

Hussein, M.I., Leamy, M.J. and Ruzzene, M., 2014. Dynamics of phononic materials and structures: Historical origins, recent progress, and future outlook. Applied Mechanics Reviews, 66.

Jensen, J.S., 2003. Phononic band gaps and vibrations in one-and two-dimensional mass–spring structures. Journal of sound and Vibration, 266(5), pp.1053-1078.

Jian-Wen, D., Peng, H. and He-Zhou, W., 2003. Broad omnidirectional reflection band forming using the combination of Fibonacci quasi-periodic and periodic one-dimensional photonic crystals. Chinese Physics Letters, 20(11), p.1963.

Jiu-Jiu, C., Bo, Q. and Jian-Chun, C., 2005. Complete band gaps for Lamb waves in cubic thin plates with periodically placed inclusions. Chinese Physics Letters, 22(7), p.1706.

John, S., 1987. Strong localization of photons in certain disordered dielectric superlattices. Physical review letters, 58(23), p.2486.

Jones, R., 1971. The golden section: A most remarkable measure. The Structurist, (11), p.44.

Khelif, A., Aoubiza, B., Mohammadi, S., Adibi, A. and Laude, V., 2006. Complete band gaps in two-dimensional phononic crystal slabs. Physical Review E, 74(4), p.046610.

Khelif, A., Choujaa, A., Benchabane, S., Djafari-Rouhani, B. and Laude, V., 2004. Guiding and bending of acoustic waves in highly confined phononic crystal waveguides. Applied physics letters, 84(22), pp.4400-4402.

Kirkman, P.D. and Pendry, J.B., 1984. The statistics of one-dimensional resistances. Journal of Physics C: Solid State Physics, 17(24), p.4327.

Kohmoto, M., Kadanoff, L.P. and Tang, C., 1983. Localization problem in one dimension: Mapping and escape. Physical Review Letters, 50(23), p.1870.

Kohmoto, M., Sutherland, B. and Iguchi, K., 1987. Localization of optics: Quasiperiodic media. Physical review letters, 58(23), p.2436.

Kohmoto, M. and Oono, Y., 1984. Cantor spectrum for an almost periodic Schrödinger equation and a dynamical map. Physics Letters A, 102(4), pp.145-148

Kola, M. and Ali, M.K., 1989. Attractors of some volume-nonpreserving Fibonacci trace maps. Physical Review A, 39(12), p.6538.

Kolář, M., 1993. New class of one-dimensional quasicrystals. Physical Review B, 47(9), p.5489.

Khelif, A., Djafari-Rouhani, B., Vasseur, J.O. and Deymier, P.A., 2003. Transmission and dispersion relations of perfect and defect-containing waveguide structures in phononic band gap materials. Physical Review B, 68(2), p.024302.

Kolá, M. and Ali, M.K., 1989. Generalized Fibonacci superlattices, dynamical trace maps, and magnetic excitations. Physical Review B, 39(1), p.426.

Kolář, M., 1993. New class of one-dimensional quasicrystals. Physical Review B, 47(9), p.5489.

Kushwaha, M.S. and Djafari-Rouhani, B., 1996. Complete acoustic stop bands for cubic arrays of spherical liquid balloons. Journal of applied physics, 80(6), pp.3191-3195.

Kushwaha, M.S. and Djafari-Rouhani, B., 1998. Giant sonic stop bands in two-dimensional periodic system of fluids. Journal of Applied Physics, 84(9), pp.4677-4683.

Kushwaha, M.S. and Halevi, P., 1994. Band-gap engineering in periodic elastic composites. Applied Physics Letters, 64(9), pp.1085-1087.

Kushwaha, M.S. and Halevi, P., 1996. Giant acoustic stop bands in two-dimensional periodic arrays of liquid cylinders. Applied Physics Letters, 69(1), pp.31-33.

Kushwaha, M.S. and Halevi, P., 1997. Stop bands for cubic arrays of spherical balloons. The Journal of the Acoustical Society of America, 101(1), pp.619-622.

Kushwaha, M.S., Halevi, P., Dobrzynski, L. and Djafari-Rouhani, B., 1993. Acoustic band structure of periodic elastic composites. Physical review letters, 71(13), p.2022.

Kushwaha, M.S., Halevi, P., Martinez, G., Dobrzynski, L. and Djafari-Rouhani, B., 1994. Theory of acoustic band structure of periodic elastic composites. Physical Review B, 49(4), p.2313.

Laude, V., 2015. Phononic Crystals: Artificial Crystals for Sonic. Acoustic and Elastic Waves Berlin: De Gruyter.

Laude, V., Achaoui, Y., Benchabane, S. and Khelif, A., 2009. Evanescent Bloch waves and the complex band structure of phononic crystals. Physical Review B, 80(9), p.092301.

Lekner, J., 1994. Light in periodically stratified media. JOSA A, 11(11), pp.2892-2899.

LENDVAI, E., 1971. Béla Bartók: An Analysis of His Music (London, Kahn & Averill).

Levine, D. and Steinhardt, P.J., 1984. Quasicrystals: a new class of ordered structures. Physical review letters, 53(26), p.2477.

Li, J., Liu, Z. and Qiu, C., 2006. Negative refraction imaging of acoustic waves by a two-dimensional three-component phononic crystal. Physical Review B, 73(5), p.054302.

Li, X.F., Ni, X., Feng, L., Lu, M.H., He, C. and Chen, Y.F., 2011. Tunable unidirectional sound propagation through a sonic-crystal-based acoustic diode. Physical review letters, 106(8), p.084301.

Li, Z.N., Wang, Y.Z. and Wang, Y.S., 2021. Tunable mechanical diode of nonlinear elastic metamaterials induced by imperfect interface. Proceedings of the Royal Society A, 477(2245), p.20200357.

Liang, B., Guo, X.S., Tu, J., Zhang, D. and Cheng, J.C., 2010. An acoustic rectifier. Nature materials, 9(12), pp.989-992.

Liang, B., Yuan, B. and Cheng, J.C., 2009. Acoustic diode: Rectification of acoustic energy flux in one-dimensional systems. Physical review letters, 103(10), p.104301.

Lima, V.D., Beli, D. and Arruda, J.R.F., 2019, September. Modeling one-dimensional phononic crystal rods using a state space formulation. In INTER-NOISE and NOISE-CON Congress and Conference Proceedings (Vol. 259, No. 2, pp. 7874-7885). Institute of Noise Control Engineering.

Lin, Y.K. and McDaniel, T.J., 1969. Dynamics of beam-type periodic structures.

Liu, Z., Zhang, X., Mao, Y., Zhu, Y.Y., Yang, Z., Chan, C.T. and Sheng, P., 2000. Locally resonant sonic materials. science, 289(5485), pp.1734-1736.

Liu, Z., Zhang, X., Mao, Y., Zhu, Y.Y., Yang, Z., Chan, C.T. and Sheng, P., 2000. Locally resonant sonic materials. science, 289(5485), pp.1734-1736.

Liu, W., Yoon, G.H., Yi, B., Choi, H. and Yang, Y., 2020. Controlling wave propagation in one-dimensional structures through topology optimization. Computers & Structures, 241, p.106368.

Lu, M.H., Feng, L. and Chen, Y.F., 2009. Phononic crystals and acoustic metamaterials. Materials today, 12(12), pp.34-42.

Lucklum, R. and Li, J., 2009. Phononic crystals for liquid sensor applications. Measurement Science and Technology, 20(12), p.124014.

Lucklum, R., Ke, M. and Zubtsov, M., 2012. Two-dimensional phononic crystal sensor based on a cavity mode. Sensors and Actuators B: Chemical, 171, pp.271-277.

Lusk, D., Abdulhalim, I. and Placido, F., 2001. Omnidirectional reflection from Fibonacci quasi-periodic one-dimensional photonic crystal. Optics Communications, 198(4-6), pp.273-279.

Maciá, E., 1998. Optical engineering with Fibonacci dielectric multilayers. Applied Physics Letters, 73(23), pp.3330-3332.

Maciá, E., 2001. Exploiting quasiperiodic order in the design of optical devices. Physical Review B, 63(20), p.205421.

Mercer, C.A. and Seavey, M.C., 1967. Prediction of natural frequencies and normal modes of skin-stringer panel rows. Journal of Sound and Vibration, 6(1), pp.149-162.

Maldovan, M. and Thomas, E.L., 2006. Simultaneous complete elastic and electromagnetic band gaps in periodic structures. Applied Physics B, 83(4), pp.595-600.

Manzanares-Martínez, B. and Ramos-Mendieta, F., 2003. Surface elastic waves in solid composites of two-dimensional periodicity. Physical Review B, 68(13), p.134303.

Markos, P., 2006. Numerical analysis of the Anderson localization. arXiv preprint cond-mat/0609580.

McColm, G.L., 2021. Cut-and-project graphs and other complexes. Theoretical Computer Science, 894, pp.172-189.

Mead, D.J., 1970. Free wave propagation in periodically supported, infinite beams. Journal of Sound and Vibration, 11(2), pp.181-197.

Mead, D.J., 1973. A general theory of harmonic wave propagation in linear periodic systems with multiple coupling. Journal of Sound and Vibration, 27(2), pp.235-260.

Mead, D.M., 1996. Wave propagation in continuous periodic structures: research contributions from Southampton, 1964–1995. Journal of sound and vibration, 190(3), pp.495-524.

Mello, P.A., Pereyra, P. and Kumar, N., 1988. Macroscopic approach to multichannel disordered conductors. Annals of Physics, 181(2), pp.290-317.

Meseguer, F., Holgado, M., Caballero, D., Benaches, N., Sanchez-Dehesa, J., López, C. and Llinares, J., 1999. Rayleigh-wave attenuation by a semi-infinite two-dimensional elastic-band-gap crystal. Physical Review B, 59(19), p.12169.

Miyashita, T., 2005. Sonic crystals and sonic wave-guides. Measurement Science and Technology, 16(5), p.R47.

Mohammadi, S. and Adibi, A., 2011. On chip complex signal processing devices using coupled phononic crystal slab resonators and waveguides. AIP Advances, 1(4), p.041903.

Mohammadi, S., Eftekhar, A.A., Hunt, W.D. and Adibi, A., 2009. High-Q micromechanical resonators in a two-dimensional phononic crystal slab. Applied Physics Letters, 94(5), p.05190

Mohammadi, S., Eftekhar, A.A., Khelif, A., Hunt, W.D. and Adibi, A., 2008. Evidence of large high frequency complete phononic band gaps in silicon phononic crystal plates. Applied Physics Letters, 92(22), p.221905.

Morini, L. and Gei, M., 2018. Waves in one-dimensional quasicrystalline structures: dynamical trace mapping, scaling and self-similarity of the spectrum. Journal of the Mechanics and Physics of Solids, 119, pp.83-103.

Morini, L., Eyzat, Y. and Gei, M., 2019. Negative refraction in quasicrystalline multilayered metamaterials. Journal of the Mechanics and Physics of Solids, 124, pp.282-298.

Morini, L., Gokay Tetik, Z., Shmuel, G. and Gei, M., 2020. On the universality of the frequency spectrum and band-gap optimization of quasicrystalline-generated structured rods. Philosophical Transactions of the Royal Society A, 378(2162), p.20190240.

Nardi, D., Zagato, E., Ferrini, G., Giannetti, C. and Banfi, F., 2012. Design of a surface acoustic wave mass sensor in the 100 GHz range. Applied Physics Letters, 100(25), p.253106.

Norris, A.N., 2008. Acoustic cloaking theory. Proceedings of the Royal Society A: Mathematical, Physical and Engineering Sciences, 464(2097), pp.2411-2434.

Ogden, R.W. and Steigmann, D.J., 2002. Plane strain dynamics of elastic solids with intrinsic boundary elasticity, with application to surface wave propagation. Journal of the Mechanics and Physics of Solids, 50(9), pp.1869-1896.

Olsson, R.H. and El-Kady, I., 2008. Microfabricated phononic crystal devices and applications. Measurement science and technology, 20(1), p.012002.

Orris, R.M. and Petyt, M., 1974. A finite element study of harmonic wave propagation in periodic structures. Journal of Sound and Vibration, 33(2), pp.223-236.

Pal, R.K., Rosa, M.I. and Ruzzene, M., 2019. Topological bands and localized vibration modes in quasiperiodic beams. New Journal of Physics, 21(9), p.093017.

Pendry, J.B. and MacKinnon, A., 1992. Calculation of photon dispersion relations. Physical review letters, 69(19), p.2772.

Peng, R.W., Huang, X.Q., Qiu, F., Wang, M., Hu, A., Jiang, S.S. and Mazzer, M., 2002. Symmetry-induced perfect transmission of light waves in quasiperiodic dielectric multilayers. Applied Physics Letters, 80(17), pp.3063-3065.

Peng, R.W., Wang, M., Hu, A., Jiang, S.S., Jin, G.J. and Feng, D., 1998. Photonic localization in one-dimensional k-component Fibonacci structures. Physical Review B, 57(3), p.1544.

Pennec, Y., Djafari-Rouhani, B., Vasseur, J.O., Khelif, A. and Deymier, P.A., 2004. Tunable filtering and demultiplexing in phononic crystals with hollow cylinders. Physical Review E, 69(4), p.046608.

Pennec, Y., Jin, Y. and Djafari-Rouhani, B., 2019. Phononic and photonic crystals for sensing applications. Advances in Applied Mechanics, 52, pp.105-145.

Pennec, Y., Vasseur, J.O., Djafari-Rouhani, B., Dobrzyński, L. and Deymier, P.A., 2010. Two-dimensional phononic crystals: Examples and applications. Surface Science Reports, 65(8), pp.229-291.

Poddubny, A.N. and Ivchenko, E.L., 2010. Photonic quasicrystalline and aperiodic structures. Physica E: Low-dimensional Systems and Nanostructures, 42(7), pp.1871-1895.

Policarpo, H., Neves, M.M. and Ribeiro, A.M.R., 2010. Dynamical response of a multi-laminated periodic bar: Analytical, numerical and experimental study. Shock and Vibration, 17(4-5), pp.521-535.

Qiu, C., Zhang, X. and Liu, Z., 2005. Far-field imaging of acoustic waves by a two-dimensional sonic crystal. Physical Review B, 71(5), p.054302.

Reinke, C.M., Su, M.F., Olsson Iii, R.H. and El-Kady, I., 2011. Realization of optimal bandgaps in solid-solid, solid-air, and hybrid solid-air-solid phononic crystal slabs. Applied Physics Letters, 98(6), p.061912.

Richards, D. and Pines, D.J., 2003. Passive reduction of gear mesh vibration using a periodic drive shaft. Journal of Sound and Vibration, 264(2), pp.317-342.

Riva, E., Di Ronco, M., Elabd, A., Cazzulani, G. and Braghin, F., 2020. Non-reciprocal wave propagation in discretely modulated spatiotemporal plates. Journal of Sound and Vibration, 471, p.115186.

Romeo, F. and Luongo, A., 2002. Invariant representation of propagation properties for bi-coupled periodic structures. Journal of sound and vibration, 257(5), pp.869-886.

Ruzzene, M. and Baz, A., 2001. Active control of wave propagation in periodic fluid-loaded shells. Smart Materials and Structures, 10(5), p.893.

Ruzzene, M., Scarpa, F. and Soranna, F., 2003. Wave beaming effects in two-dimensional cellular structures. Smart materials and structures, 12(3), p.363.

Sainidou, R. and Stefanou, N., 2006. Guided and quasiguided elastic waves in phononic crystal slabs. Physical Review B, 73(18), p.184301. 6.

Sánchez-Dehesa, J., Garcia-Chocano, V.M., Torrent, D., Cervera, F., Cabrera, S. and Simon, F., 2011. Noise control by sonic crystal barriers made of recycled materials. The Journal of the Acoustical Society of America, 129(3), pp.1173-1183.

Sánchez-Pérez, J.V., Caballero, D., Mártinez-Sala, R., Rubio, C., Sánchez-Dehesa, J., Meseguer, F., Llinares, J. and Gálvez, F., 1998. Sound attenuation by a two-dimensional array of rigid cylinders. Physical Review Letters, 80(24), p.5325.

Shechtman, D., Blech, I., Gratias, D. and Cahn, J.W., 1984. Metallic phase with long-range orientational order and no translational symmetry. Physical review letters, 53(20), p.1951.

Shi, J., Lin, S.C.S. and Huang, T.J., 2008. Wide-band acoustic collimating by phononic crystal composites. Applied Physics Letters, 92(11), p.111901.

Shmuel, G. and Band, R., 2016. Universality of the frequency spectrum of laminates. Journal of the Mechanics and Physics of Solids, 92, pp.127-136.

Sibilia, C., Masciulli, P. and Bertolotti, M., 1998. Optical properties of quasiperiodic (self-similar) structures. Pure and Applied Optics: Journal of the European Optical Society Part A, 7(2), p.383.

Sigalas, M. and Economou, E.N., 1993. Band structure of elastic waves in two dimensional systems. Solid state communications, 86(3), pp.141-143.

Sigalas, M.M., 1992. Elastic and acoustic wave band structure. Journal of sound and vibration, 158(2), pp.377-382.

Sigalas, M.M., 1997. Elastic wave band gaps and defect states in two-dimensional composites. The Journal of the Acoustical Society of America, 101(3), pp.1256-1261.

Sigalas, M.M., 1998. Defect states of acoustic waves in a two-dimensional lattice of solid cylinders. Journal of Applied Physics, 84(6), pp.3026-3030.

Sigmund, O. and Søndergaard Jensen, J., 2003. Systematic design of phononic band–gap materials and structures by topology optimization. Philosophical Transactions of the Royal Society of London. Series A: Mathematical, Physical and Engineering Sciences, 361(1806), pp.1001-1019.

Sivaraman, R., 2020. Exploring Metallic Ratios. Mathematics and Statistics, 8(4), pp.388-391.

Sorokin, V.S., 2019. Longitudinal wave propagation in a one-dimensional quasi-periodic waveguide. Proceedings of the Royal Society A, 475(2231), p.20190392.

Spadoni, A. and Daraio, C., 2010. Generation and control of sound bullets with a nonlinear acoustic lens. Proceedings of the National Academy of Sciences, 107(16), pp.7230-7234.

Spadoni, A., Gonella, S., Ruzzene, M. and Scarpa, F., 2007, September. Wave propagation and band-gap characteristics of chiral lattices. In ASME 2007 International Design Engineering Technical Conferences and Computers and Information in Engineering

Srivastava, A., 2016. Metamaterial properties of periodic laminates. Journal of the Mechanics and Physics of Solids, 96, pp.252-263.

Steigmann, D.J. and Ogden, R., 1997. Plane deformations of elastic solids with intrinsic boundary elasticity. Proceedings of the Royal Society of London. Series A: Mathematical, Physical and Engineering Sciences, 453(1959), pp.853-877.

Steurer, W. and Deloudi, S., 2008. Fascinating quasicrystals. Acta Crystallographica Section A: Foundations of Crystallography, 64(1), pp.1-11.

Steurer, W. and Sutter-Widmer, D., 2007. Photonic and phononic quasicrystals. Journal of Physics D: Applied Physics, 40(13), p.R229.

Steurer, W., 2004. Twenty years of structure research on quasicrystals. Part I. Pentagonal, octagonal, decagonal and dodecagonal quasicrystals. Zeitschrift für Kristallographie-Crystalline Materials, 219(7), pp.391-446.

Steurer, W., Deloudi, S., 2008. Fascinating quasicrystals. Acta Crystals A64, 1–11.

Sukhovich, A., Jing, L. and Page, J.H., 2008. Negative refraction and focusing of ultrasound in two-dimensional phononic crystals. Physical Review B, 77(1), p.014301.

Swinteck, N., Robillard, J.F., Bringuier, S., Bucay, J., Muralidharan, K., Vasseur, J.O., Runge, K. and Deymier, P.A., 2011. Phase-controlling phononic crystal. Applied Physics Letters, 98(10), p.103508.

Tamura, S. and Nori, F., 1989. Transmission and frequency spectra of acoustic phonons in Thue-Morse superlattices. Physical Review B, 40(14), p.9790.

Tanaka, Y. and Tamura, S.I., 1998. Surface acoustic waves in two-dimensional periodic elastic structures. Physical Review B, 58(12), p.7958.

Timorian, S., Petrone, G., De Rosa, S., Franco, F., Ouisse, M. and Bouhaddi, N., 2019. Spectral analysis and structural response of periodic and quasi-periodic beams. Proceedings of the Institution of Mechanical Engineers, Part C: Journal of Mechanical Engineering Science, 233(23-24), pp.7498-7512.

Tol, S., Degertekin, F.L. and Erturk, A., 2017. Structurally embedded reflectors and mirrors for elastic wave focusing and energy harvesting. Journal of Applied Physics, 122(16), p.164503.

Torrent, D. and Sánchez-Dehesa, J., 2009. Radial wave crystals: radially periodic structures from anisotropic metamaterials for engineering acoustic or electromagnetic waves. Physical review letters, 103(6), p.064301.

Torres, M.D.E.F., De Espinosa, F.M., Garcia-Pablos, D. and Garcia, N., 1999. Sonic band gaps in finite elastic media: surface states and localization phenomena in linear and point defects. Physical Review Letters, 82(15), p.3054.

Trabelsi, Y., Kanzari, M. and Rezig, B., 2009. Microwave properties of the generalized Fibonacci quasi-periodic multilayered photonic band gap structure. Optica Applicata, 39(2).

Trainiti, G. and Ruzzene, M., 2016. Non-reciprocal elastic wave propagation in spatiotemporal periodic structures. New Journal of Physics, 18(8), p.083047.

Trainiti, G., Xia, Y., Marconi, J., Cazzulani, G., Erturk, A., Ruzzene, M., 2019. Timeperiodic stiffness modulation in elastic metamaterials for selective wave filtering: Theory and experiment. Phys. Rev. Lett. 122, 124301.

Tschichold, J., 1991. The form of the book: essays on the morality of good design. Point Roberts: Hartley & Marks.

Ungar, E.E., 1966. Steady-state responses of one-dimensional periodic flexural systems. The

Vasseur, J.O., Djafari-Rouhani, B., Dobrzynski, L., Kushwaha, M.S. and Halevi, P., 1994. Complete acoustic band gaps in periodic fibre reinforced composite materials: the carbon/epoxy composite and some metallic systems. Journal of Physics: Condensed Matter, 6(42), p.8759.

Vatanabe, S.L., Paulino, G.H. and Silva, E.C., 2014. Maximizing phononic band gaps in piezocomposite materials by means of topology optimization. The Journal of the Acoustical Society of America, 136(2), pp.494-501.

Waters, T.P., 2019. A chirp excitation for focussing flexural waves. Journal of Sound and Vibration, 439, pp.113-128.

Willis, J.R., 2016. Negative refraction in a laminate. Journal of the Mechanics and Physics of Solids, 97, pp.10-18.

Wilson, R., Reboud, J., Bourquin, Y., Neale, S.L., Zhang, Y. and Cooper, J.M., 2011. Phononic crystal structures for acoustically driven microfluidic manipulations. Lab on a Chip, 11(2), pp.323-328.

Wu, T.T., Hsu, J.C. and Sun, J.H., 2011. Phononic plate waves. IEEE transactions on ultrasonics, ferroelectrics, and frequency control, 58(10), pp.2146-2161.

Wu, T.T., Huang, Z.G. and Lin, S., 2004. Surface and bulk acoustic waves in two-dimensional phononic crystal consisting of materials with general anisotropy. Physical review B, 69(9), p.094301.

Wu, T.T., Wu, L.C. and Huang, Z.G., 2005. Frequency band-gap measurement of two-dimensional air/silicon phononic crystals using layered slanted finger interdigital transducers. Journal of Applied Physics, 97(9), p.094916.

Xia, Y., Erturk, A. and Ruzzene, M., 2020. Topological edge states in quasiperiodic locally resonant metastructures. Physical Review Applied, 13(1), p.014023.

Yablonovitch, E., 1987. Inhibited spontaneous emission in solid-state physics and electronics. Physical review letters, 58(20), p.2059.

Yuan, C., Jing, L., Jingdong, Z., Tao, H., Minggang, Z. and Yuan, Y.D., 2014. Phononic first band gap of quaternary layered periodic structure with the lumped-mass method. Shock and Vibration, 2014.

Zhang, H.F., 2017. Investigations on the two-dimensional aperiodic plasma photonic crystals with fractal Fibonacci sequence. AIP Advances, 7(7), p.075102.

Zhang, X. and Liu, Z., 2004. Negative refraction of acoustic waves in two-dimensional phononic crystals. Applied Physics Letters, 85(2), pp.341-343.

Zhao, M., Xie, Y.Z., Zhang, X.G. and Gao, J., 2013. Band gaps of Lamb waves propagating in one-dimensional periodic and nesting Fibonacci superlattices thin plates. Thin Solid Films, 546, pp.439-442.

Zheng, L.Y., 2017. Granular monolayers: wave dynamics and topological properties (Doctoral dissertation, Le Mans).

Zheng, X., Zhang, X., Chen, T.T. and Watanabe, I., 2023. Deep Learning in Mechanical Metamaterials: From Prediction and Generation to Inverse Design. Advanced Materials, p.2302530.

Zhu, X., Zhong, S., Sun, D., Ye, A. and Deng, F., 2014. Investigation of phononic band gap structures considering interface effects. Physica B: Condensed Matter, 450, pp.121-127.